SAPIENZA
UNIVERSITÀ DI ROMA

Setup of Modulated Temperature FTIR technique to investigate thermal transitions of polymers

PhD in Chemical Sciences, XXXI Cycle
Faculty of Mathematical, Physical and Natural Sciences
Department of Chemistry
Sapienza University of Rome, 2018

Doctoral thesis by
Valerio Di Lisio

Supervisor
Prof. Andrea Martinelli

1. INTRODUCTION

Since early 1900s the discover of polymeric materials profoundly changed human technology, revolutionizing the human approach to the material science. Since then, polymer science had played a fundamental role in the development of new synthetic polymers for a wider range of application. Simultaneously, the necessary understanding of physical and chemical properties of polymeric materials to define application ranges and uses pushed the improvement of investigation techniques and the development of new ones. The principal analysis utilized to study the behaviour of polymers thermodynamic in bulk was the thermal analysis. Thermal analysis studies the behaviour of polymer materials in the principal physical state of condensed matter, namely liquid, glass, crystalline state, and the relative transition from one to another. The study and the understanding of thermal transitions of a polymeric material is crucial to infer the applicability and the future development of new materials.

The PhD research can be divided in four main issues. The first concerns the development of a new spectroscopic investigation technique, namely the Modulated Temperature FTIR (MTFTIR), exposing the theory and the mathematical elaboration in the experimental section of the thesis.

Furthermore, in the second part of the research, in combination with calorimetric DSC and FSC measurements performed in collaboration with PhD Daniele Cangialosi of Material Physics Center (CFM) in San Sebastian, the MTFTIR technique was used to study and give further insights on two different transitions of difficult interpretation, namely the glass transition with the related relaxation recovery and the physical aging of PET and poly(L-lactide). The extensive study on the conformational transitions occurring in the glassy and liquid state of amorphous PET will be exposed in Chapter 3. Regarding the investigation on poly(L-lactide), the effects of the rejuvenation process, defined as a short-term isothermal annealing slight above the glass transition, on the glassy PLLA was studied by MTFTIR, in Chapter 4.

The third part deals with the application of MTFTIR and quasi-isothermal FTIR to investigate the reversible melting and crystallization phenomena of isotactic polypropylene. In Chapter 5, these techniques were combined successfully to the Quasi-isothermal DSC in order to give new insights in the molecular mechanisms of the reversible crystallization and melting of isotactic polypropylene.

In conclusion, the research conducted in collaboration with PhD Daniele Cangialosi of Material Physics Center (CFM) was showed in the Appendix, consisting in an improvement of the Temperature Modulated Fast Chip Calorimetry in order to study the glass transition of PS under confinement effect.

1.1 THERMAL ANALYSIS

Thermal analysis is a branch of materials science that includes any investigation technique regarding the study of the properties of a material in function of the temperature. [1,2] There are many classifications for describing material properties on the basis of different factors. Most important classifications are the following:

Depending on the dependency of the extension of the material

- Intensive (e.g. Temperature, Pressure)
- Extensive (e.g. Volume, n° of mole)

Depending on the kind of property

- Thermodynamic (e.g. heat capacity, enthalpy, volume)
- Mechanical
- Optical
- Dielectric
- Spectroscopic (vibrational spectrum, electron and neutron scattering spectrum)

Depending on the length scale

- Macroscopic
- Microscopic

In the present PhD research, the thermal properties of 3 polymers were studied by using two different investigation techniques. The first is the Differential Scanning Calorimetry (DSC) for determining the macroscopic thermodynamic properties of the system as the specific heat (c_p) and the enthalpy of phase transitions (ΔH), and the second is the study of the change with temperature of the infrared vibrational spectrum of polymers by Fourier Transformation Infrared Spectroscopy (FTIR).

1.1.1 Differential Scanning Calorimetry

Differential Scanning Calorimetry (DSC) is the most important investigation technique to study the thermodynamic properties of a material.[3-6] It allows to measure the heat exchange (δQ) of a system as function of the temperature, and as follows the enthalpy change (dH), the heat capacity (C), and the specific heat (c). In the case of a closed system, in which the pressure is kept constant and no work is done other than thermal expansion, the four system properties are linked by the thermodynamic expression:

$$\delta Q = dH = C_p dT = \frac{c_p}{m} dT \qquad \text{Eq 1.1}$$

where C_p and c_p are respectively the heat capacity and the specific heat at a constant pressure, T is the temperature of the system and m is the mass.

The experimental data obtained by a Differential Scanning Calorimeter is defined thermogram. A thermogram displays the heat flux ($\delta Q/dt$) [Watt] as function of the temperature T. In general DSC scans are performed by changing the temperature with a constant heating or cooling rate, and recording simultaneously the heat flux involved. As an example, Figure 1.1 shows a thermogram of an amorphous Poly (Ethylene Terephthalate) heated at 10 °C/min from 25 to 280 °C, with highlighted the physical state of the matter and the principal phase transitions.

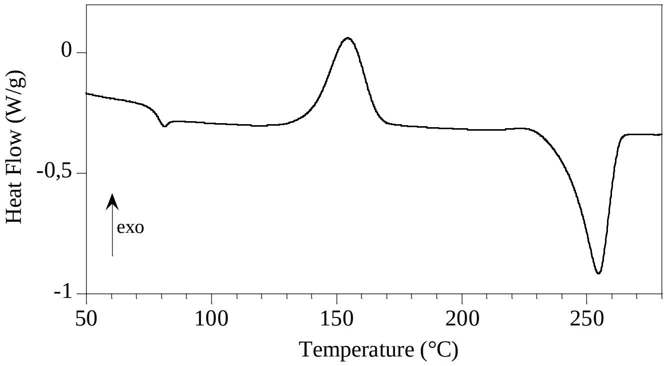

Figure 1.1. Heat flow as function of the temperature for a PET amorphous sample.

From the thermogram it is possible to calculate the specific heat of the system (Equation 1.2), that is a macroscopic property and it is defined as the amount of heat needed per unit mass to increase the temperature of a degree[3] (it has as IS measure unit J g^{-1} K^{-1}).

$$c_p = -\frac{1}{m\beta}\frac{\delta Q}{dt} \qquad \text{Eq 1.2}$$

where $\delta Q/dt$ is the heat flux, m is the mass of the sample and β is the heating/cooling rate. Note that the negative sign is needed when the heat is considered positive when released by the system.

The importance of this property lies in the fact that the specific heat is linked to the properties of single macromolecules present in the system. In quantomechanical terms, the specific heat is proportional to the degree of freedom of the system, constitute of the sum of all vibration, rotation and translation normal modes.[3] In the case of linear macromolecules, the macroscopic specific heat was explained by a microscopic model of thermal motion. For an overall description, four different contributions of thermal motion to the specific heat of a macromolecule are distinguished:

1. Vibrational motion of the overall atomic groups of the macromolecule in a fixed position (small amplitude motions)
2. Conformational motions, namely the rotation of a part of the macromolecule around a bond
3. Translation of a macromolecule as a whole
4. Rotation of a macromolecule as a whole

For large macromolecules the contributes of type 3 and 4 are negligible because of the little amount of energy involved in these motions. So, type 1 and 2 motions contribute mostly to the specific heat of a macromolecular material in equilibrium conditions in absence of phase transitions.

Another additional contribution to the specific heat is related to the heat absorbed or released by the system to change its physical state, e.g. liquid to solid. The so called “latent specific heat” is defined as the energy required to change the physical state of a unitary mass of the material in isothermal conditions, and it coincides to the change of enthalpy per unit of mass of a phase transition.

The study of the temperature dependent specific heat of a linear macromolecule and its separation in vibrational, conformational and latent heat contributions represented a real challenging issue for calorimetry in the last decades of 1900s, because of the huge amount of vibrational and conformational states implied in the thermal motion of polymers. In order to interpret the specific heat of linear macromolecules, in the 1980s a collection of specific heat measurements was made for a large number of linear polymers, known as Advanced THermal Analysis System (ATHAS)[7]. Furthermore, the system describes the specific heat of the solid state as the sum of the overall vibrational contribution calculated by IR and Raman vibrational spectrum at low temperatures. The conformational contribution is added for describing the specific heat of liquid phases, in which the macromolecular system acquires the mobility of the backbone chain. As far as temperature dependent specific heat of solid and liquid phases, the temperature dependent latent heat of fusion and crystallization was calculated for each polymer.

1.1.2 Modulated Differential Scanning Calorimetry

In the year 1992 an improvement of the standard DSC was developed by Reading and its coworkers,[6] defined Modulated Differential Scanning Calorimetry (MDSC or MTDSC). The basic principle of MDSC is to measure the heat flow response of a sample during a modulated temperature program. The latter is composed by a linear heating or cooling ramp with superimposed a small-amplitude periodic perturbation of the temperature. Although many different oscillating functions may be used, the common and simpler to elaborate is the sinusoidal perturbation. Hence, a sinusoidal temperature program can be written in mathematical terms as:

$$T(t) = T_0 + \beta t + A_T \sin \omega t \qquad \text{Eq 1.3}$$

where T is the actual temperature, T_0 is the start temperature, β is the heating/cooling rate, A_T the modulating temperature amplitude and ω the angular frequency.

Thus, the heating/cooling rate can be expressed as the sum of a linear and an oscillating component:

$$\frac{dT}{dt}(t) = \beta + A_{HR} \cos \omega t \qquad \text{Eq 1.4}$$

where

β is the linear part of the heating/cooling rate

$\omega A_T \cos \omega t$ is the oscillating part in which $A_{HR} = \omega A_T$ is the oscillating heating/cooling rate amplitude

The heat flow response, $HF(t)$, similarly to the heating/cooling rate, can be expressed as the sum of the linear, $\langle HF \rangle$, and the oscillating heat flow:

$$HF(t) = \frac{\delta Q}{dT} = \langle HF \rangle + A_{HF} \cos(\omega t + \varphi) \qquad \text{Eq 1.5}$$

where

$\langle HF \rangle$ is the average, or total heat flow (linear part)

$A_{HF}\cos(\omega t + \varphi)$ is the oscillating part, in which A_{HF} represents the heat flow oscillating amplitude and φ the phase lag respect to the heating rate modulation.

It is worth to notice in the oscillating heat flow response the introduction of a phase lag term, considering the dissipative phenomena that can occur in the sample.

Furthermore, by a deconvolution procedure based on Discrete Fourier Transform, the heat flow signal is decomposed into one part that follows the periodic perturbation, namely the *reversing* component, and one that does not, the *non-reversing* part. For the determination of the *reversing* heat capacity, the use of complex notation is often useful. The complex heat capacity $\hat{C}$ is calculated from the oscillating part of the heat flow and heating rate, by means of Equation 1.6.

$$\hat{C} = C' - iC'' = \frac{A_{HF}}{A_{HR}} e^{-i\varphi} \qquad \text{Eq 1.6}$$

and

$$C' = C^{rev} = \frac{A_{HF}}{A_{HR}} \cos\varphi \quad \text{is the phase-corrected reversing heat capacity} \qquad \text{Eq 1.7}$$

$$C'' = \frac{A_{HF}}{A_{HR}} \sin\varphi \quad \text{is the out-of-phase, or kinetic heat capacity} \qquad \text{Eq 1.8}$$

For the determination of the phase-corrected *non-reversing* heat capacity, the phase-corrected *reversing* heat capacity is subtracted to the *total* or *apparent* heat capacity C^{tot}, that is the ratio between the total heat flow and the linear heating/cooling rate, reported in Equations 1.4 and 1.5:

$$C^{nr} = C^{tot} - C^{rev} = \frac{\langle HF \rangle}{\beta} - \frac{A_{HF}}{A_{HR}} \cos\varphi \qquad \text{Eq 1.9}$$

The separation of the thermal response of a polymeric material into its *reversing* and *non-reversing* components is often useful to study in detail polymeric thermal transition, such as melting, crystallization and glass transition, or chemical reaction, such as curing, polymerization, degradation. As an example, one of the major advantages of Modulated DSC is that of separate the heat capacity or specific heat from latent heat contributions given by phase transitions such as the crystallization. The heat capacity is always affected by the small-amplitude modulation, hence it appears in the *reversing* response of the system. On the other hand, transitions that occur spontaneously, namely with a decrease of Gibbs free energy (G) once initiated they cannot be reversed by modulation, hence they appear in the *non-reversing* part of the heat flow. In Table 1.1 it is shown the characteristics of a list of physical transitions and chemical reaction occurring in polymer system in response to the temperature modulation, analysed by DSC.

Table 1.1 Behaviour of phase transitions and chemical reactions of polymers in response to the temperature modulation. "*Reversing*" stands for a transition that follows the temperature modulation, that is reversed by heating/cooling cycles.

Transition	***Characteristic***
Heat capacity	Reversing
Glass transition	Reversing (frequency dependent)
Melting	Reversing (frequency and amplitude dependent) + Non-reversing
Melt-crystallization	Reversing + Non-reversing
Cold-crystallization	Non-reversing
Relaxation	"
Curing	"
Evaporation	"
Oxidation	"
Decomposition	"

It is worth to notice that the melting and the melt-crystallization of polymers are partially affected by the modulation, hence the MDSC technique allows to separate the *reversing* part from the *non-reversing* part of such transitions. Moreover, the characteristics of *reversing* transition may be affected by temperature modulation parameters, namely the frequency and the amplitude of the oscillation. As an example, it was studied that the glass transition temperature increases with increasing the frequency,[56,57] meanwhile the reversing part of polymer melting increase in intensity by decreasing the frequency and increasing the amplitude of modulation.[15,16]

1.1.3 Time-resolved Infrared Spectroscopy

Since the second half of 1900s, the study of the variation of the vibrational spectrum of polymers as function of the temperature was developed and gained a relevant importance to understand the thermal behaviour of polymers.[10-11] In particular, two major techniques were used until nowadays, namely Infrared spectroscopy[8-12] and Raman spectroscopy[12,13].

Infrared spectroscopy involves the interaction of an infrared radiation with molecules composing the examined system. Infrared spectroscopy exploits the fact that molecules absorb at frequencies that are characteristic of their structure[8]. These absorptions occur at resonant frequencies, that are associated with the normal modes corresponding to the molecular electronic ground state potential energy surface. The resonant frequencies are also related to the strength of the bond and the mass of the atoms. Thus, the frequency of the vibrations is associated in general with a particular normal mode of motion and a particular bond type. In order for a vibrational mode in a sample to be "IR active", it must be associated with changes in the dipolar momentum, namely the transition dipole momentum, of a group of two or more atoms. A molecule can vibrate in many ways, and each way is called a *vibrational mode.* For molecules with N number of atoms, linear molecules have 3N – 5 degrees of vibrational modes, whereas nonlinear molecules have 3N – 6 degrees of vibrational modes. The simplest or fundamental IR bands arise from the excitations of normal modes, the simplest distortions of the molecule, from the ground state with vibrational quantum number v = 0 to the first excited state with vibrational quantum number v = 1.

In the case of molecules with a large number of atoms, it was experimentally proven that the physical state of the system affects the presence, the resonance frequency and the strength of vibrational modes. In fact, the vibrational spectrum of a macromolecule is influenced by inter and intra-molecular interactions, conformational or structural changes of the material.

For sake of clarity, the vibrational absorption bands of a macromolecule can be classified in four different types depending on the influence of the microscopic properties of the macromolecule[14] (configuration, conformation, short-long scale structural order):

1. Stereoregularity band
2. Conformational band
3. Regularity band
4. Crystalline band

A stereoregularity band (1) is sensible to a precise arrangement of adjacent chiral centers within a macromolecule, e.g. the same vibrational mode possesses two different resonance frequency for isotactic and syndiotactic polypropylene. Conformational bands (2) are sensitive to conformational isomerism of atomic groups that allows rotation through one bond, e.g. the case of two different absorption bands for the gauche and trans conformation of the ethylenic group of PET. A regularity band (3) arises when an arrangement of ordered conformers sequences appears in the molecular chain. In this case, intra-molecular interactions play a substantial role in particular vibrational modes relative to the coupling of the oscillators in the ordered structure. Crystalline band (4) arises when a long-range order of the polymer chains, comprises conformational spatially ordered structures, generates a resonant vibration given by the combination of intra- and inter-molecular coupling of oscillators. Type 4 band are uncommon in polymers, because the loose packing of the polymers crystalline structures does not allow enough inter-molecular interaction for the oscillators coupling. Examples of polymers that possess crystalline bands in the vibrational spectrum are polyethylene and poly(L-lactide), due to the high density of the polymer chains packing in the crystal lattice.

1.2 PHASE TRANSITIONS AND RELAXATIONS OF POLYMERS

Generally, a thermoplastic polymer exhibits different physical states, or phases, based on the temperature of observation.[2,3] Briefly, a physical state of matter can be characterized by the strength of the interactions, the mobility, and the spatial order between molecules. Based on these parameters, three condensed states can be assumed for a polymeric system:

- Liquid state: characterized by high mobility and low structural order;
- Amorphous glassy state: low mobility, low structural order;
- Crystalline state: low mobility, high structural order.

Each physical state is characterized by a defined set of state variables, such as temperature, volume, enthalpy, entropy. The Gibbs free energy ($G = H - TS$) is an important state variable to measure the thermodynamic stability. Thermodynamic systems tend to minimize Gibbs free energy.

By varying the temperature of the system, polymeric materials may have phase transitions, defined as the change between a physic state to another. The main phase transitions for a polymeric system are:

- Crystallization
- Melting
- Glass transition

The crystallization and the melting phase transition are associated to the transformation of the liquid phase, or only a fraction of it, in the crystal phase and vice versa. By cooling a liquid phase at the transition temperature, macromolecular chains order conformationally and spatially forming the crystal phase, in which large-amplitude motions of the chains stop and thermodynamic state variables as entropy, enthalpy and volume decreases abruptly. On the contrary, by heating a crystal phase, the system gains mobility by a disordering process that brings about the liquid phase. These transitions are classified as first-order transition, because of the latent heat involved in the change of intra- and inter-molecular interactions. Figure 1.2 shows the Gibbs free energy profiles as function of the temperature of the system.

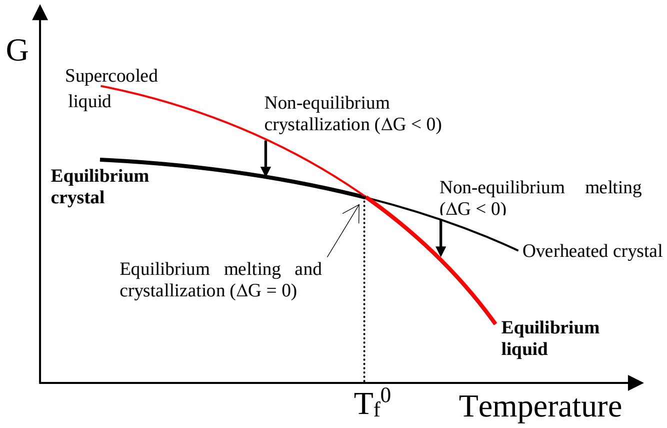

Figure 1.2. Gibbs free energy as function of the temperature for liquid and crystal phase. At the equilibrium melting/crystallization temperature (T_f^0) the equilibrium crystallization (on cooling) and melting (on heating) occur. The equilibrium system follows the bold pathway. Black arrows show two isothermal crystallization and melting in non-equilibrium conditions (ΔG < 0)

The equilibrium melting (on heating) or crystallization (on cooling), occur in correspondence of the intersection of the Gibbs free energy profiles of the liquid and crystal states (Figure 1.2). Therefore, the equilibrium melting and crystallization occur with no free energy change (ΔG = 0) at the equilibrium melting/crystallization temperature (T_f^0)[15,16]. Commonly, the crystallization or melting of polymeric materials may occur at different temperatures respect to the equilibrium temperature. In this case, a transient state is involved, in which the system evolves spontaneously as function of time toward the equilibrium condition by decreasing the amount of Gibbs free energy[3]. For sake of clarity, in Figure 1.2 are shown two examples of spontaneous ($\Delta G < 0$) non-equilibrium transitions, in which the system evolves kinetically from supercooled liquid to equilibrium crystal (non-equilibrium crystallization) and from overheated crystal to equilibrium liquid (non-equilibrium melting).

The glass transition involves the transformation of a system from the liquid state to an amorphous solid state and vice versa.[3,17-20] By cooling a liquid phase, large-amplitude motions of macromolecular chains decrease. The liquid system become less mobile up to the glass transition temperature, in which large-amplitude motions of polymer chains stop. The system freezes in a glassy state that possesses a structure similar to the liquid, but the thermal motion is restrained to vibrations. The glass transition is classified as a “pseudo” second-order transition, in which thermodynamic state variables do not change abruptly, and no heat exchange is involved. At the glass transition temperature, the heat capacity (C_p) of the system decrease passing from liquid to glass, because of the inactivation of large-amplitude, conformational and orientational motions.[3] It is worth to notice that the glass transition can occur also in semi-crystalline systems, involving only the amorphous fraction.

In Figure 1.3 is reported the Gibbs free energy of the liquid and glassy phases as a function of temperature.

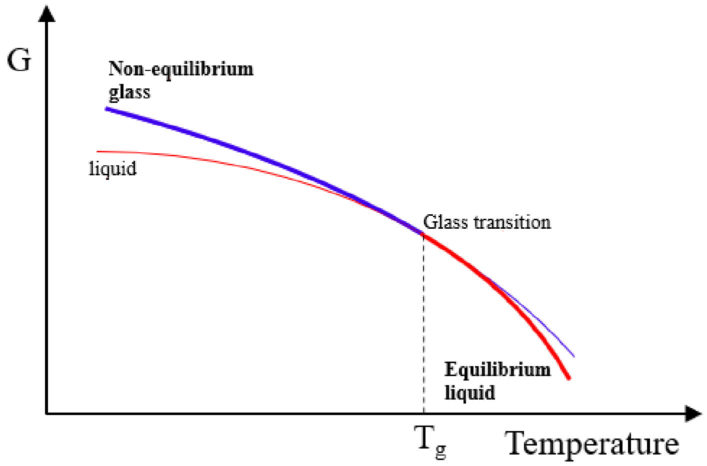

Figure 1.3. Gibbs free energy as function of the temperature for the liquid and the glassy state. The system follows the bold pathway by changing the temperature, the glass transition is shown at T_g.

By extrapolating the Gibbs free energy of the liquid state at temperatures below the glass transition, it is observed that the amount of free energy of the liquid is always lower than that of the glass. So, the glass transition can be considered as the loss of the equilibrium condition of the liquid phase, microscopically explained as the arrest of the molecular large-amplitude motions. In thermodynamic terms, the vitrification of a liquid is not considered properly a phase transition, because of its kinetics nature. For example, the glass transition temperature and the glass properties depend on the thermal history of the formation of the glass, e.g. the cooling rate. The upper part of Figure 1.4 shows the variation of the glass properties (Volume and Enthalpy) and the change of the glass transition temperature for two different cooling rates v_1 and $v_{2,}$ as a function of the temperature. On the lower graph of Figure 1.4 the kinetics factor of the molecular mobility as function of the temperature is compared to the cooling rates v_1 and $v_{2.}$ At temperatures above the glass transition the high molecular mobility allow the material to remain in the equilibrium liquid state. By cooling the system, the molecular mobility decreases and, at the glass transition temperature, the system is not able to rearrange in order to follow the equilibrium properties. Hence, the liquid system vitrifies by falling out from equilibrium, being the kinetic factor of the molecular rearrangements lower than that of the external temperature change. By increasing the cooling rate ($v_2 > v_1$, Figure 1.4) the glass transition temperature increase, leading to the formation of more unstable glasses (*glass 2*, Figure 1.4) with properties further away from equilibrium.

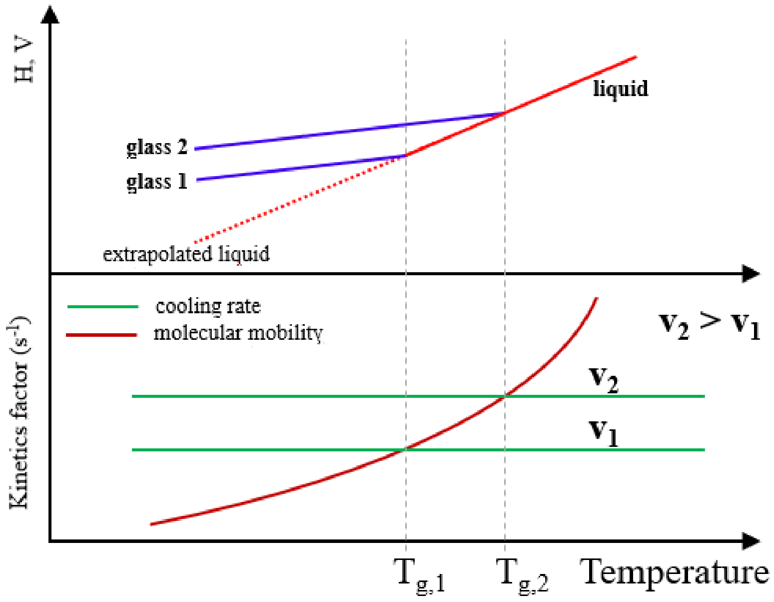

Figure 1.4. Upper side: Enthalpy and Volume properties for a glass-former system, cooled at two cooling rates, v_1 (slow) and v_2 (fast), as function of the temperature. Lower side: Comparison

between the kinetics factor of the molecular mobility of the system and the two different kinetics of cooling.

As discussed previously, the glassy state of a system is in thermodynamic terms an out-of-equilibrium state[3,19]. As far as the kinetics of molecular motions is low but not null, the properties of a glass evolve as function of time toward a thermodynamic equilibrium, namely the liquid equilibrium. Hence, if a polymeric material is kept at the glassy state, a relaxation phenomenon takes place. Such process was defined "physical aging" by Struik[21] and consists in the activation of structural, conformational and orientational rearrangements of polymer chains in order to minimize the internal energy of the glassy system. The driving force of the physical aging is the offset from the equilibrium, considered as the liquid equilibrium properties extrapolated at the actual temperature of the glass.

The physical aging of glassy systems is considered a "thermo-reversible" phenomenon[21], because of its erasing at temperature around T_g, at which the glassy relaxed system regains the structural mobility and a "relaxation recovery" occurs by reaching the liquid equilibrium. The physical aging and the subsequent relaxation recovery can be easy visualized by following thermodynamic properties in a temperature cycle. Figure 1.5 shows the thermal trend of volume and enthalpy in a cooling-isothermal-heating cycle departing from the liquid state.

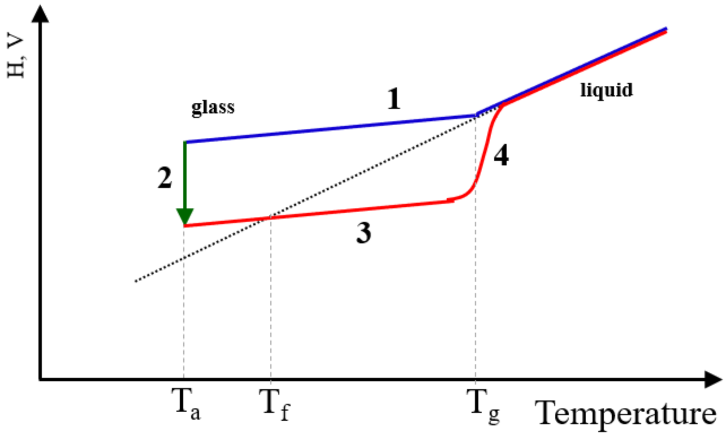

Figure 1.5. Changes in Enthalpy and Volume as function of the temperature in a cooling-isothermal-heating cycle.

By cooling the system, at T_g the liquid falls out from the equilibrium, becoming a glass (1). If the glass is kept in isothermal conditions at the aging temperature T_a (2), an exothermic *physical aging* occurs by lowering the enthalpy and volume of the system, in order to reach the extrapolated liquid equilibrium value. In the subsequent heating (3) the thermodynamic properties of the relaxed glass are lower than those in the cooling step, intersecting the extrapolated equilibrium liquid values at a temperature defined *fictive temperature* (T_f). In proximity of T_g an abrupt increase of volume and enthalpy takes place, the sample retrieving the equilibrium liquid properties. Microscopically, frozen macromolecules acquire enough segmental mobility such as to reactivate large-amplitude thermal motions and undergo the glass transition superimposed to the endothermic *relaxation recovery*, that erase the thermal history of the glass.

Being the physical aging of glassy systems an out-of-equilibrium relaxation phenomenon, the glass property evolution shows dependency from aging time and temperature.[17-24] The time evolution of a glass property $\phi(t)$, as volume or enthalpy, toward the extrapolated liquid equilibrium follows a "stretched exponential" relaxation behaviour, described by Kohlrausch-William-Watts equation[22,23] (Equation 1.3). This relationship takes into account that there is a distribution of relaxation times whose average and breadth are parametrized by the characteristic time τ and the stretching parameter β, respectively.

$$\phi(t) = exp\left[-(t/\tau)^{\beta}\right] \qquad \text{Eq 1.3}$$

Being linked to the residual mobility in the glass state, the relaxation of glassy systems shows a strong temperature dependence, in which the characteristic time of the relaxation process increase with decreasing aging temperature. Commonly, the temperature dependent relaxation time follows a Vogel-Tamman-Fulcher (VTF) relationship[24-26] (Equation 1.4), that postulates a Vogel temperature for the glass $T_0 = T_g - 30$ °C, at which the characteristic time of relaxation diverges and the glassy system freezes completely.

$$\ln \tau = \ln \tau_0 + \frac{B}{(T - T_0)}$$

where τ_0 is the characteristic time extrapolated at infinite temperature and B is the Vogel activation energy.

1.3 EFFECTS OF THERMAL TREATMENTS ON POLY-ETHYLENE TEREPHTHALATE IN THE GLASS TRANSITION REGION

Poly(ethylene terephthalate) (PET) is a thermoplastic polymer belonging to the family of polyesters. PET is one of the most used polymeric materials in the packaging of food containers[27].

The characteristics of strength, transparency, workability, low oxygen permeability, low production costs and recyclability have allowed it to replace glass in the bottling of carbonated drinks, oils and mineral waters. Its uses are very extensive, including films, tubes, labels and textile fibres. PET is a semi-crystalline polymer with a fusion temperature of about 260 °C, and degradation temperature of 300 °C. PET crystallizes in a temperature range between 230 – 90 °C. If quenched from the melt in liquid nitrogen or ice-water an amorphous glass can be obtained, with the glass transition in a temperature range of 70-80 °C.[28]

The repetitive unit of PET is showed in Figure 1.6 and it is composed by a terephthalate unit and an ethylene unit bonded by means of a glycolic bond (II).

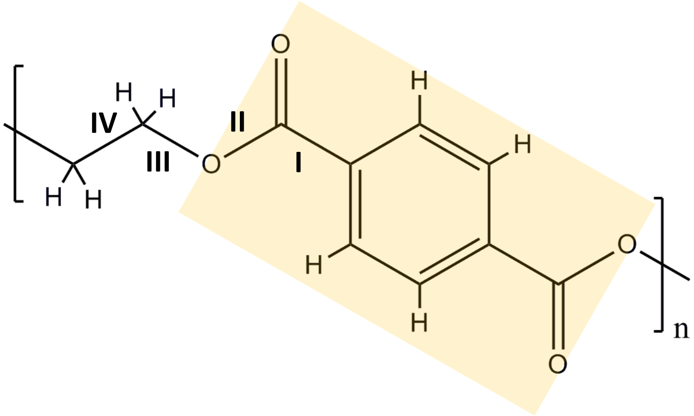

Figure 1.6 Repeating unit of poly(ethylene terephthalate). The four kind of torsional bonds in the repeating unit are reported, the C-C bond between the phenyl ring and the carbonyl unit (I), the ester bond (II), glycolic (III) and ethylenic (IV) bonds. The shaded area represents the terephthalate unit.

1.3.1 Conformational study of PET

One of the preliminary stages to understand the thermal behavior of PET is the study of the conformations assumed by the macromolecular chains and their spatial arrangement in the amorphous and crystalline states[29-30]. Chain dynamics in amorphous PET were performed by molecular dynamics simulations in literature[31,32]. In particular, the torsional potentials for the four single bonds contained in a repetitive unit (I-II-III-IV, Figure 1.6) were calculated using different force fields. The potential as function of torsional angle calculated by Boyd et al.[31] is displayed in Figure 1.7

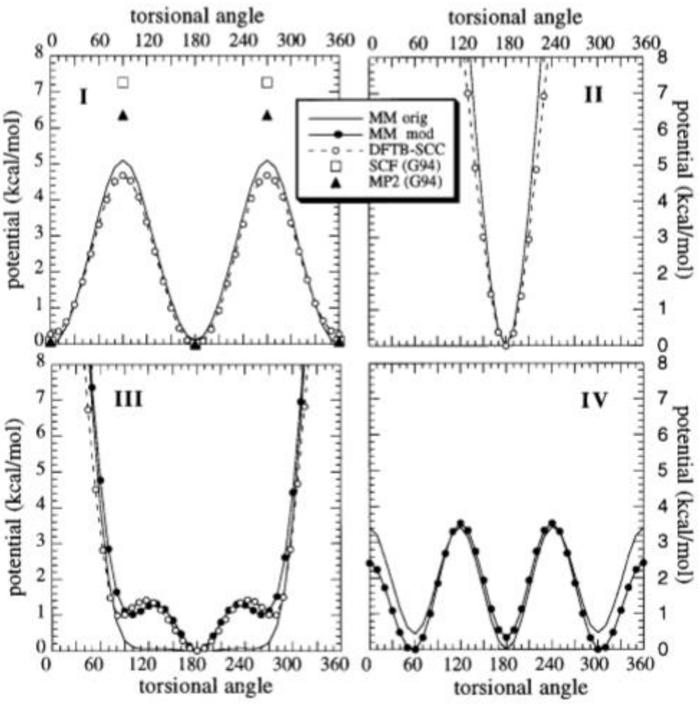

Figure 1.7. Torsional potentials as function of torsional angles for the four bonds in the repeating unit of poly(ethylene terephthalate). The potentials are calculated by means of different force fields.

The study of potential maps for the four bonds of PET gives two different minima in the potential energy for bonds I, III and IV, meanwhile only one minimum for bond II. This means that the rotation around the ester bond (II) is prevented, hence the two ester groups of the terephthalate unit is always planar respect to the phenyl ring. The phenyl link (I), the glycolic (III) and ethylenic (IV) bonds exhibit conformational isomerism.

Newman representations for PET rotamers[30] are displayed in Figure 1.8. In the terephthalate unit the two ester groups can be in *cis* (C_B) or *trans* (T_B) positions respect each other. The torsion around the glycolic bond gives *trans* (*t*) and *gauche* (*g*) conformers, as the ethylenic bond, with *trans* (*T*) and *gauche* (*G*) conformations.

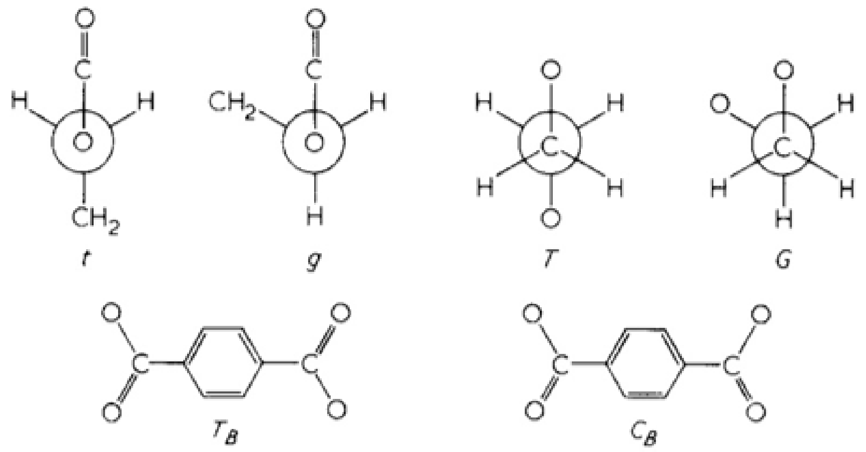

Figure 1.8. Schematic representation of conformational forms of poly(ethylene terephthalate)

The study of the conformational distribution in the disordered phase of PET by infrared spectroscopy[33] showed that the more stable conformation of the repeating unit in liquid and glassy PET is the *Gg* concerning ethylenic and glycolic conformers, with no direct evidences about the cis-trans distribution (C_B-T_B) of terephthalic unit. Nevertheless, the crystalline form of PET consists in spatially and conformationally ordered chains with T_{B},T,t conformations, that form a rigid planar stripe packed in a triclinic unit cell, with cell parameters a = 4,56 Å, b = 5,94 Å, c = 10,75 Å, α = 98,5°, β = 118°, γ = 112°. This gives the density of the crystals as 1,455 g/cm^3. The conformational and spatial order calculated by Bunn et al.[34,35] by wide angle x-ray diffraction (WAXD) of a crystal of PET is showed in Figure 1.9.

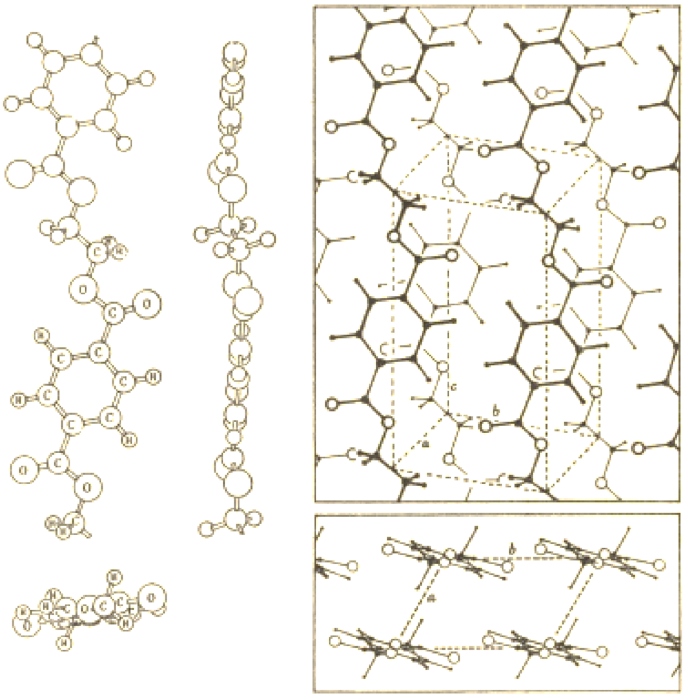

Figure 1.9. Conformational (left) and spatial (right) arrangements of PET chains in crystal structure.

1.3.2 Conformational analysis by infrared spectroscopy

Infrared spectroscopy is one of the most useful technique able to analyse the conformational arrangement of amorphous and crystalline PET, because of its sensibility to conformational or structural changes. The mid-infrared spectrum of PET is characterized by different conformational bands that are assigned to different conformational isomers in the molecular chain. By literature[30,36], the assignment of vibrational modes, reported in Table 1.2, shows different absorption bands for the *gauche* and *trans* conformers of the ethylenic group (*G*, *T*), as well as for the gauche and trans conformers of glycolic bond (*g*, *t*). No direct evidence is found to distinguish vibrational bands of *cis* and *trans* terephthalic unit (T_B, C_B).

Table 1.2. Band assignments for the mid-infrared spectrum of PET. Normal modes are labelled in the following way: stretching (ν), bending (*δ*), wagging (*w*) and rocking (*r*). Blue shades highlight the conformational bands assigned to the *gauche (G)* and *trans (T)* conformers of ethylenic group vibrations. Red shades highlight the stretching mode of the *gauche (g)* and *trans (t)* glycol group vibrations.

Wavenumber (cm^{-1})	***Normal modes***	***Conformer assignment***
1723	*ν* C=O	
1615	*ν* ring C=C	
1577	*ν* ring C-C	
1505	*ν* ring C-C	
1505	*ν* ring C-H	
1471	*δ* CH_2	T
1454	*δ* CH_2	G
1439	*δ* CH_2	G
1409	*δ* (ring C-H in plane)	
1385	*δ* ring C-H	
1368	*w* CH_2	G
1342	*w* CH_2	T
1286	*ν* C-O ester	
1269	*ν* (C=O)-O	
1247	ring-ester in plane mode	
1178	*δ* C-H in plane	
1127	*δ* ring C-H in plane	

1101	ν O-CH$_2$	
1045	ν O-CH$_2$	g
1022	δ ring C-H in plane	
1017	δ ring C-H in plane	
971	ν O-CH$_2$	t
902	r CH$_2$	G
873	ν C-H out of the plane	
848	r CH$_2$	T
795	δ C=O + CCO	
730	δ ring C-C	

1.3.3 Infrared spectroscopy factor analysis for semi-crystalline PET

In the late 1900' a spectroscopic method was developed by Koenig et al.[33], and subsequently improved by Cole et al.[37] , in order to determine the spectra of the pure crystalline and pure amorphous PET. The analysis method was performed by collecting infrared spectra of PET samples with different crystallinity and performing a factorial analysis. It allows to obtain the spectra of pure components and the amount of each component in the analysed samples. Factor analysis results indicated that three principal components were needed to represent the spectral variation caused by crystallinity change. Hence, the three pure component spectra were assigned to three different conformational arrangements of PET according to the ethylenic and terephthalic conformations, called G, TX and TC. In particular:

- G pure spectrum: accounts for PET arrangements with the ethylenic *gauche* conformation (G) and disordered terephthalate conformations (mixture cis-trans);
- TX pure spectrum: the ethylenic bond is in *trans* conformation (*T*) and the terephthalate is in disordered conformation;

- TC pure spectrum: typical of ordered crystalline structures, with ordered sequences of ethylenic, glycolic and coplanar terephthalate units in trans conformation (T,t,T_B).

Figure 1.10 shows the three spectra of G, TX, TC, calculated by Cole et al., in a spectral window between 1800-600 cm^{-1}. A tentative assignation of the pure component spectra to the microstructural domains typical of semi-crystalline PET was made, results are listed in Table 1.3.

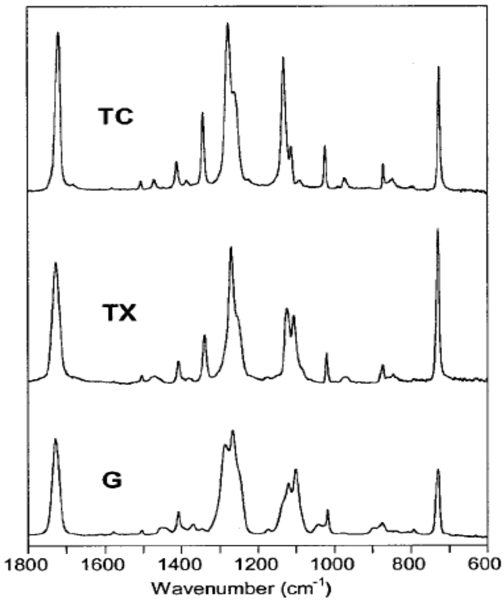

Figure 1.10. G, TX, TC pure components infrared spectra of PET, obtained by factor analysis.

Table 1.3. Assignation of G, TX and TC spectra to the microstructural domains in semi-crystalline PET. The expected conformational arrangements of ethylenic and terephthalic groups in different microstructural domains are listed in the second and third column.

Microstructural domains	***Ethylenic conformation***	***Terephthalate conformation***	***Assignment***
Crystalline	Trans (extended)	Trans (extended)	TC
Crystalline (chain folds)	Gauche	Disordered	G (+ TC?)
Intermediate (constrained)	Trans (extended)	Disordered	TX
Amorphous	Trans (isolated)	Disordered	TX (+ G?)
Amorphous	Gauche	Disordered	G

Although the infrared spectroscopy-factor analysis produced results difficult to interpret concerning the precise assignment of glycolic, ethylenic and terephthalate conformational rearrangements, it was able to study the crystallization behaviour of PET in terms of gauche-trans conformational transition of the ethylenic bond.

1.3.4 State of the art on the study of the physical aging and glass transition of PET by infrared spectroscopy

For explaining the change in thermodynamic properties of glassy PET such as enthalpy and volume towards equilibrium on aging, for the first time Kovacs et al.[38] suggested that some kind of structural rearrangements have to occur in the glass, in order to reach the properties of the liquid equilibrium extrapolated at low temperatures.

Infrared spectroscopy studies[39] analysed the temperature dependence of ethylenic conformers distribution for PET in the glassy and liquid state prior to crystallization. In particular, they followed the trend of the area of two conformational bands in a step-cooling scan from 95 to 45 °C. The analysed bands are centred at 1340 cm^{-1} and 1370 cm^{-1}, assigned to the CH_2 wagging respectively in *gauche* (G) and *trans* (T) conformations. Furthermore, also the ratio 1340/1370, proportional to the conformational ratio *T/G*, was analysed. Figure 1.11 shows the trends of the 1340 cm^{-1} (up left), 1370 cm^{-1} (down left) and their ratio as function of the temperature.

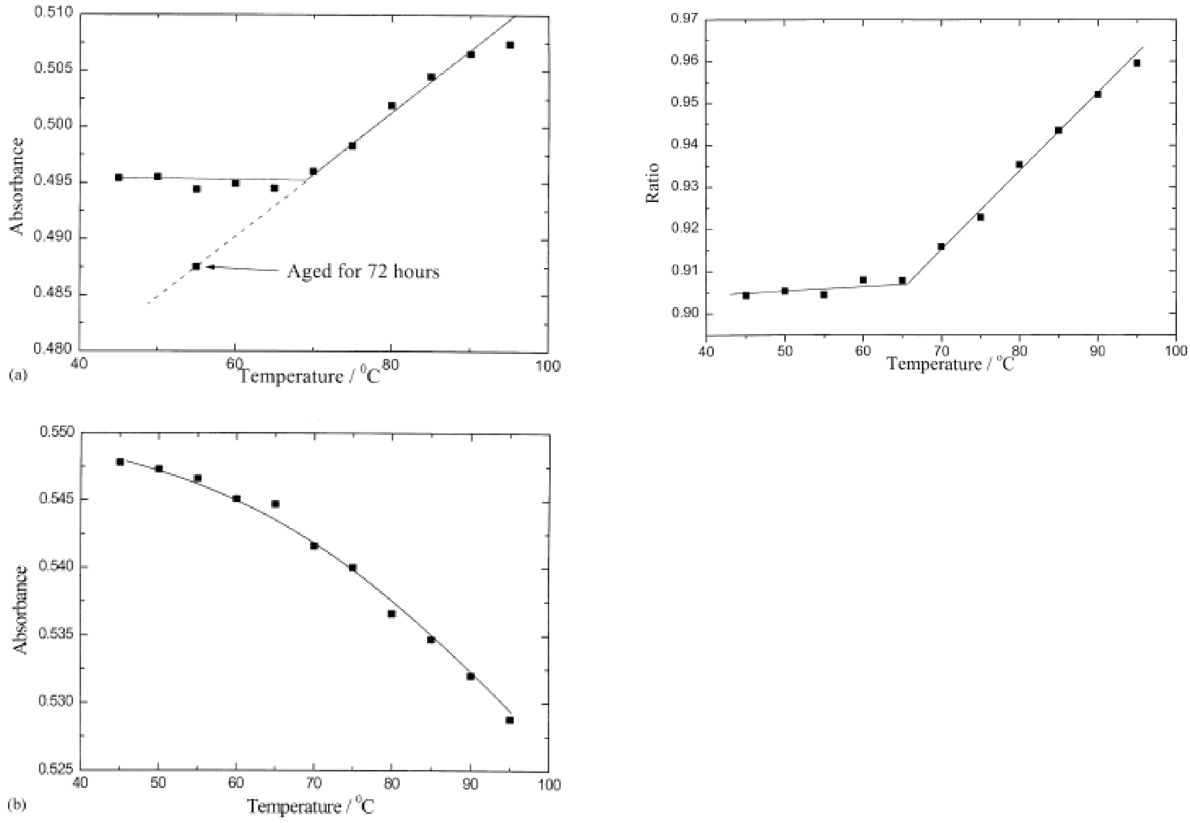

Figure 1.11. Integral absorbance as function of the temperature for PET absorption bands. Up left 1340 cm^{-1}, Down left 1370 cm^{-1}, Up right Ratio 1340/1370.

By analysing the area ratio 1340/1370, the glass transition temperature was taken at the slope abrupt change at about 65 °C, temperature at which the system falls out of the equilibrium. The trend of the area ratio in the liquid region was associated to the conformational *gauche-trans* equilibrium. Moreover, an aging at 55 °C for 72 h was performed, and the area of the 1340 cm^{-1} band (T conformers) was found equal to that extrapolated by the liquid equilibrium. Surprisingly, the physical aging studied by FTIR was addressed to the conformational transition from *trans* ethylenic conformers to *gauche*, even though the *trans* isomer is the lower energy conformer and it allows the chain packing in the crystal structure (Figure 1.9). Hence, it was suggested that *gauche* ethylene conformers allow a better packing of polymer chains in amorphous phase.

Qian studies on the effects of physical aging upon heating by FTIR spectroscopy[40,41] determined quantitively the percentage content of ethylenic *trans* conformer in PET samples aged at different temperatures (T_a = 40, 50, 60 °C) in a subsequent heating scan at 1 °C/min. Firstly, an absorptivity ratio between 1340 and 1370 cm^{-1} bands of 6.6 was calculated from the slope of the linear fit between 1340 and 1370 cm-1 integral absorbances for PET samples with different crystallinity (Figure 1.12).

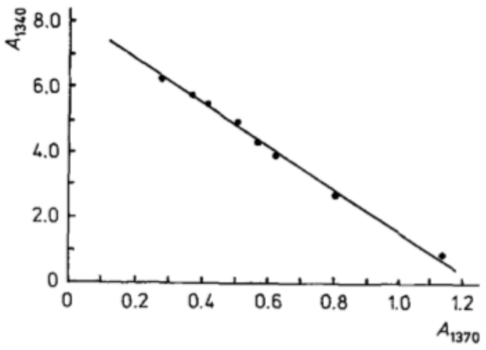

$$T = \frac{A_{1340}}{A_{1340} + 6.6 \times A_{1370}}$$

$$G = \frac{6.6 \times A_{1370}}{A_{1340} + 6.6 \times A_{1370}}$$

Figure 1.12. Plot of integral absorbance of 1340 cm^{-1} band vs. 1370 cm^{-1} band for PET samples with different crystallinities. The absolute value of the angular coefficient (6.6) is used for quantitative determination of *trans* (T) and *gauche* (G) conformers.

The *trans* percentage population (*T*), determined by means of the equation in Figure 1.12, was reported in Figure 1.13 for an ice-water quenched PET (MQ) and three PET samples aged at 40 °C for 192 h (AN40), 50 °C for 96 h (AN50) and 60 °C for 48h (AN60) as function of the temperature. The percentage rate of increase of *trans* population per unit °C was also reported.

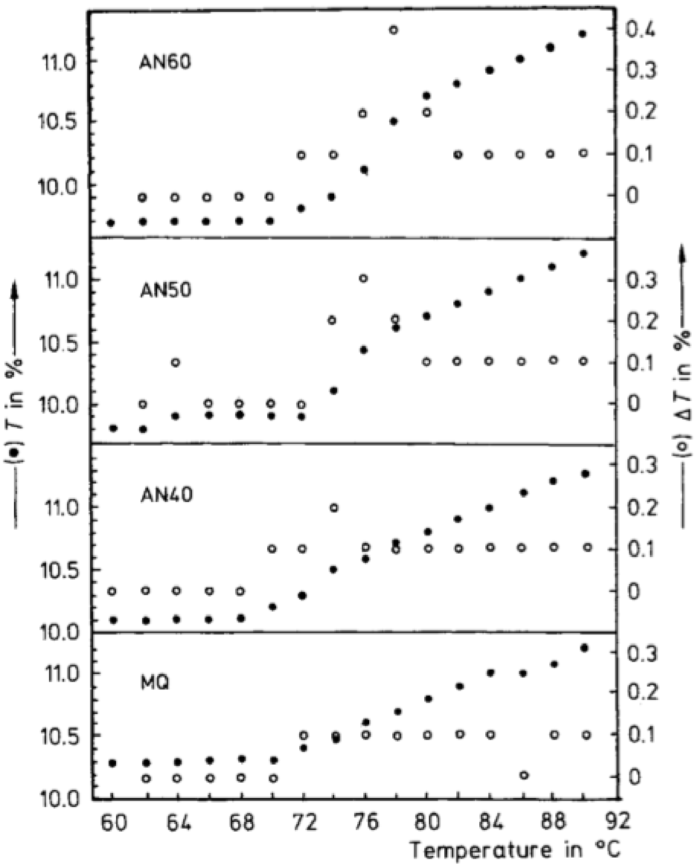

Figure 1.13. Changes of the percentage population (filled circle) and rate of increase (empty circles) of trans conformers as a function of temperature.

In the glassy state, below 70 °C, the *trans* conformer populations remain constant. It is observed for different samples a decrease of *trans* content with increasing the physical aging temperature, in accordance with Hay[39]. In a temperature range between 70 and 80 °C, the glass transition takes place for all samples, with the recovery of the *gauche-trans* equilibrium. In order to regain the equilibrium conformational distribution in the liquid region (80-90 °C), aged samples AN40, AN50 and AN60 shows a sharp transition from *gauche* to *trans* conformers, highlighted by the peak in the rate increase of *trans* conformers at about 75 °C, in correspondence to the glass transition. The ethylenic conformational transition *gauche*→*trans* superimposed to the glass transition was assigned to the “conformational recovery” of the previous aging treatment, which leads to the complete erase of the thermal history of the glass.

1.3.5 The effect of physical aging on cold crystallization of PET studied by DSC, FSC and FTIR

It is generally considered that physical aging is “thermo-reversible”, because the heating to temperatures higher than the glass transition erases the aging that developed in the glassy state. DSC was used to measure the extent of the enthalpic recovery towards equilibrium as a function of the aging time.[42-47] For sake of clarity Figure 1.14 displays the progressive increase in the endothermic peak on the DSC heating curves for samples aged at 60 °C for different times. The relative heat flow in the ordinate was calculated by subtracting the DSC curve of a quenched PET from the aged one.

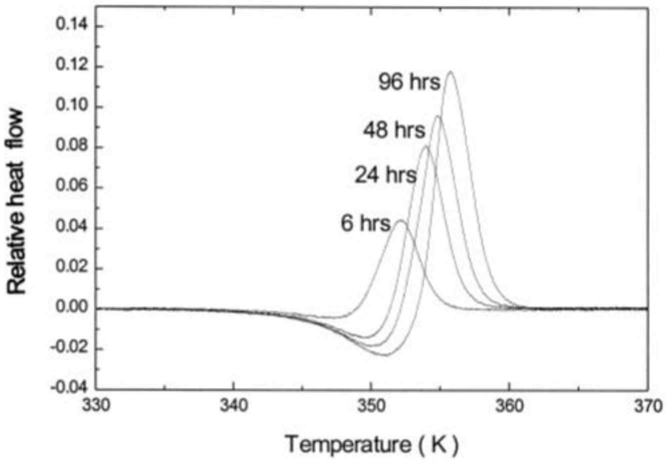

Figure 1.14. Evolution of relative heat flow curves with aging time in the glass transition range as function of the temperature.

The endothermic peak, associated to the enthalpic recovery after the physical aging, increased in size and shifted to higher temperatures by increasing the aging time. The time dependent enthalpy change $\Delta H(t_a)$ during the recovery at the glass transition was calculated by integrating as function of time the relative heat flow curves. Figure 1.15 displays the enthalpy recovery as function of aging time for PET aged at 40, 50, 60 and 70 °C. [42]

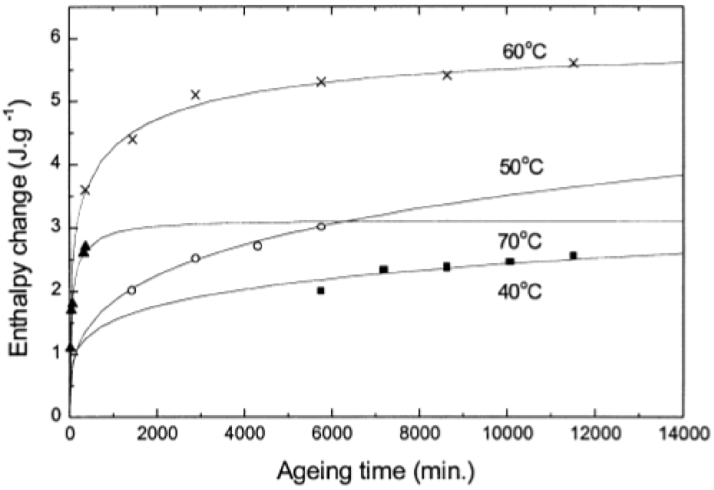

Figure 1.15 Enthalpy recovery as function of time for different aging temperatures. Dots are experimental DSC data, lines are the fitting model.

Table 1.4. Calculated parameters for enthalpy recovery of PET

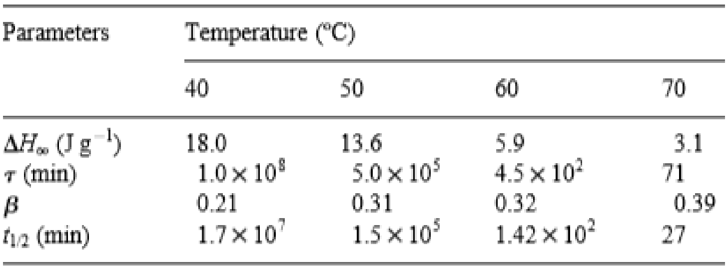

Parameters	Temperature (°C)			
	40	50	60	70
ΔH_∞ (J g^{-1})	18.0	13.6	5.9	3.1
τ (min)	1.0×10^8	5.0×10^5	4.5×10^2	71
β	0.21	0.31	0.32	0.39
$t_{1/2}$ (min)	1.7×10^7	1.5×10^5	1.42×10^2	27

The experimental enthalpy recovery was fitted by Cowie and Ferguson's relationship combined with a Kohlrausch-William-Watts equation, showed in equation 1.3.

$$\Delta H(t_a) = \Delta H_\infty(1 - \exp\left[-\left(\frac{t_a}{\tau}\right)^\beta\right]) \qquad \text{Eq 1.3}$$

Where ΔH_∞ is the enthalpy recovery when glass reach the extrapolated liquid equilibrium, τ is the average relaxation time and β the stretching parameter, reported in Table 1.4. The half-time of the relaxation process, increasing with decreasing aging temperature, appeared to follow an Arrhenius relationship, with an activation energy of 470 ±20 kJ/mol, in accordance with the 370 ± 50 kJ/mol of other result.[47] Similar results were obtained for the activation energy of the glass transition measured by TMDSC, by following the change of the glass transition temperature as function of the modulation frequency.[56,57] A value of 328 kJ/mol was found for a fully amorphous PET, close to the activation energy calculated for the relaxation process in the glassy state, that is related to the cooperative relaxation process characteristic of the glass transition.

DSC and infrared studies on the physical aging of PET[42,43,58] reported that physical aging in the glassy state altered the kinetic parameters of a subsequent isothermal cold crystallization of PET, with an increase of nucleation density and decrease of half conversion times. They explained that the structural rearrangements on aging can induce inter-chain cohesion with a short-range parallel alignment of neighbouring chain segments. It is believed that these dense zones of the material, defined cohesional entanglements[40,41] by Qian were the precursor to nucleation and increased rate of crystallization. For example, it is showed in Figure 1.16 the dynamic cold-crystallization during a DSC heating scan at 10 °C/min for samples aged at 70 °C for different aging times. At about 75 °C, the evolution as function of aging time of the endothermic peak, namely enthalpic recovery, is highlighted. With increasing aging time causes the shift to lower temperatures of the cold-crystallization exothermic peak located at about 135 °C.

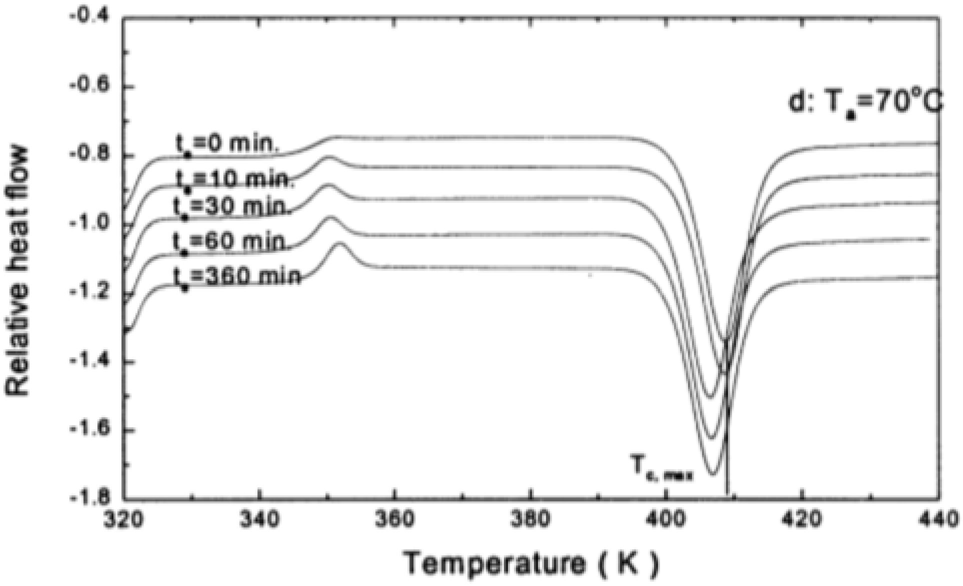

Figure 1.16. DSC curves for PET aged at 70 °C for different times.

Moreover, FSC studies were performed on PET[55] and other polymers[54] to investigate the interplay between the physical aging and the homogeneous nucleation in the glassy state. The Tamman two-stage temperature protocol[55] was used, involving an annealing treatment in the glassy state for different aging times and a growth-stage step for each aging, in order to obtain a detectable heat flow signal from the melting of the crystalline phase developed from homogeneous nuclei that can eventually form in the annealing treatment. It was found a general behaviour of polymer systems, that is, the homogeneous nucleation can occur also in the glassy state few degrees below the glass transition soon after the end of the enthalpy relaxation. This observation, reported in Figure 1.17 for PLLA, and verified also for other polymers,[54] was explained considering the competition between the cooperative rearrangement of the enthalpic recovery and the formation of nuclei of proper dimensions. For a non-equilibrated glass, the large-scale cooperative rearrangements, commonly in the order of 3 nm, due to enthalpy relaxation prevent the growth of stable homogeneous nuclei formed by spontaneous thermal fluctuations. On the other hand, in a glass that has reached the extrapolated liquid equilibrium, the cooperative rearrangements due to enthalpy relaxation cease, and homogeneous nuclei can survive and grow to over-critical size and eventually to small crystals.

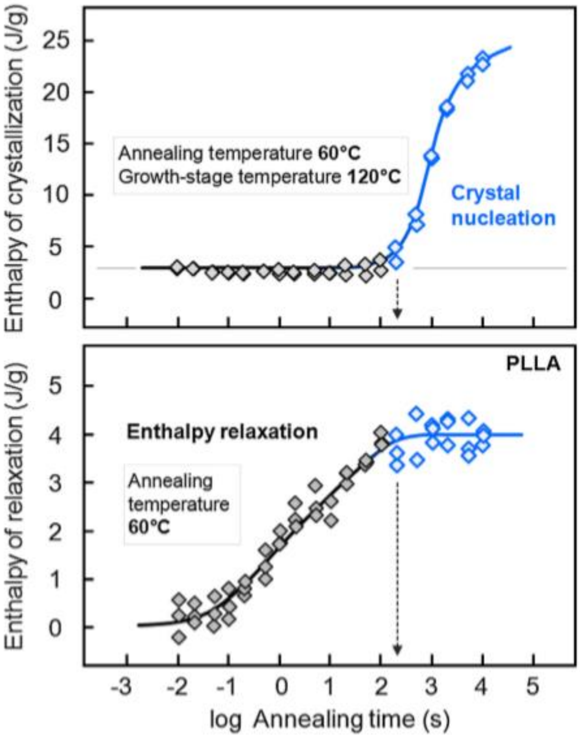

Figure 1.17 Enthalpy recovery of PLLA annealed at 60 °C (T_g = 66 °C at 1000 °C/s heating rate) for different time (bottom panel) and the enthalpy of crystallization calculated after a growth-stage at 120 °C for 70 s (upper panel) as a function of the annealing time.

With variable temperature infrared spectroscopy, Shen[44] followed the temperature dependency of the *trans* ethylenic fraction (*T%*) in a heating scan from 80 to 180 °C at 1 °C/min for PET samples melt-quenched and aged at 65, 75 and 85 °C for 48 h. The results, showed in Figure 1.18, highlighted that the cold-crystallization, seen by the increase of *trans* conformers, shift to lower temperatures by increasing the aging temperature, in accordance with DSC results[42].

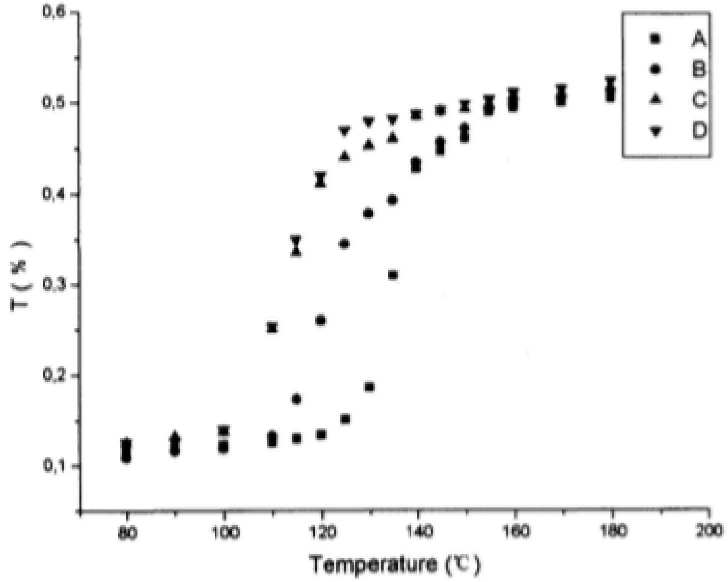

Figure 1.18. Change of the fraction of *trans* conformers as a function of temperature in a heating scan at 1 °C/min for PET (A) melt-quenched, and aged at 65 (B), 75 (C), 85 °C (D) for 48 h.

1.3.6 Evidences of double physical aging mechanisms in polymer glasses

Recently, DSC was utilized to study the kinetics of the enthalpic recovery of narrow molecular weight poly(styrene) and poly(carbonate) at aging temperature significantly below the glass transition[48]. The study showed for lower aging temperatures a non-monotonic trend of the enthalpic recovery consisting in a double-step relaxation with an intermediate plateau. The enthalpy recovered after the overall relaxation corresponds to that extrapolated from liquid equilibrium. For sake of clarity, the results reported by Cangialosi et al.[48] about of the time-dependent enthalpic recovery for a 85 kDa poly(styrene) aged at different temperatures are displayed in Figure 1.19.

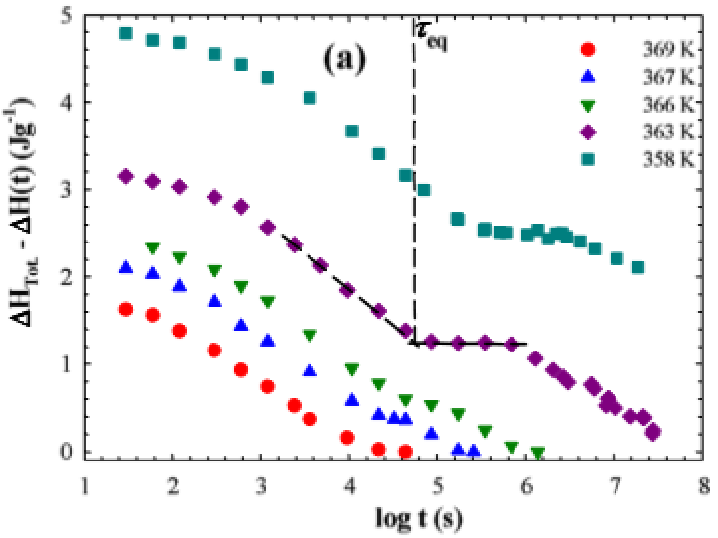

Figure 1.19. Difference between enthalpy recovery at equilibrium and actual enthalpy recovery as function of aging time for PS aged at different temperatures.

The enthalpy recovery evolution for temperature in proximity of the glass transition ($T_{g\ PS}$= 375 K) resembles a Kohlrausch-William-Watts stretched exponential decay that finishes at the extrapolated enthalpy recovery at liquid equilibrium. By lowering the aging temperature, the relaxation becomes slower and at 363 K the trend splits in two relaxation mechanism separated by an intermediate plateau. The two-step enthalpy recovery indicates the presence of two different time scales for glass equilibration. The first relaxation is faster but allows a partial recovery of the enthalpy until a relative minimum in the energy landscape (1° plateau of Figure 1.19). The second relaxation is slower and allows the material to reach the extrapolated liquid equilibrium properties (2° plateau). Figure 1.20 shows an enthalpy, volume vs. temperature graph for the visualization of the two-step decay mechanism.

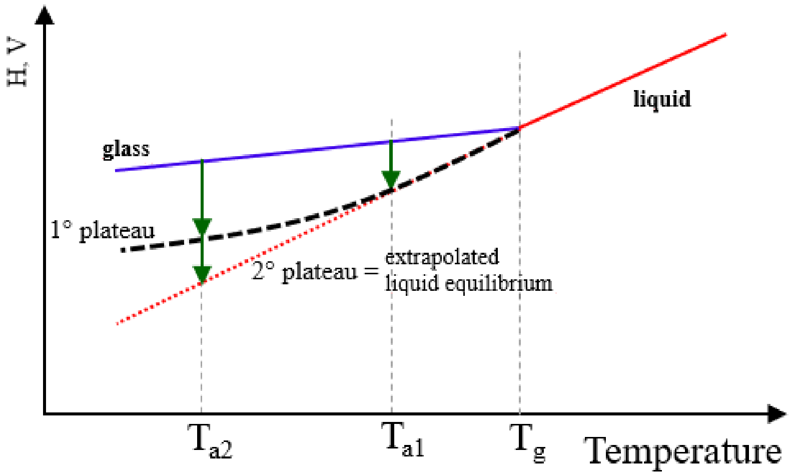

Figure 1.20 Schematic representation of enthalpy and volume as function of the temperature for a liquid-glass system. The glass aged in proximity of the Tg (T_{a1}) evolves directly toward the extrapolate liquid equilibrium (2° plateau) by one-step decay. At lower temperatures (T_{a2}) the glass evolves toward a metastable equilibrium (1° plateau) and subsequently the second decay allow the reach of liquid equilibrium.

Cangialosi et al.[48,50] provided first clear evidences of two different mechanisms of glass relaxation toward equilibrium, involving the existence of an intermediate metastable equilibrium glass. An intuitive explanation was provided for the two-steps decay, by supposing that the first decay was generated by structural rearrangements of short chain segments or lateral groups, meanwhile the second decay involved cooperative large-amplitude rearrangements of the backbone polymer chains.

Even though the two-steps aging mechanism was studied only for a few non-crystalline glass-former polymers, it is believed that the process is a general behaviour of the glassy state of polymers[49], even for crystallizable macromolecules such as PET. However, the study of the double aging mechanism is restrained to the calorimetric investigation of enthalpic recovery until nowadays.

Further investigation on the conformational transitions during the physical aging of PET by Infrared Spectroscopy will be provided in this doctoral thesis, that confirm the existence of a double aging mechanism also for PET.

1.3.7 Conformational ordering process of PET prior to the cold-crystallization

A key problem in the study of the crystallization of materials deals with the formation of crystalline nuclei. Kinetic and thermodynamic studies on crystal nucleation [51] are based on the concept that crystallization can be initiated by localized fluctuations of some order parameter such as density. When these fluctuations are larger than some critical size, nucleation starts. Imai et al. [51,52] reported a series of comprehensive studies focused on the orientation fluctuations and parallel ordering of PET chains occurring in the induction period of the cold-crystallization. In particular, isothermal crystallization kinetics of a PET and deuterated PET samples slight above the glass transition (80 and 110 °C) were followed by Wide and Small Angle X-Ray Scattering (WAXD, SAXS), Small Angle Neutron Scattering (SANS), Depolarized Light Scattering (DLS). Imai's results highlighted an increase of rigid chain segments of PET and a spinodal decomposition by parallel ordering occurring in the induction period prior to the spherulite growing of PET. It was hypothesized that PET annealed above the glass transition undergo a conformational rearrangement of the ethylene groups from the gauche to the trans form, being the most stable chain conformation in crystal. This conformational change increases the length of the rod-like chain segments, that became stiffer and able to order parallelly, in order to form the crystalline nuclei. This suggests that for a polymer able to crystallize the amorphous liquid state is not a stable equilibrium, but unstable, and the parallel ordering of polymer segments occurs due to the increase of the polymer chain rigidity.

Until nowadays Imai's hypothesis on the conformational rearrangements from gauche to trans ethylenic conformers in the induction period remain argument of debate. Huang et al.[53] by combining NMR and DSC results provided an evidence of the trans content increase prior to the crystallization for a PET sample annealed at 100 °C (Figure 1.21). *Trans* fraction resulted to increase with a faster kinetics and in major content respect to the crystallinity, suggesting the existence of the conformational pre-ordering and of a *trans*-rich phase at the edge of lamellar crystals of PET.

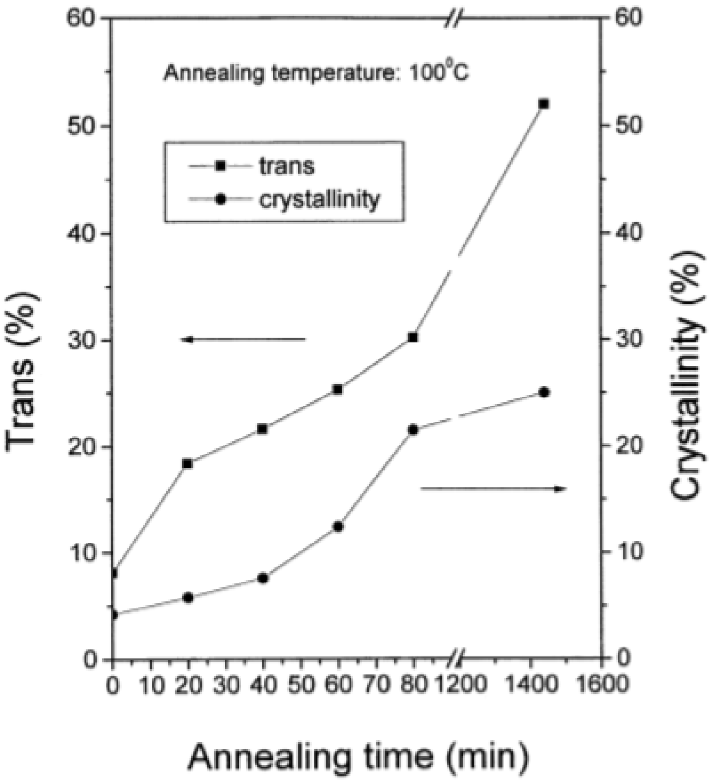

Figure 1.21. Trans content calculated by NMR solid state spectroscopy and crystallinity calculated by DSC of PET as a function of annealing time at 100 °C.

1.4 REFERENCES

(1) Haines, P. J. (2012). Thermal methods of analysis: principles, applications and problems. Springer Science & Business Media.B

(2) Turi, E. (Ed.). (2012). Thermal characterization of polymeric materials. Elsevier.

(3) Wunderlich, B. (2005). Thermal analysis of polymeric materials. Springer Science & Business Media.

(4) Höhne, G. W. H., Hemminger, W., & Flammersheim, H. J. (1996). Theoretical fundamentals of differential scanning calorimeters. In Differential Scanning Calorimetry (pp. 21-40). Springer, Berlin, Heidelberg.

(5) Schick, C. (2009). Differential scanning calorimetry (DSC) of semicrystalline polymers. Analytical and bioanalytical chemistry, 395(6), 1589.

(6) Reading, M., Luget, A., & Wilson, R. (1994). Modulated differential scanning calorimetry. Thermochimica Acta, 238, 295-307.

(7) Wunderlich, B. (1995). The ATHAS database on heat capacities of polymers. Pure and applied chemistry, 67(6), 1019-1026.

(8) Poliakoff, M., & Weitz, E. (1986). Time-Resolved IR Spectroscopy. Advances in organometallic chemistry, 25, 277.

(9) Stuart, B. (2005). Infrared spectroscopy. Kirk-Othmer Encyclopedia of Chemical Technology.

(10) Zbinden, R. (1964). Infrared spectroscopy of high polymers.

(11) Koenig, J. L. (1984). Fourier transform infrared spectroscopy of polymers. In Spectroscopy: NMR, Fluorescence, FT-IR (pp. 87-154). Springer, Berlin, Heidelberg.

(12) Siesler, H. W. (1980). Infrared and Raman spectroscopy of polymers. Practical spectroscopy; v. 4.

(13) Boerio, F. J., & Koenig, J. L. (1971). Raman spectroscopy of polymers. In POLYMER CHARACTERIZATION Interdisciplinary Approaches (pp. 1-13). Springer, Boston, MA.

(14) Zerbi, G., Ciampelli, F., & Zamboni, V. (1964). Classification of crystallinity bands in the infrared spectra of polymers. In Journal of Polymer Science Part C: Polymer Symposia (Vol. 7, No. 1, pp. 141-151). New York: Wiley Subscription Services, Inc., A Wiley Company.

(15) Okazaki, I., & Wunderlich, B. (1997). Reversible melting in polymer crystals detected by temperature-modulated differential scanning calorimetry. Macromolecules, 30(6), 1758-1764.

(16) Okazaki, I., & Wunderlich, B. (1997). Reversible local melting in polymer crystals. Macromolecular rapid communications, 18(4), 313-318.

(17) Gibbs, J. H., & DiMarzio, E. A. (1958). Nature of the glass transition and the glassy state. The Journal of Chemical Physics, 28(3), 373-383.

(18) Turnbull, D., & Cohen, M. H. (1961). Free‐volume model of the amorphous phase: glass transition. The Journal of chemical physics, 34(1), 120-125.

(19) DiMarzio, E. A. (1981). Equilibrium theory of glasses. Annals of the New York Academy of Sciences, 371(1), 1-1.

(20) Edwards, S. F. (1976). Theory of glasses. Polymer, 17(11), 933-937.

(21) Struik, L. C. E. (1977). Physical aging in amorphous polymers and other materials.

(22) Alvarez, F., Alegra, A., & Colmenero, J. (1991). Relationship between the time-domain Kohlrausch-Williams-Watts and frequency-domain Havriliak-Negami relaxation functions. Physical Review B, 44(14), 7306.

(23) Hodge, I. M. (1983). Effects of annealing and prior history on enthalpy relaxation in glassy polymers. 4. Comparison of five polymers. Macromolecules, 16(6), 898-902.

(24) Fulcher, G. S. (1925). Analysis of recent measurements of the viscosity of glasses. Journal of the American Ceramic Society, 8(6), 339-355.

(25) Rault, J. (2003). Ageing of glass: role of the Vogel–Fulcher–Tamman law. Journal of Physics: Condensed Matter, 15(11), S1193.

(26) Angell, C. A., Ngai, K. L., McKenna, G. B., McMillan, P. F., & Martin, S. W. (2000). Relaxation in glassforming liquids and amorphous solids. Journal of Applied Physics, 88(6), 3113-3157.

(27) Lepoittevin, B., & Roger, P. (2011). Poly (ethylene terephthalate). Handbook of Engineering and Speciality Thermoplastics, 3, 97-126.

(28) Wypych, G. (2016). Handbook of polymers. Elsevier.

(29) Cunningham, A., Ward, I. M., Willis, H. A., & Zichy, V. (1974). An infra-red spectroscopic study of molecular orientation and conformational changes in poly (ethylene terephthalate). Polymer, 15(11), 749-756.

(30) Štokr, J., Schneider, B., Doskočilová, D., Lövy, J., & Sedláček, P. (1982). Conformational structure of poly (ethylene terephthalate). Infra-red, Raman and nmr spectra. Polymer, 23(5), 714-721.

(31) Boyd, S. U., & Boyd, R. H. (2001). Chain dynamics and relaxation in amorphous poly (ethylene terephthalate): A molecular dynamics simulation study. Macromolecules, 34(20), 7219-7229.

(32) Hedenqvist, M. S., Bharadwaj, R., & Boyd, R. H. (1998). Molecular dynamics simulation of amorphous poly (ethylene terephthalate). Macromolecules, 31(5), 1556-1564.

(33) Lin, S. B., & Koenig, J. L. (1982). Spectroscopic characterization of the rotational conformations in the disordered phase of poly (ethylene terephthalate). Journal of Polymer Science: Polymer Physics Edition, 20(12), 2277-2295.

(34) Daubeny, R. D. P., Bunn, C. W., & Brown, C. J. (1954). The crystal structure of polyethylene terephthalate. Proc. R. Soc. Lond. A, 226(1167), 531-542.

(35) Fakirov, S., Fischer, E. W., & Schmidt, G. F. (1975). Unit cell dimensions of poly (ethylene terephthalate). Die Makromolekulare Chemie: Macromolecular Chemistry and Physics, 176(8), 2459-2465.

(36) Djebara, M., Stoquert, J. P., Abdesselam, M., Muller, D., & Chami, A. C. (2012). FTIR analysis of polyethylene terephthalate irradiated by MeV He+. Nuclear Instruments and Methods in Physics Research Section B: Beam Interactions with Materials and Atoms, 274, 70-77.D'esposito, L., & Koenig, J. L. (1976). Application of Fourier transform infrared spectroscopy to the study of semicrystalline polymers: poly (ethylene terephthalate). Journal of Polymer Science: Polymer Physics Edition, 14(10), 1731-1741.

(37) Cole, K. C., Ajji, A., & Pellerin, E. (2002). New insights into the development of ordered structure in poly (ethylene terephthalate). 1. Results from external reflection infrared spectroscopy. Macromolecules, 35(3), 770-784.

(38) Kovacs, A. J. (1963). Glass transition in amorphous polymers: a phenomenological study. Adv. Polym. Sci, 3(3), 394-507.

(39) Atkinson, J. R., Biddlestone, F., & Hay, J. N. (2000). An investigation of glass formation and physical ageing in poly (ethylene terephthalate) by FT-IR spectroscopy. Polymer, 41(18), 6965-6968.

(40) Qian, R., Shen, D., Sun, F., & Wu, L. (1996). The effects of physical ageing on conformational changes of poly (ethylene terephthalate) in the glass transition region. Macromolecular Chemistry and Physics, 197(4), 1485-1493.

(41) Wang, Y., Shen, D., & Qian, R. (1998). Subglass-transition-temperature annealing of poly (ethylene terephthalate) studied by FTIR. Journal of Polymer Science Part B: Polymer Physics, 36(5), 783-788.

(42) Lu, X., & Hay, J. N. (2000). The effect of physical aging on the rates of cold crystallization of poly (ethylene terephthalate). Polymer, 41(20), 7427-7436.

(43) McGonigle, E. A., Daly, J. H., Gallagher, S., Jenkins, S. D., Liggat, J. J., Olsson, I., & Pethrick, R. A. (1999). Physical ageing in poly (ethylene terephthalate)—its influence on cold crystallisation. Polymer, 40(17), 4977-4982.

(44) Zhang, W., & Shen, D. (1998). The effects of thermal histories on crystallization of poly (ethylene terephthalate). Polymer journal, 30(4), 311.

(45) Zhao, J., Yang, J., Song, R., Linghu, X., & Fan, Q. (2002). The effect of annealing on the subsequent cold crystallization of amorphous poly (ethylene terephthalate). European polymer journal, 38(4), 645-648.

(46) Aref-Azar, A., Biddlestone, F., Hay, J. N., & Haward, R. N. (1983). The effect of physical ageing on the properties of poly (ethylene terephthalate). Polymer, 24(10), 1245-1251.

(47) Aref-Azar, A., Arnoux, F., Biddlestone, F., & Hay, J. N. (1996). Physical ageing in amorphous and crystalline polymers. Part 2. Polyethylene terephthalate. Thermochimica Acta, 273, 217-229.

(48) Cangialosi, D., Boucher, V. M., Alegría, A., & Colmenero, J. (2013). Direct evidence of two equilibration mechanisms in glassy polymers. Physical review letters, 111(9), 095701.

(49) Cangialosi, D. (2018). Glass Transition and Physical Aging of Confined Polymers Investigated by Calorimetric Techniques. Handbook of Thermal Analysis and Calorimetry, 6, 301-337.

(50) Perez-De Eulate, N. G., & Cangialosi, D. (2018). The very long-term physical aging of glassy polymers. Physical Chemistry Chemical Physics, 20(18), 12356-12361.

(51) Imai, M., Mori, K., Mizukami, T., Kaji, K., & Kanaya, T. (1992). Structural formation of poly (ethylene terephthalate) during the induction period of crystallization: 1. Ordered structure appearing before crystal nucleation. Polymer, 33(21), 4451-4456.

(52) Imai, M., Kaji, K., Kanaya, T., & Sakai, Y. (1995). Ordering process in the induction period of crystallization of poly (ethylene terephthalate). Physical Review B, 52(17), 12696.

(53) Huang, J. M., Chu, P. P., & Chang, F. C. (2000). Conformational changes and molecular motion of poly (ethylene terephthalate) annealed above glass transition temperature. Polymer, 41(5), 1741-1748.

(54) Androsch, R., Zhuravlev, E., Schmelzer, J. W., & Schick, C. (2018). Relaxation and crystal nucleation in polymer glasses. European Polymer Journal, 102, 195-208.

(55) Androsch, R., Schick, C., & Rhoades, A. M. (2015). Application of Tammann's two-stage crystal nuclei development method for analysis of the thermal stability of homogeneous crystal nuclei of poly (ethylene terephthalate). Macromolecules, 48(22), 8082-8089.

(56) Okazaki, I., & Wunderlich, B. (1996). Modulated differential scanning calorimetry in the glass transition region. V. Activation energies and relaxation times of poly (ethylene terephthalate) s. Journal of Polymer Science Part B: Polymer Physics, 34(17), 2941-2952.

(57) Wunderlich, B., & Okazaki, I. (1997). Modulated differential scanning calorimetry in the glass transition region: VI. Model calculations based on poly (ethylene terephthalate). Journal of Thermal Analysis and Calorimetry, 49(1), 57-70.

(58) Shieh, Y. T., Lin, Y. S., Twu, Y. K., Tsai, H. B., & Lin, R. H. (2010). Effect of crystallinity on enthalpy recovery peaks and cold-crystallization peaks in PET via TMDSC and DMA studies. Journal of applied polymer science, 116(3), 1334-1341.

2. EXPERIMENTAL PART

In the following section the technical aspects of thermal analysis techniques employed to characterize polymeric materials were described. Firstly, we will focus on the apparatus used for the Fourier Transform Infrared spectroscopy (FTIR) analysis, the different imposed temperature programs and the elaboration of the spectral signal, with particular attention to the mathematical elaboration of the Modulated Temperature FTIR (MTFTIR). Following up, the technical aspect of the calorimetric analysis, performed by means of the conventional Differential Scanning Calorimetry, and by the Fast Scanning Calorimetry, were exploited. Moreover, the signal elaboration performed on calorimetric experiments were described.

2.1 FOURIER TRANSFORM INFRARED SPECTROSCOPY (FTIR)

For Fourier Transform Infrared spectroscopy measurements, the following instruments were used:

- FTIR spectrometer: Nicolet 6700 FT-IR spectrometer;
- Sample cell holder: SPECAC variable temperature measuring cell;
- Thermo-programmer: Ascon Y series temperature controller model YL-POROO-2 with operating range -200/300 °C;
- Temperature measurement: CENTER 301 Type K thermocouple reader;
- K-factor voltage stabilizer model MCU-8.

The experimental apparatus used for FTIR analysis consists in the FTIR spectrometer interfaced by a computer for the acquisition of spectra, a thermo-programmer for temperature control and a thermocouple also connected to the computer for the sample temperature acquisition. In order to have reliable data, the spectrometer and the thermo-programmer are connected to a current stabilizer and located in a dedicated room, equipped with an air conditioner. This was necessary to minimize oscillations in the signal due to potential changes in the power network and changes in the temperature of the environment.

The apparatus is suitable for measurements in variable temperature and time-resolved FTIR in transmission mode, using samples supported on a KBr windows of 13 mm diameter, a transparent material in the infrared spectral range used (4000-400 cm^{-1}).

The supported sample is inserted into the SPECAC variable temperature cell holder. The device is equipped with two thermocouples, one internal and one external. The internal thermocouple has the function to regulate the power delivered by the thermo-programmer to the heating resistance inside the cell. The sample temperature is acquired by the external thermocouple, that is interfaced to the computer for temperature acquisition and it is placed in contact with the KBr window. After positioning the sample, the cell holder is fixed inside the FTIR spectrometer. The apparatus was used to perform different type of experiments depending on the temperature program imposed to the sample, both in isothermal and in variable temperature. In fact, the great stability of the spectral signals over time allowed to follow in an accurate and precise way the spectroscopic evolution of samples during isothermal treatments up to 400 h.

2.1.1 Time-resolved FTIR spectroscopy

Time-resolved FTIR experiments consist in performing sequential acquisition of the infrared spectra during an isothermal treatment of the sample. The overall quality of the vibrational spectrum depends on the signal-to-noise ratio (S/N) and the signal saturation. The optimization of the spectral signal was performed by choosing the correct thickness of the sample in order to not exceed the unitary Absorbance, and by varying the spectral resolution and the cumulative spectra parameter to maximise the signal-to-noise ratio.

2.1.2 Modulated Temperature FTIR spectroscopy

For MTFTIR measurements, the sample was subjected to a modulated heating or cooling program, composed by a linear heating or cooling ramp, defined as the mean temperature of the experiment as function of time (T^M) with superimposed a periodic oscillation of the temperature, characterized generally by a temperature amplitude (A_T) and a period (p) . The infrared spectra are acquired sequentially during the modulated ramp. A schematic temperature program and its parameters are showed in Figure 2.1

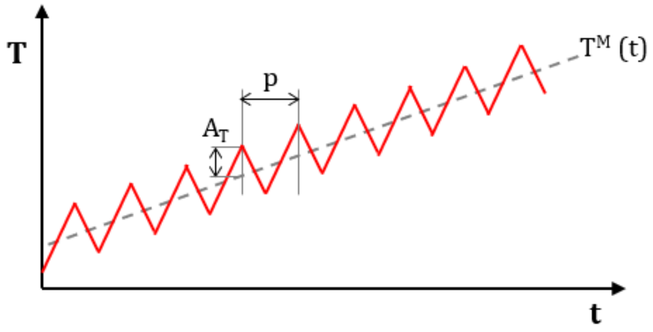

Figure 2.1. Temperature program of a Modulated Temperature FTIR analysis. T^M is the mean temperature, A_T the modulated amplitude and p the period of oscillation.

2.1.3 Quasi-isothermal FTIR

The Quasi-isothermal FTIR measurements is a variation of the MTFTIR. This time the temperature program consists by oscillating the temperature with amplitude A_T and period p around a constant mean temperature for an equilibration time (t_{eq}). Hence, the oscillating program was repeated step by step for other mean temperatures. Figure 2.2 shows an illustrative quasi-isothermal program. In general, the equilibration time is chosen adequately to allow the material to reach the stationary condition.

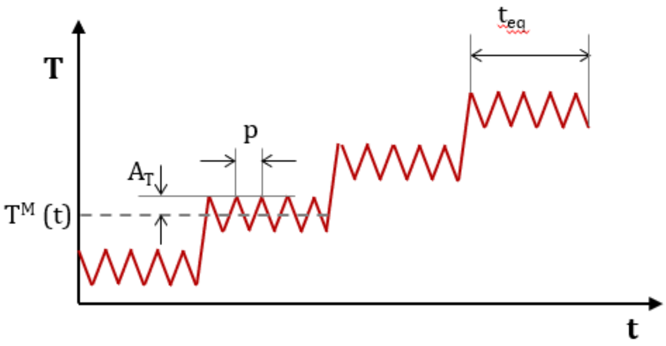

Figure 2.2. Temperature program of a Quasi-isothermal FTIR analysis

2.1.4 Temperature Calibration

For the calibration of the temperature two low molecular weight compounds were used that possess a melting temperature included in the thermal range investigated in the experiments performed on polymer materials. It was decided to use benzoic acid (T_f = 122 ° C) and biphenyl (Tf = 72 ° C). The two compounds were subjected prior of every set of MTFTIR and Quasi-isothermal experiments to a temperature program with the same experimental conditions to those used for the sample. Two kinds of thermal lags were calculated for the modulated experiments, the first consisting in the deviation of the experimental melting temperature from the actual melting temperature, the second regarding the phase lag between the spectral signal oscillation and the temperature oscillation. These experiments did not show any thermal lag between the thermocouple and the samples, both in MTFTIR and Quasi-isothermal experiments.

2.1.5 Infrared spectra signals acquisition

The study of the spectroscopic behavior of samples was carried out by the measure of the spectral characteristics of selected infrared bands. For each spectrum, the intensity or the area of absorption bands were acquired, giving a suitable baseline. The latter consist of a linear function passing through two minimum points of the spectrum, and it must be insensitive to the spectral variations due to changes in temperature or sample transitions.

In the case of resolved bands in the infrared spectrum, the calculation of the area was preferred, being more sensible to sample transformations. Meanwhile, for overlapped bands the measure of the height was chosen. For each band the area or intensity was baseline corrected. Moreover, the algorithm for acquiring the intensity and area for absorption bands was repeated for all the spectra composing a time-resolved FTIR or MTFTIR analysis. Finally, the spectral characteristics acquired for the vibrational bands was associated with the time and temperature of each spectrum.

2.1.6 Data elaboration for the Modulated Temperature FTIR analysis and Quasi-isothermal FTIR

The potentiality of the Modulated Temperature thermal analysis, as introduced in 1993 by the invention of the Modulated Temperature DSC[1], consist in the separation of the thermal response of a sample into the thermally reversing and the non-reversing components of the sample signal. For calorimetric measurements, this improvement of the conventional DSC technique allowed to separate the thermal transitions of materials occurring in thermodynamic equilibrium (reversing component) independently on the experimental time, from those that occur kinetically, hence out-of-equilibrium (non-reversing component). As such as the MTDSC technique, also the MTFTIR technique utilizes a temperature program comprises a linear temperature ramp with superimposed an oscillating function:

$$T(t) = T^M(t) + \tilde{T}(t) \qquad \text{Eq. 2.1}$$

where T is the actual temperature, T^M is the mean temperature and $\tilde{T}$ is the oscillating temperature.

During the temperature program, time resolved sample spectra are acquired sequentially. Similarly to the temperature program, the integrated intensity response $I_{\bar{\nu}}(t)$ for a generic spectral band absorbing at wavenumber $\bar{\nu}$ as a function of time can be described as a sum between a mean component and a periodic function with the same frequency of the temperature oscillation:

$$I_{\bar{\nu}}(t) = I^M{}_{\bar{\nu}}(t) + \tilde{I}_{\bar{\nu}}(t) \qquad \text{Eq. 2.2}$$

Where $I_{\bar{\nu}}$ is the actual signal, $I^M{}_{\bar{\nu}}$ is the mean signal and $\tilde{I}_{\bar{\nu}}$ is the oscillating signal.

Mean temperature T^M and mean intensity $I^M{}_{\bar{\nu}}$ were calculated by a moving average algorithm. This consists in averaging $T(t)$ and $I_{\bar{\nu}}(t)$ over a limited data box that corresponds to one period of oscillation and assigning the mean value to the average time of the period. This process is looped into the whole data interval shifting the data box. Moreover, oscillating functions for temperature $\tilde{T}(t)$ and intensities $\tilde{I}_{\bar{\nu}}(t)$ as a function of time were calculated by subtracting mean values from the actual ones, simply rearranging Equations 2.1 and 2.2. The mean intensity as a function of mean temperature $I^M{}_{\bar{\nu}}(T^M)$ was defined as the total intensity $I^{Tot}{}_{\bar{\nu}}$.

Additionally, it can be expressed as the sum of two terms, the reversing intensity $I^R{}_{\bar{\nu}}$ and the non-reversing intensity $I^{NR}{}_{\bar{\nu}}$ (Equation 2.3)

$$I^{Tot}{}_{\bar{\nu}}(T^M) = I^R{}_{\bar{\nu}}(T^M) + I^{NR}{}_{\bar{\nu}}(T^M) \qquad \text{Eq 2.3}$$

The calculation of the reversing intensity started from oscillating temperature and intensity and was performed by a three steps procedure:

1. Calculation of the frequency dependent complex intensity $I^*{}_{\bar{\nu}}(\omega)$ and the complex temperature $T^*(\omega)$ by means of Sliding Fast Fourier Transformation (Equations 2.4-2.5). As seen for the moving average, the FFT algorithm is performed on a limited interval of data

comprising a period of oscillation and is repeated shifting the data box into the whole data interval, in order to obtain a temperature profile for both complex values.

$$I^*_{\bar{\nu}}(\omega) = I'_{\bar{\nu}} + iI''_{\bar{\nu}} = \int_{t_0}^{t_0+p} \tilde{I}(t)e^{-i\omega t}dt \qquad \text{Eq 2.4}$$

$$T^*(\omega) = T' + iT'' = \int_{t_0}^{t_0+p} \tilde{T}(t)e^{-i\omega t}dt \qquad \text{Eq 2.5}$$

Where
$I^*_{\bar{\nu}}$, $I'_{\bar{\nu}}$ and $I''_{\bar{\nu}}$ are the complex, the in-phase and the out-of-phase intensity
T^*, T', T'' are the complex, the in-phase and the out-of-phase temperature
ω is the angular frequency
t_0 is the start time for the Fourier Transformation
p is the period of the oscillation.

For the present research, only the complex values relative to the base frequency $\omega_0 = \frac{2\pi}{p}$ are considered.

2. Calculation of the temperature dependent phase lag $\varphi(T^M)$ between complex intensity and complex temperature (Equation 2.6):

$$\varphi(T^M) = \tan^{-1}\frac{I''_{\bar{\nu}}}{I'_{\bar{\nu}}} - \tan^{-1}\frac{T''}{T'} \qquad \text{Eq 2.6}$$

3. Integration in the whole temperature range of the ratio between the in-phase intensity $I'_{\bar{\nu}} = |I^*_{\bar{\nu}}|\cos\varphi$ and the complex temperature modulus $|T^*|$ (Equation 2.7):

$$I^R_{\bar{\nu}}(T^M) = \int_{T_0}^{T} \frac{|I^*_{\bar{\nu}}|\cos\varphi}{|T^*|} dT^M \qquad \text{Eq. 2.7}$$

The initial value of the reversing intensity $I^R_{\bar{\nu}}(T^M = T_0)$ is chosen arbitrarily.
It is important to remark that for an MTFTIR experiment the in-phase component of the complex intensity $I'_{\bar{\nu}}$ can assume both positive and negative values, depending on the absorption band behavior as function of temperature.

Finally, the non-reversing intensity $I^{NR}_{\bar{\nu}}$ as a function of the mean temperature was calculated by subtracting $I^R_{\bar{\nu}}$ from $I^{Tot}_{\bar{\nu}}$, simply rearranging the equation 2.3.

Concerning the quasi-isothermal FTIR measurements, the temperature program is slightly different to that used for MTFTIR. In this case, the temperature is oscillated with amplitude A_T and period p around a constant mean temperature for an equilibration time. Then, after the completion of the step, the mean temperature is changed, and the oscillating temperature program repeated. Analogously to the MTFTIR elaboration discussed above, the Fourier algorithm is applied, and the frequency dependent complex intensity $I^*_{\overline{\nu}}(\omega)$, the complex temperature $T^*(\omega)$ and the phase lag φ was calculated by means of Sliding Fast Fourier Transformation (Equations 2.4/2.6) for each temperature step. Differently from MTFTIR measurements, in which the reversing intensity $I^R_{\overline{\nu}}$ was calculated, as well as the total $I^{Tot}_{\overline{\nu}}$ and non-reversing intensity $I^{NR}_{\overline{\nu}}$ in quasi-isothermal protocol (QIFTIR) only the first derivative of the reversing intensity was calculated by the relationship of Equation 2.8:

$$\frac{dI^R_{\overline{\nu}}}{dT}(t,T^M) = \frac{|I^*_{\overline{\nu}}|\cos\varphi}{|T^*|} \qquad \text{Eq 2.8}$$

Commonly, during an acquisition step at the same mean temperature $\frac{dI^R_{\overline{\nu}}}{dT}$ may vary over time, because of non-stationary condition caused by material reorganization, relaxations, or heat transfer. If the system reaches the stationary condition after a certain time, the $\frac{dI^R_{\overline{\nu}}}{dT}$ remain constant over time. In this case, the first derivative of the reversible intensity $\left(\frac{dI^R_{\overline{\nu}}}{dT}\right)^\infty$ can be calculated by QIFTIR experiments. It is worth to notice that a distinction of the "reversing" term from "reversible" is made, by considering "reversing" the intensity signal that follows the temperature modulation calculated in non-stationary condition, and using "reversible" only when the system is proved to be in stationary condition (Table 2.1).

Table 2.1 Symbolism and terminology used to indicate the first derivative of intensity that follows the temperature modulation.

Symbol	***Stationary condition***	***Terminology***
$\frac{dI^R_{\overline{\nu}}}{dT}(t,T^M)$	No (change over time)	Reversing
$\left(\frac{dI^R_{\overline{\nu}}}{dT}\right)^\infty (T^M)$	Yes	Reversible

2.1.7 Determination of the fictive temperature for time-resolved FTIR

The fictive temperature (T_f) is a measure of the thermodynamic state of a glass and is defined as the intersection of the extrapolated glass line and the extrapolated equilibrium liquid line in an enthalpy vs. temperature plot. For time-resolved FTIR measurements, the calculation of the fictive temperature was performed on the intensity variation of selected absorption bands, by utilizing a variation of the conventional Moynihan method.[2] To determine the evolution of the fictive temperature T_f (t) as a function of time during an isothermal aging process an additional MTFTIR measurement in heating scan at the end of the experiment is necessary in order to extrapolate the equilibrium liquid line and the glass line for the sample, otherwise not accessible from isothermal measurements. From the MTFTIR data elaboration the total intensity and the reversible component of the selected band was calculated. This component is translated to coincide with the total absorbance data above the Tg, to define the liquid equilibrium line (red line in Figure 4.4), and the glass isostructural line, hence not due to the modification of the sample structure below the Tg (yellow line in Figure 4.4).

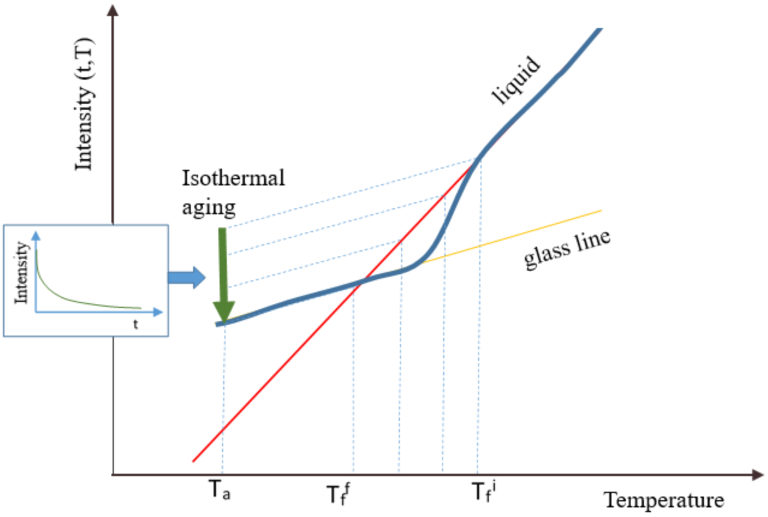

Figure 2.3: Example diagram for the determination of the fictive temperature (Tf) during an isothermal annealing process.

The T*f* is determined as a projection of the data of *I(t)* (green arrow) on the equilibrium line as a function of the temperature along parallel lines to that of glass (isostructural) through the equation 2.9:

$$T_f(t) = \frac{I(t) - m_g T_a - q_l}{m_l - m_g} \qquad \text{Eq 2.9}$$

where:

I(t) is the band intensity or area as a function of the time;

m_g is the slope of the glass line;

m_l is the slope of the equilibrium liquid line;

q_l is the intercept of the liquid line;

T_a is the annealing temperature.

The terms m_g, m_l and q_l of Equation 2.8 are derived from the lines in Figure 2.3.

The advantage of this procedure is the possibility to determine the trend of the T_f as a function of the annealing time (relaxation profile) using a single time-resolved FTIR analysis combined with a subsequent heating scan. As showed in the following pages, the procedure for determining the T_f by DSC analysis requires different heating scans for each annealing time.

2.2 DIFFERENTIAL SCANNING CALORIMETRY

The Differential Scanning Calorimetry (DSC) is a conventional thermal analysis based on the measure of the heat exchange between a sample and the external system. Generally, two kind of DSC are in commerce, the power compensating DSC and the heat flux calorimeter. The research focuses on the experiment of the second kind of calorimeter, composed schematically by a temperature-controlled furnace, that constitutes the closed system, and two temperature monitored slots within. In these slots the sample and the reference are placed. The heat flux from the sample to the external environment or vice versa is calculated by the departure of the measured temperatures between the sample slot and the reference slot when the system is heated or cooled. Generally, the sample absorbs heat because of the intrinsic heat capacity of the substance of which is composed, causing a thermal lag respect to the reference. Additionally, endothermic and exothermic transitions cause further heat flux, caught by means of additional thermal lag. In the present research, two different heat flux calorimeters were used, a standard DSC and the more recent Fast Scan Calorimetry.

2.2.1 Standard DSC and Quasi-isothermal DSC

For standard DSC measurements the Mettler Toledo DSC 822e heat flux calorimeter was employed, equipped with a ceramic sensor FRS 5 and a liquid nitrogen cooler. A flux of dry nitrogen gas with flow rate of 30 ml/min was utilized to purge the furnace. Standard samples are generally prepared by placing 2-5 mg of polymer into sealed aluminum pans with 40 μl volume capacity. In the reference slot is generally placed an empty pan. Calibrations for the temperature, the heat flow and the tau lag were performed using indium and zinc.

A standard measurement consists in heat the sample at a constant rate, generally 10 °C/min, and recording the heat flux of the sample. In the thesis, also a Quasi-isothermal measurement was employed, in order to obtain thermodynamic information on the reversibility of the thermal transitions occurring in the sample. In this case, a temperature program similar to that of the Quasi-isothermal FTIR was performed, hence by oscillating the temperature around a constant mean temperature for a certain time, and proceeding with the variable temperature analysis by varying mean temperature step-by-step. With this method, all the kinetic contribution to the heat flux were suppressed, and the reversible component of the heat flux can be measured. Specifically, considering the previous discussion in Paragraph 1.1.3 on Modulated DSC techniques, the reversing specific heat c_p^{rev} was calculated by means of equation 2.9.

$$c_p^{rev}(T^M) = \frac{A_{HF}}{m \cdot A_{HR}} \qquad \text{Eq 2.10}$$

where A_{HF} is the amplitude of the oscillating heat flow, m is the mass of the sample and A_{HR} is the amplitude of the oscillating heating/cooling rate.

2.2.2 Fast Scanning Calorimetry (FSC)

Typically, the heating/cooling rates of standard DSC are around 10 °C/min, but heating rates up to 600 °C/min can be reached by fine calibration of thermal lag. Nevertheless, the standard calorimetry was not able to detect kinetic and thermodynamic transitions that occur in a shorter time-scale. Typical examples of rapid kinetics phenomena are the formation, rearrangements and relaxation of highly metastable mesomorphic phases and glassy phases. Another issue concerning the low achievable cooling rate is the ability to obtain amorphous glasses by melt-quenching a crystallizable polymer with fast kinetics of crystallization, for example PET and the most part of polyolefins, hence, with.

Recently, in order to increase the maximum achievable heating/cooling rates, new experimental techniques based on fast scanning calorimetry (FSC) have been developed. [3] These techniques are based on the same principles of heat flux standard calorimeters. Generally, the two slots inside the furnace for sample and reference are replaced by a silicon membrane-based chip, formed by two identical active zones, or furnaces, as showed in Figure 2.4. The sample is placed directly on one of the two active zones of the chip that possess integrated thermocouples for detection of the temperature. Fast heating is assured by means of an integrated resistance, meanwhile the higher cooling rate is achieved by the ballistic cooling of the thin chip respect to the external environment, generally

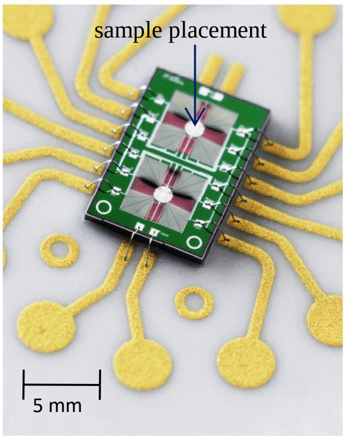

Figure 2.4. Chip sensor of METTLER TOLEDO Flash DSC. The crossed squares are the two furnaces for the sample and the reference. Active zones are placed in the middle of the cross, with 400 μm^2 surface area.

For FSC measurements, the METTLER TOLEDO ’Flash DSC 1’ was employed, equipped with a Huber TC100 intra-cooler. The device uses a chip sensor based on MEMS processes, showed in Figure 2.4.[3,4] The operative temperature range of Flash DSC 1 ranges from -95 to 450 °C and scan rates has an operative widow within 6 to 12000 °C/min on cooling and from 30 to 24000 °C/min on heating.[4] A flux of dry nitrogen gas with flow rate of 20 ml/min was utilized to purge the furnace, in order to avoid water condensation.

The sample preparation involves the placement of a tiny piece of the polymeric substance, generally ranging from 50 to 500 ng, on the top of the chip active area by means of an optical microscope and a single hair brush. Though, the sample weighting is not possible even employing the most accurate balances available. Hence, thermal properties like the melting enthalpy and heat capacity step at the glass transition are used to estimate the sample mass.[4] In the present research, the sample mass was calculated from the heat flow step *ΔHF* at the glass transition temperature by means of equation 2.10:

$$m = \frac{\Delta HF}{\beta \Delta c_p} \qquad \text{Eq 2.10}$$

where m is the mass of the sample, ΔHF the heat flow step at the glass transition temperature, β is the heating rate and Δc_p is the theorical step in the specific heat at the glass transition.

2.2.3 Fictive Temperature calculation from DSC and FSC measurements

In order to determine the fictive temperature in a DSC or FSC analysis the heating scan after an aging treatment below the glass transition is considered. In thermograms obtained in the range of the glass transition temperature, generally an overshoot peak appears, caused by the aging treatment for a certain time, superimposed to the heat flow step of the glass transition. The fictive temperature T_f of the glass can be calculated graphically as schematized in Figure 2.5.

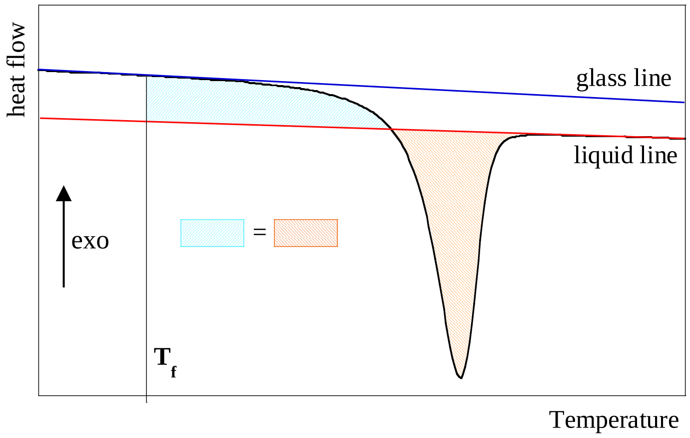

Figure 2.5. Fictive temperature calculation for the heating scan of DSC and FSC.

The glass and liquid lines are constructed by linear fitting of the heat flow or specific heat data of the thermogram respectively well below and well above the glass transition. The fictive temperature of the glass is the temperature at which the two areas (orange shaded area and light blue shaded area) matches.

Alternatively, the calculation of the fictive temperature is carried out mathematically by following the Moynihan relationship[2] (equation 2.11):

$$\int_{T\gg T_g}^{T\ll T_g}\left(c_p^{liquid}-c_p^{glass}\right)dT=\int_{T\gg T_g}^{T\ll T_g}\left(c_p(T)-c_p^{glass}\right)dT \qquad \text{Eq 2.11}$$

where c_p^{liquid} and c_p^{glass} are the specific heat capacities of the liquid and the glass respectively, and $c_p(T)$ is the experimental specific heat capacity measured in a DSC or FSC heating scan. It is worth noticing that the calculation of the fictive temperature could be performed by Equation

2.11 using the heat flow values alternatively to the specific heat capacities. As stated previously, the time evolution of the fictive temperature during an isothermal treatment of the glass requires a heating scan for each aging time.

2.3 REFERENCES

(1) Gill, P. S., Sauerbrunn, S. R., & Reading, M. (1993). Modulated differential scanning calorimetry. *Journal of Thermal Analysis*, *40*(3), 931-939.

(2) Moynihan, C. T.; Easteal, A. J.; De Bolt, M. A.; Tucker, J. Dependence of the Fictive Temperature of Glass on Cooling Rate. J. Am. Ceram. Soc. 1976, 59, 12–16.

(3) Mathot, V.; Pyda, M.; Pijpers, T.; Vanden Poel, G.; van de Kerkhof, E.; van Herwaarden, S.; van Herwaarden, F.; Leenaers, A. The Flash DSC 1, a Power Compensation Twin-Type, Chip-Based Fast Scanning Calorimeter (FSC): First Findings on Polymers. Spec. Issue Interplay Nucleation Cryst. Glass Transit. 2011, 522 (1–2), 36–45.

(4) Schawe, J. E. K.; Pogatscher, S. Part I. Material Characterization by Fast Scanning Calorimetry: Practice and Applications. In Fast Scanning Calorimetry; Schick, C., Mathot, V., Eds.; Springer International Publishing, 2016; pp 3–80.

3. INSIGHT IN THERMAL TRANSITIONS OF AMORPHOUS POLY(ETHYLENE TEREPHTHALATE) IN GLASSY AND LIQUID STATES BY MODULATED TEMPERATURE FTIR, TIME-RESOLVED FTIR, DSC AND FSC

3.1 INTRODUCTION

The potentiality of conventional thermal analysis has been improved by the superimposition of a temperature modulation to a constant cooling or heating rate. It gives, indeed, the opportunity to resolve material thermal transformations in their reversing and non-reversing components, allowing a deeper insight in the mechanism ruling complex or superimposed transitions. Modulated temperature programs were successfully used in various thermal analysis techniques, including DSC, TMA and TGA as well ellipsometry.[1-4] Differently from the conventional thermal techniques, which follows only one signal output, namely heat flow, sample dimension or weight, variable temperature FTIR (VTFTIR) could be used as a multi-signal analysis able to characterize materials at molecular level, being sensitive to inter- or intra-molecular interactions, conformation or structure changes occurring during sample transformation. The comparison among the different dependencies of absorption band intensities with temperature, can be employed, in fact, to explore transition details, such as sequential ordering in polymer crystallization process, mesophase formation and melting, conformer concentration variation, polymorphic transitions, all of these features not easily or not detectable by conventional thermal analyses.[5,6] Moreover, VTFTIR allows the investigation of slow processes occurring at low temperature or heating rate that, otherwise, can not be studied by conventional DSC because of the low heat flux involved in the transformation.[7,8]

In the first part of the chapter, we investigated PET thermal transitions by following time resolved FTIR spectra evolution during a modulated temperature ramp (modulated temperature FTIR, MTFTIR) in the glass transition region. In particular, the effect of the physical aging of quenched amorphous PET on the glass transition, relaxation recovery and cold-crystallization was studied. The intensities of some absorption bands as a function of time were elaborated by a deconvolution procedure and the components of reversing and non-reversing transformation were obtained for a series of PET samples melt-quenched and aged at different temperature below the glass transition temperature. The results evidenced that MTFTIR is able to give new insight on polymer transformations otherwise not accessible by other conventional thermal analysis.

The obtained results on PET behavior encouraged a deeper study of the conformational transitions of PET during the physical aging process which, despite a number of researches dealing with it,[9-17] is still not completely understood.

Firstly, the systematic study of the PET spectrum was performed during the heating of aged and quenched samples by means of the factorial analysis, in order to assign in a more precise way the conformations or conformational sequences to peculiar infrared absorption bands. Moreover, an extensive study on the kinetics of the relaxation during the isothermal physical aging below the glass transition, and on the annealing above the glass transition was performed using a combination of time-resolved FT-IR, DSC and Fast Scan Calorimetry (FSC). The results obtained allowed to obtain a new general insight on the conformational transitions occurring in the glassy and liquid state of PET, allowing the understanding of the effects of such structural rearrangement on the cold-crystallization.

3.2 EXPERIMENTAL PART

Poly(ethylene terephthalate) (PET, M_v=18000), trifluoroacetic acid (TFA), chloroform and spectroscopy grade KBr were purchased from Sigma-Aldrich and used without any purification.

For Infrared measurements, polymer films were obtained by spin-coating on a KBr disk support 50µl of TFA/$CHCl_3$ (1/10 v/v) PET solution (2.5 wt%). The spin-coater angular rotation was set at 2000 rpm for 120 s. After drying under vacuum overnight, the thickness of the films was about 4-6 µm. In order to achieve amorphous polymer, the films were melted at 290 °C for 5 min and rapidly quenched in liquid nitrogen. To eliminate previous thermal history, the samples were reheated at 85 °C for 5 minutes and cooled down at 2 °C min^{-1} up to the aging temperature. Unaged samples were cooled down up to 40 °C and immediately analyzed. The physical aging treatment conditions for PET samples are reported in Table 3.1. At the end of the aging, the samples were cooled at 40 °C and immediately analyzed.

Table 3.1 Sample experiment codes defining physical aging conditions of PET

Sample	Aging temperature T_a (°C) (T_a±0.1 °C)	Aging time t_a (h)
Q	-	-
A84	84.0	90
A83	82.5	90
A81	81.0	90
A80	80.0	90
A76	76.2	70
A74	74.3	40
A73	72.8	65
A70	70.3	90
A68	68.4	110
A65	65.1	415

Infrared spectra were acquired by a Nicolet 6700 FTIR equipped with a SPECAC variable temperature cell driven by a HELLMA temperature controller. The sample temperature was measured by a K-thermocouple in contact with the KBr disk and recorded on a PC. No temperature lag between the thermocouple and the sample was detected, as determined by following the melting process two standard compounds (diphenyl, T_m=72 °C, and benzoic acid, T_m=122 °C) by MTFTIR in the same experimental conditions used for PET analyses.

For time-resolved FTIR measurements spectra were acquired during the isothermal aging of the samples listed in Table 3.1, by co-adding 400 scan per spectrum at a resolution of 4 cm^{-1}. Spectra were acquired every 300 s.

For MTFTIR measurements, a temperature program comprises a linear heating at 0.21 K min^{-1} superimposed to a periodic modulation characterized by an amplitude of 2.7 °C and a period of

480 s. The overall temperature range goes between 40 °C to 120 °C. By co-adding 40 scans per spectrum at a resolution of 4 cm^{-1}, a time and mean temperature resolution of 30 s and 0.1 °C were obtained, respectively. MTFTIR experiments on unaged and aged PET samples were repeated twice. The observed spectral variations as a function of temperature were reproducible. The selected results shown below are referred to aged and unaged samples showing approximatively the same overall spectrum intensity.

The intensity of the peak, or the area of selected bands, defined generally I_λ, per each spectrum was recorded, given a suitable baseline. Table 3.2 lists all the recorded absorption bands, with the vibrational mode assignment and the baseline applied. The detailed signal transformation used to obtain the total band intensity variation ($I^{Tot}{}_\lambda$) and the reversing ($I^{R}{}_\lambda$) and non-reversing ($I^{NR}{}_\lambda$) components as a function of the mean temperature (T^M) is reported in the paragraph 2.1.6 "Data elaboration for the Modulated Temperature FTIR analysis".

Table 3.2. Band assignment and experimental parameter of signal acquisition. "*G*" and "*T*" are the assignment for ethylenic *gauche-trans* isomerism, meanwhile "*g*" and "*t*" are used for glycolic *gauche-trans* conformations.

Wavenumber (cm^{-1})	Parameter type	Assignment	Conformer assignment	Baseline (cm^{-1})
1370	Area	CH_2 wagging	*G*	1358-1329
1340	Area	CH_2 wagging	*T*	1391-1359
1048	Area	O–CH_2 stretching	*g*	1059-1030
973	Area	O–CH_2 stretching	*t*	1032-999
841	Intensity	CH_2 rocking	*T*	858-827

3.3 RESULTS AND DISCUSSION

3.3.1 MTFTIR results on melt-quenched and aged PET

In order to study the conformational changes occurring in PET samples during a modulated heating ramp by Modulated Temperature FTIR analysis, infrared spectra were acquired every 30 s simultaneously to the temperature program. For sake of clarity, Figure 3.1 displays a waterfall plot of mid-IR spectra in a spectral window between 1800-700 cm^{-1}, acquired between 50 and 125 °C for the quenched PET sample.

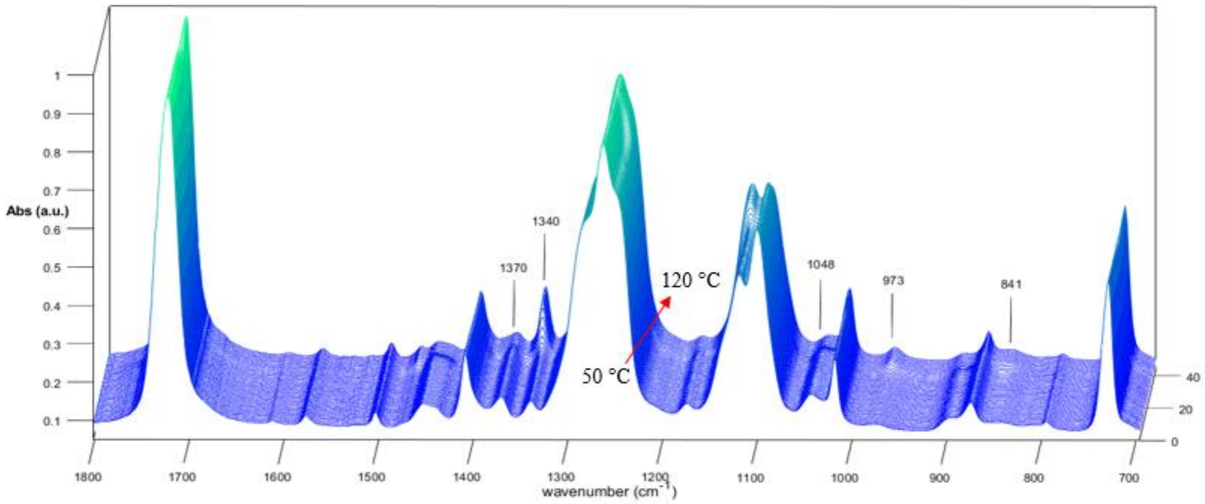

Figure 3.1. Acquired spectra of melt-quenched PET (Q) in a modulated heating ramp between 50 and 120 °C.

In order to standardize the initial amorphous structure, the quenched samples were equilibrated few degrees above the glass transition. Moreover, to avoid sub-T_g relaxations before the analysis, they were rapidly cooled down to the starting temperature. In the explored temperature range (50-120 °C), the amorphous PET experienced the glass transition and the cold-crystallization process. It was chosen to follow the temperature variation of the intensity or the area for six different conformational bands, associated to the CH2 and O-CH2 vibrations of the *trans* and *gauche* conformers of PET. Table 3.2 reports the assignation of conformational bands and the baseline used to calculate the integrated intensity. In Figure 3.2 A, the temperature and the integrated intensity (I_{1340}) of the peak at 1340 cm^{-1}, assigned to the wagging of the ethylene CH$_2$ in trans conformation, of unaged amorphous PET were reported as a function of time.[18,19]

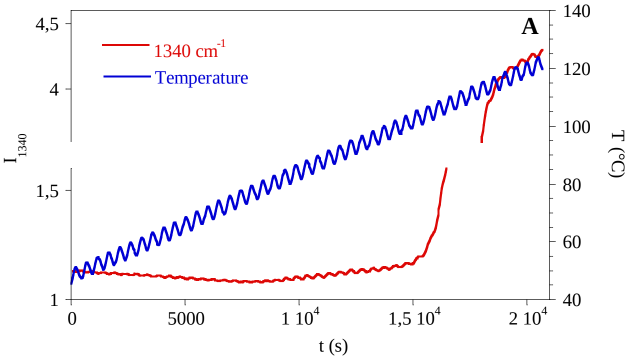

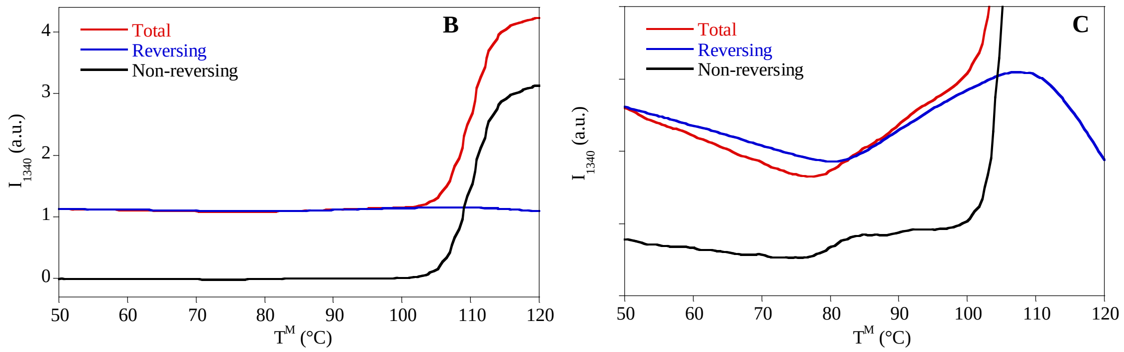

Figure 3.2. Integrated intensity of the peak at 1340 cm^{-1} (I_{1340}) and modulated temperature recorded as a function of time (A). Total intensity of the peak at 1340 cm^{-1} (I^{Tot}_{1340}) and its reversing (I^{R}_{1340}) and non-reversing (I^{NR}_{1340}) components as a function of mean temperature (T^M) as obtained by raw data elaboration (B). Detail of panel B (C).

The processing of time-resolved areas or intensities for given absorption bands gives the I^{Tot}_{λ} values and the reversing I^{R}_{λ} and non-reversing I^{NR}_{λ} components as a function of the mean temperature (T^M). It is worth to notice that the trend of I^{Tot}_{λ} vs. T^M is approximatively the same to that achievable by a variable temperature FTIR experiment carried out by using a constant heating rate.

In general, in absence of non-reversing transitions, the peak intensity changes linearly with temperature. This behavior is ascribed mainly to the variation of the absorption coefficient ($d\varepsilon_{\lambda}/dT$) and in lesser extent to sample density variation ($d\rho/dT$).[20] In the temperature region whereas the structural mobility allows conformational rearrangements, e.g. at temperatures above the glass transition, the change of conformers equilibrium concentration (*gauche-trans* equilibrium) affects also the slope of the reversing intensity. The results, reported in Figure 3.2 B, shows that the largest spectral modification occurred during the non-reversible cold-crystallization process, as evidenced by the abrupt variation of I^{Tot}_{1340} and I^{NR}_{1340} at about 105 °C. In correspondence of this transition, the I^{R}_{1340} inflection was due to the change of $d\varepsilon_{\lambda}/dT$ and $d\rho/dT$ between the amorphous and crystalline phases, as well as the perturbation of the *gauche-trans* equilibrium distribution, caused by the crystallization. In order to appreciate the small intensity variation at lower temperature, the plot of Figure 3.2 B was expanded in Figure 3.2 C. The glass transition, being affected by the temperature modulation (reversing event), appears as a slope change of I^{R}_{1340} as a function of temperature. The T_g value (T_g =80°C) was taken in correspondence the intersection point of the two straight lines interpolating I^{R}_{1340} data before and after the transition. This determination results quite difficult if carried out on I^{Tot}_{1340} data, being superimposed by another process. In fact, both total and non-reversing component showed a continuous decrease of the trans conformers up to the T_g, followed by a step increase overlapped to the glass transition. These phenomena, associated to the polymer non-isothermal sub-T_g relaxation (here defined as dynamic physical aging) and recovery, respectively, will be discussed later.

In order to better interpret the observed spectral changes and to appreciate the effect of physical aging on the PET thermal behavior on subsequent heating, the PET melt-quenched (Q) and aged at 70°C (A70) trends were compared. To exclude sample thickness variation, the ratio between the total intensity ($R^{Tot}=I^{Tot}_{1340}/I^{Tot}_{1370}$), reversing ($R^{R}=I^{R}_{1340}/I^{R}_{1370}$) and non-reversing ($R^{NR}=R^{Tot}-R^{R}$) components of the peaks at 1340 cm^{-1} and 1370 cm^{-1} (assigned to CH_2 bending of the ethylene unit in trans and gauche conformation, respectively) were investigated (Figure 3.3). The R ratio is proportional to the conformational ethylene *trans* (T) abundancy,[11,12] with the following relationship:

$$R = \frac{\varepsilon_{1340}}{\varepsilon_{1370}} \cdot \frac{[T]}{[G]} \qquad \text{Eq. 3.1}$$

where $\frac{\varepsilon_{1340}}{\varepsilon_{1370}}$ is the ratio between absorptivity coefficients of 1340 and 1370 cm^{-1} bands, $\frac{[T]}{[G]}$ is the ethylene *trans-gauche* concentration ratio.

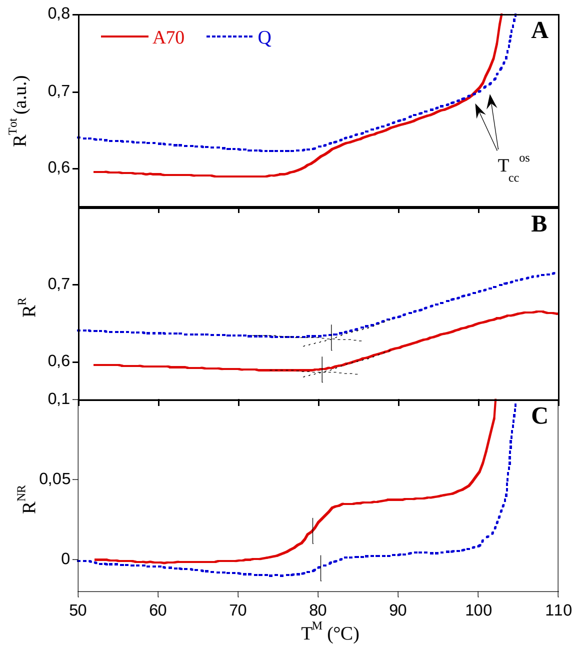

Figure 3.3. Variation as a function of the mean temperature (T^{M}) of $R^{Tot}=I^{Tot}_{1340}/ I^{Tot}_{1370}$ (A, total) $R^{R}=I^{R}_{1340}/I^{R}_{1370}$ (B, reversing component) and $R^{NR}=R^{Tot}-R^{R}$ (C, non-reversing

component). The arrows indicate the cold-crystallization onset temperature (T_{cc}^{os}). The vertical bars in R^R indicate the glass transition temperature and in R^{NR} the relaxation recovery temperature.

In the temperature range below the T_g, values of the Q unaged sample was always higher than those of the aged polymer, that is the physical aging increased the relative amount of gauche conformers, as observed by other.[10-12] Above the glass transition, at about 80 °C, the A70 and Q R^{Tot} values nearly coincide, as a result of the equilibrium recovery and the erase of glass thermal history. At about 100 °C the departure from linearity suggests the cold crystallization onset, a few degrees below for the aged sample A70.

The partition of the total spectral changes as a function of temperature in the reversing and non-reversing components allowed a deeper analysis of the sample thermal transformations. The temperature range up to the cold-crystallization can be divided in three regions. From the beginning of the experiment to about 70 °C, as previously outlined, the unaged sample was subjected to a continuous non-reversing decrease of the trans conformation relative content, as evidenced by R^{NR} decrease. It was due to the non-isothermal physical aging during the slow heating process. The aged sample, on the other hand, showed an approximately null non-reversing transformation since it has undergone relaxation during the isothermal annealing at 72 °C for 19 h. Between 70 and 80 °C, the reversible glass transition overlapped the non-reversing recovery of the sub-T_g relaxation. However, MTFTIR allowed the separation of the two transformations. In fact, the glass transition was clearly revealed from the slope change of the linear dependence of R^R with temperature at 80°C for both samples.

As far as the non-reversing components R^{NR}, it can be observed the presence of a step-wise increase of the relative amount of trans conformers from about 75 °C, due to the structural reorganization allowed by the chain segmental mobility acquired at T_g. This phenomenon is analogue to that observed by DSC as endothermic peak (called overshoot or enthalpic recovery) superimposed to the glass transition of aged polymers.[9,16,17] The step increase of R^{NR} was larger for the aged sample because the isothermal physical aging at 70 °C (A70 sample) has been more effective on the conformer relaxation than the dynamic aging (Q sample). The reversing component R^R changes linearly with the temperature before and after the glass transition (figure 3.3 B). Above the T_g, it represents the relative equilibrium concentration of the two conformers in liquid PET. It is important to observe that the temperature-dependent *trans-gauche* equilibrium concentration was not affected by physical aging, being nearly equal the slopes of the R^R vs T^M linear trend of A70 and Q samples. However, the small R^{NR} rise from above T_g up to the crystallization on-set (figure 3.3 C) indicates a slight non-reversing increase of ethylenic *trans* conformers that evidences a subtle non-equilibrium ordering phenomenon prior to the cold-crystallization in both liquid polymer samples.

The possibility to investigate the behavior of single bonds or atom groups comprising the repeating unit during material transformation trough the analysis of different absorption band is one of the advantages of the FTIR analysis respect to the conventional calorimetric techniques. Then, in addition to the absorbance ratio *R*, the band at 1048 cm^{-1}, related to the stretching of O-CH$_2$ in *gauche* (*G*) conformers was taken into account.[18,19] In figure 3.4, the comparison of I_{1048} total, reversible and non-reversible variations of the quenched and the aged at 70 °C samples are reported as a function of T^M up to the cold-crystallization.

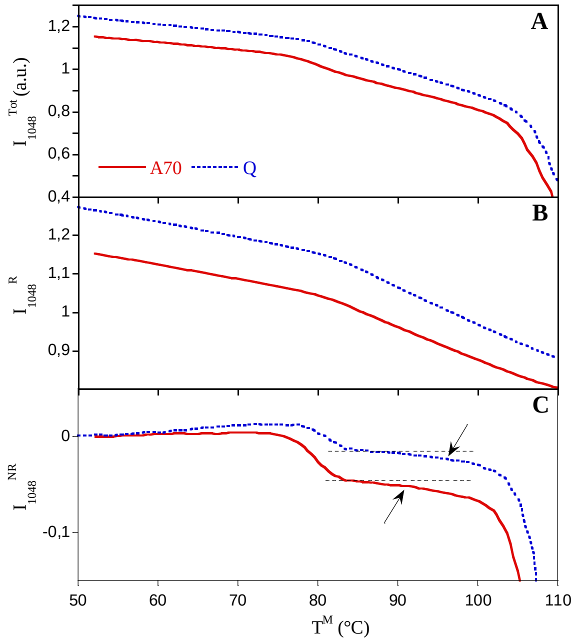

Figure 3.4. Variation as a function of the mean temperature (T^M) of total I_{1048}^{Tot} (A), reversing I_{1048}^{R} (B), and non-reversing I_{1048}^{NR} (C) intensities for Q and A70 PET samples. In panel C arrows indicate the non-reversing transition in the liquid state.

Some differences respect to the *R* behavior can be observed, mostly concerning the general trend and the behavior of non-reversible component. Firstly, being the 1048 cm^{-1} band relative to the glycolic *gauche* (*g*) conformer, the general behavior of the total intensity is expected to be reversed respect to the R ratio, related to ethylene *trans* (T) relative abundance. Moreover, the absence of any normalization brings about a slight difference in the total area of different samples, because of the different thickness of the PET films.

Briefly, the temperature-dependent glycolic conformational distribution (*g* and *t*) behaved very similar to that of ethylenic conformers (*G* and *T*). The *g* conformer is the low energy isomer in amorphous phase. In the physical aging, as well as dynamic aging, the *g* conformer concentration increased, meanwhile the relaxation recovery at about 80 °C led to a decrease of *gauche* conformation (Figure 3.4 C). The non-reversing cold-crystallization at about 100°C caused a consistent decrease of glycolic *gauche* conformers, seen in I_{1048}^{Tot} and I_{1048}^{NR}.

It worth noticing that in the I_{1048}^{NR} component (Figure 3.4 C), as soon as the relaxation recovery finishes, a non-reversing decrease of *gauche* conformers took place in the liquid state for both samples analyzed (arrows of Figure 3.4 C). The decrement of I_{1048}^{NR} at $T>T_g$ was more intense than that of R^{NR} (Figure 3.3 C).

MTFTIR results suggests that in the liquid state two structural rearrangements caused by different factors were active. The first and more pronounced was the temperature reversible *gauche-trans* equilibrium for ethylenic and glycolic conformers that follow Boltzmann distribution relationship (Equation 3.2), in which the *trans* isomer is favored at higher temperatures for both conformers.[11]

$$\frac{[T]}{[G]}, \frac{[t]}{[g]} = A \exp\left(-\frac{\Delta E}{kT}\right) \qquad \text{Eq. 3.2}$$

where $\frac{[T]}{[G]}, \frac{[t]}{[g]}$ are the *trans-gauche* ratio for ethylenic and glycolic isomers respectively, A is the pre-exponential factor, ΔE the energy difference between the two conformers, k the Boltzmann constant and T the temperature.

The second conformational rearrangement of glycolic, and in a minor part ethylenic, functions from the *gauche* to the *trans* isomer was non-reversible. It can be caused by the conformational evolution of the amorphous phase toward the more stable crystalline structure, composed by *trans* isomers, as hypothesized by Imai.[22,23] A more detailed study on the kinetics of the pre-ordering phenomenon prior to the crystallization will be discussed later.

3.3.2 Factor analysis on the heating of quenched and aged PET

In order to retrieve quantitative information on conformational rearrangements of PET during the heating scan for quenched (Q) and aged (A70) PET, the acquired spectra by MTFTIR experiment were analyzed by means of factor analysis. This elaboration allows to calculate the pure component spectra and the relative amount of the more recurrent conformational distributions of the chains. As mentioned in the Introduction, the chain conformation of PET plays a very important role in determining the crystalline and the amorphous structure. The molecular chain of PET has three different degree of rotational freedom, two of which concerning the rotation around the C-C ethylenic bond and the C-O glycolic bond. These rotations lead to the *gauche* and *trans* forms for ethylene unit CH_2-CH_2 (G, T), and for the glycolic unit CH_2-O (g, t). The third degree of freedom is the rotation around the phenyl-carbonyl bond of the terephthalate unit. The two carbonyl bonds adjacent to each benzene ring lies in the same plane of the ring, giving the cis (C_B) or the trans (T_B) arrangement with respect to each other.[24] The chain conformation in the crystalline phase of PET is well-studied in literature and it is formed by chains arranged in all-trans conformation (TtT_B).[25,26] Chain arrangements in the amorphous phase of PET is poorly characterized instead, because of the great amount of degree of freedom of the PET chain. It is generally believed that the *gauche* conformation of the ethylenic group (G) is predominant in the amorphous phase,[10-12,21,24] because it allows the chain to fold and organize in coil structures. Raman and FTIR studies[11,12,24] calculated that the amount of ethylenic gauche conformers in the liquid state range from 70 to 90%, depending on which absorption band was used. Retrieving information on the amount of *gauche-trans* conformations around the glycolic bond C-O is more difficult, an NMR study[18] reported that in the amorphous phase of PET a great amount of glycolic groups is in *trans* (t) form, about 75%. Regarding conformational rearrangements of the terephthalic unit, some Raman and infrared studies,[18,24] as well as theoretical calculation,[27] sustained that the planar trans (T_B) and cis (C_B) form are equally favorable. Nevertheless, non-planar ring-carbonyl isomers may be present in the amorphous phase, because of the low-energetic rotational barrier between the two forms.

The use of the factor analysis on PET infrared spectra aims to reduce the components, or factors, that influence the spectral variation due to conformational rearrangements during the glass transition and the cold-crystallization. The factor analysis of the following study was performed by using the “MCR-ALS” MATLAB add-on. Infrared spectra acquired between 60 and 120 °C of quenched (Q) and aged at 70 °C (A70) PET, were analyzed. A set of 43 spectra per each of the two samples were prepared by means of sliding average over 16 spectra acquired during the MTFTIR analysis. The averaging process, corresponding to one period of the temperature modulation, was used to maximize the signal-to-noise ratio and to erase the contribution of temperature oscillations. The spectral window between 1800-700 cm^{-1} was chosen.

The preliminary analysis of eigenvalues suggested that three factors, or “pure components”, account for most of the spectral variation. Simplifying, all the PET spectra could be represented by combining in different proportions three "pure component", representing three spectra associated to different phases of PET. By literature suggestion,[21,24] the three components were assigned to a crystalline PET (TC), an amorphous *gauche*-rich phase (G), and an amorphous *trans*-rich phase (TX). Nevertheless, in order to obtain physically and chemically significative spectra of the three pure components, a "component input" is needed. The latter consists in a set of three spectra that resembles the expected spectroscopic features of the three different phases. Differently from Cole's method,[24] the TC_i, TX_i and G_i input spectra were calculated by means of spectral subtraction. Firstly, three IR spectra were taken into account, at 85 (I_{85}), 95 (I_{95}) and 105 °C (I_{105}), corresponding to a low temperature *gauche*-rich liquid phase, a high temperature *trans*-rich liquid and a semi-crystalline PET respectively (Figure 3.5). Furthermore, we proceeded to spectral weighted subtraction (Equations 3.3/3.5), in which *a* and *b* are the weight coefficients.

$$G_i = \frac{I_{85} - a \cdot I_{95}}{1 - a} \qquad \text{Eq 3.3}$$

$$TX_i = \frac{I_{95} - a \cdot I_{85}}{1 - a} \qquad \text{Eq 3.4}$$

$$TC_i = \frac{I_{105} - b \cdot I_{95}}{1 - b} \qquad \text{Eq 3.5}$$

The G_i input spectrum was obtained by subtracting from a *gauche*-rich liquid phase (85 °C) the *trans*-rich liquid (95 °C) and trying to eliminate the absorption bands known to be associated with the trans conformation of the ethylene *trans* conformer, particularly the strong CH_2 wagging peak near 1340 cm^{-1}. We know from MTFTIR analysis that a *gauche-trans* equilibrium is established in the liquid phase of PET, with an interconversion from *gauche* to *trans* form by increasing the temperature. For this reason, the TX_i spectrum was calculated by subtracting from the liquid at 95 °C the spectrum recorded at 85 °C with the same weight coefficient of G_i. The TC_i spectrum, instead, was obtained by weighted subtraction of the liquid phase from the semi-crystalline PET, in order to obtain a spectrum without the absorption bands characteristic of the ethylene and glycolic *gauche* forms, in particular the 1370 and 1048 cm^{-1} peaks.

The factorial analysis results, comprising the optimized pure component spectra, G, TX and TC, were reported in Figure 3.6.

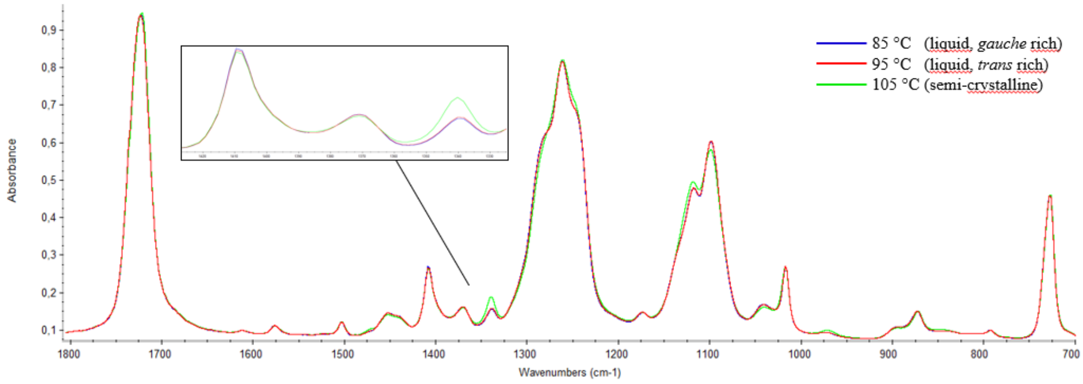

Figure 3.5 Mid-infrared spectra between 1800-700 cm^{-1} of A70 PET at 85, 95, 105 °C during heating at 0.2 °C/min utilized for the calculation of G_i, TX_i and TC_i input spectra for factor analysis. Inner box is a detail of the 1408, 1370 and 1340 cm^{-1} absorption bands change.

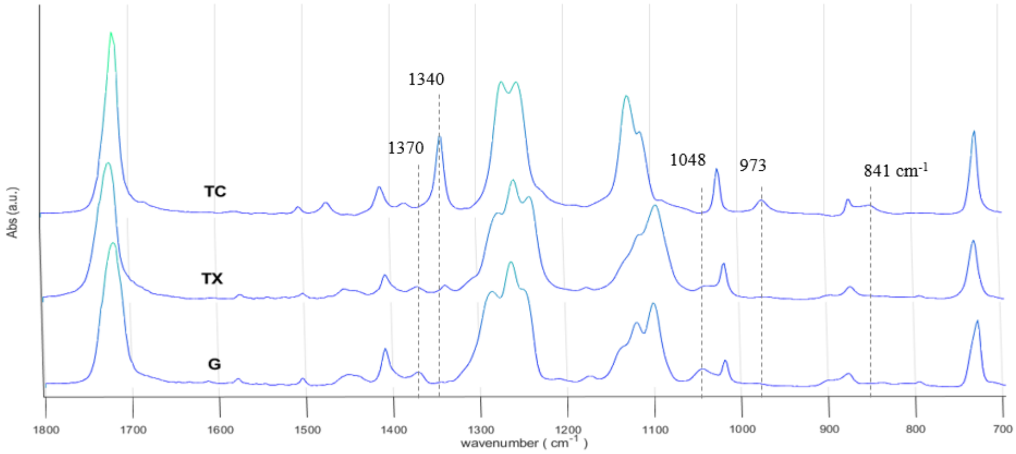

Figure 3.6. Pure component spectra of gauche-rich amorphous (G), trans-rich amorphous (TX) and trans crystalline (TC) PET in the 1800-700 cm^{-1} spectral range.

By analysing the spectral features of the three pure component spectra, some considerations have to be made. First of all, the PET crystalline spectrum TC differentiates more respect to TX and G amorphous spectra, possessing narrower and more intense absorption bands. The complete absence of 1370 cm^{-1} (*gauche* CH_2 wagging) and 1048 cm^{-1} (*gauche* O-CH_2 stretching) suggests than the chain is in all-trans conformation. It is worth noticing that the 841 cm^{-1} (*trans* rocking CH2) band was present only in the TC spectrum, indicating that this band emerge only in case of an all-trans rearrangement of the monomeric unit (TtT_B).

The differences between the G and TX amorphous spectra, as expected, are milder. The G spectrum possesses the typical absorption bands of ethylene *gauche*, 1370 cm^{-1}, and the glycol *gauche*, 1048 cm^{-1}. Hence, the G spectrum can be assigned to a PET amorphous phase with exclusively *gauche* glycolic and ethylenic conformers (*Gg*). In the TX spectrum, these two bands are still present in minor intensity. Contemporarily the 1340 cm^{-1} band (*trans* ethylene) appears with lower intensity and red-shifted respect to the crystalline form. Moreover, a small band appear at 973 cm^{-1}, associated to the C-O stretching in *trans* form. The assignment of the TX phase appears more difficult though. It possesses both *gauche* and *trans* forms of the functional group, with no indication respect to the terephthalate conformation. Hence, the TX phase was associated to an amorphous phase containing a combination of *Gt* , *Tg* and *Tt* forms of the O-CH_2-CH_2-O glycolic unit.

Based on the analysis of the pure component spectra by factor analysis and literature suggestions, a more specific assignments to the bands of interest were made, showed in Table 3.3. Specifically, the 1340 cm^{-1} band was decomposed in two absorption band, assigned to two different conformational arrangements, the isolated *trans* ethylenic form *T* in the amorphous phase of PET, centered at 1340 cm^{-1} with low absorptivity, and the ordered all-trans chain (TtT_B), that appears in the crystalline form at 1343 cm^{-1} and possesses a higher intensity. Results confirmed that the band at 1048 cm^{-1} was associated to *Gg* sequences of adjacent ethylene and glycolic bonds. Moreover, the 973 cm^{-1} band was assigned to a combination of *Gt* and *Tt* forms of the O-CH_2-CH_2-O in the amorphous phase absorbing weakly, meanwhile the band shifts at 971 cm^{-1} and increase in absorptivity in the crystalline phase, being sensible to the all-trans form TtT_B. Furthermore, the band centered at 841 cm^{-1} is related only to the TtT_B ordered sequences in the crystalline phase.

Table 3.3. Assignation of PET absorption bands to conformational rearrangement of the chain

Wavenumber (cm^{-1})	Assignment	Intensity	Conformational arrangement
1370	CH_2 wagging	medium	*G*
1343	“	strong	TtT_B
1340	“	medium	*T*
1048	O–CH_2 stretching	medium	*Gg*
973	“	weak	*Tt* + *Gt*
971	“	medium	TtT_B
841	CH_2 rocking	weak	TtT_B

In the following section the phase composition of PET as function of the temperature, calculated by the factorial analysis was discussed. The variation of the relative fraction of the G, TX and TC phases during the heating scan of quenched and aged PET results are showed in Figure 3.7 and Figure 3.8.

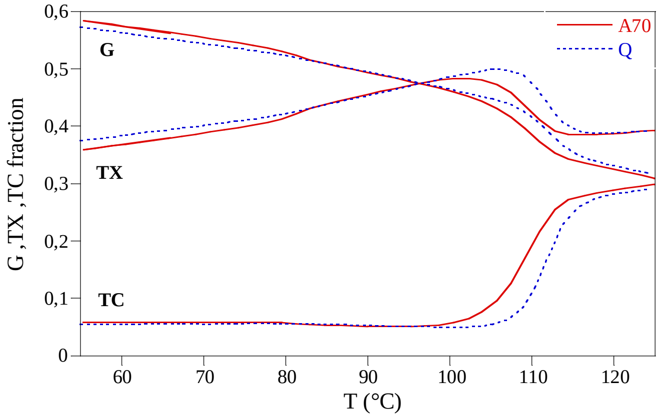

Figure 3.7. Variation of Gauche (G), trans amorphous (TX) and trans crystalline (TC) fractions as function of the temperature for A70 and Q PET samples, heated from 50 to 120 °C.

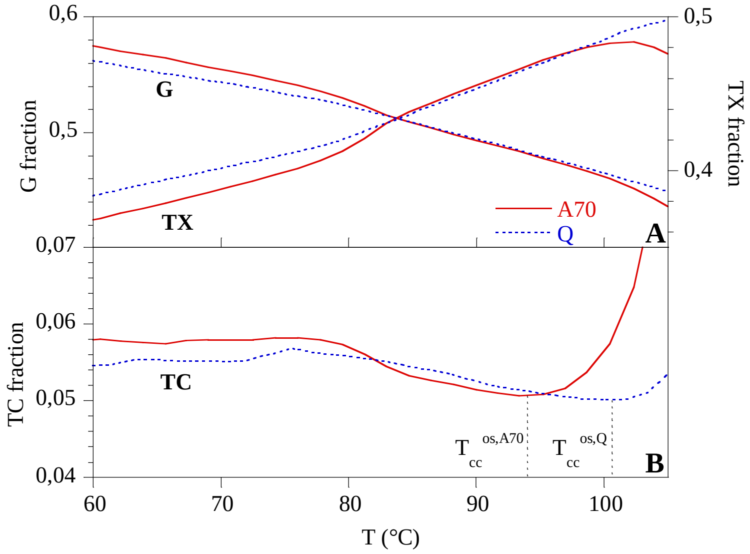

Figure 3.8. Enlargement of Figure 3.7. G and TX components fraction (panel A), and TC fraction (panel B) as function of the temperature. $T_{cc}^{os,Q}$ and $T_{cc}^{os,A70}$ are the cold-crystallization onset temperatures for Q and A70 samples, respectively.

The value for the fraction of G phase (56-57 %) appears to be lower than the data available in literature, quoted at about 70-90 %, [21,24] meanwhile the TC fraction is in accordance with the crystallinity content calculated by DSC and FTIR analysis.[18,28] The underestimation of the G fraction was due to the fact that the TX "*trans*-rich" amorphous also contains a little amount of *gauche* forms, hence the overall *gauche* conformation fraction was distributed between G and TX.

The overall trend of the three fractions as function of the temperature for melt-quenched PET (Q) was analysed (Figure 3.7). By increasing the temperature, an interchange from the G to the TX form was observed up to the onset of the cold-crystallization at 100 °C. At the glass transition temperature (80 °C) an abrupt change of the G and TX slope indicates that the G→TX conversion is greater in the liquid phase, as expected. In the cold-crystallization region (100-115 °C), the crystalline TC phase underwent a steep increase from 5 % up to 30 % at the expense of both G and TX amorphous phases. The A70 sample showed the same features, but cold-crystallization occurred at lower temperatures (Figure 3.7).

By comparing the thermal behaviour of the two samples in the glass transition region, some differences can be observed (Figure 3.8). Firstly, in the glassy state (60 - 80 °C), the distribution fractions of G, TX and TC phases were different for the A70 and Q sample. The physical aging treatment at 70 °C for 90 h of the A70 sample caused an increase of G phase from 56 % to 57 % and a simultaneous decrease of the TX from 38 to 37 %. The TC crystalline form, still present in a minor fraction of 5.5 % in the melt-quenched PET, slightly increased with the physical aging process, indicating that an ordering process, such as the formation of crystalline nuclei, nanocrystals or mesophase occurred.[24] Superimposed to the glass transition, the recovery of physical aging took place by a G→TX conversion, in order to retrieve the equilibrium fractions between G and TX (Figure 3.8 A). So, in the liquid phase A70 and Q compositions are almost the same. Concerning the TC phase (Figure 3.8 B), its fraction remained almost constant in the glassy and the liquid states of PET. At the glass transition temperature an abrupt decrease in the A70 sample was observed, suggesting that the relaxation recovery leads to the disruption of the ordered structures formed during the aging process. Nevertheless, the crystallization occurs earlier, the onset being taken at the first increase of the TC fraction, giving $T_{cc}^{os,\,Q}$ = 101 °C for the melt-quenched sample and $T_{cc}^{os,\,Q}$ = 94 °C for the aged one. This result highlighted that ordered structures formed during the physical aging were not disrupted totally after the relaxation recovery, as stated in other studies.[9,11-17] Ordered structures persisted in the liquid phase, acting as crystal nuclei and causing the early crystallization. Unfortunately, the factor analysis method, such other investigation techniques, does not possess the adequate sensibility to individuate such persisting structures in the liquid phase.

In conclusion, the factorial analysis was performed on the heating scan of a melt-quenched and an aged PET to individuate the different thermal behaviour caused by the physical aging. The infrared spectra associated to three different structural arrangements of PET were individuated, namely a *gauche*-rich amorphous (G), a *trans*-rich amorphous (TX), and an all-trans crystalline (TC). Based on the spectral features found in these spectra, a more detailed assignment of the 1370, 1340, 1048, 973 and 841 cm^{-1} conformational bands were made. Furthermore, the temperature dependence of the G, TX and TC fractions in the heating scan of the two samples were analysed. It was observed that by increasing the temperature the amorphous TX contribution increased at the expense of the low-energy amorphous G fraction both in the glassy and in the liquid phase. The "G to TX" conversion represented the *gauche-trans* conformational equilibrium in the liquid phase of PET. The less pronounced conformational rearrangement observed in the glass can be explained by considering a residue mobility of small segments of the chain that allows the partial interconversion between G and TX. The crystalline TC phase, in less amount in amorphous phase, did not participate to the *gauche-trans* equilibrium. Finally, at about 100 °C, the cold-crystallization took place with an increase of the crystalline TC at the expense of amorphous G and TX fractions. The physical aging treatment on PET caused an increase of the lower energy G phase and simultaneously a slight increase of TC, associated to the formation of ordered structures or all-trans chain portions. On heating, superimposed to the glass transition, the relaxation recovery took place with the recovery of equilibrium G fraction and the disruption of the ordered segments formed during aging. Although not observed directly, the thermal history of the glass was not erased completely by the relaxation recovery, residual ordered structures acted as crystalline nuclei and anticipated the crystallization of the aged PET respected the melt-quenched sample.

3.3.3 Effects of aging treatments on the cold-crystallization of PET

The effects of isothermal treatments at different temperatures (T_a) below the glass transition (sub-T_g aging) on the subsequent heating were investigated by MTFTIR analysis. Figure 3.9 shows the variation of the total $R=I_{1340}/I_{1370}$ ratio as function of the mean temperature for 5 different isothermal treatment at 74.3, 72.8, 70.3, 68.0, 65.0 °C and for a melt-quenched PET sample (reference to codes in Table 3.1).

The abrupt increase of the R^{Tot} ratio at about 100 °C indicated the increase of *trans* conformers due to the cold-crystallization of PET. For aged samples a significative shift of crystallization temperature at lower temperatures respect to the melt-quenched PET was observed. The R ratio at the end of the cold-crystallization showed slight differences in the final crystallinity for different samples. Concerning the kinetics of the cold-crystallization, it was not observed a significative increase with aging treatments, meanwhile the crystallization onset shifted at lower temperatures. The half-conversion crystallization temperature $T_c^{X=0.5}$ was calculated for all samples from R^{Tot} results and reported as function of the aging temperature in Figure 3.10.

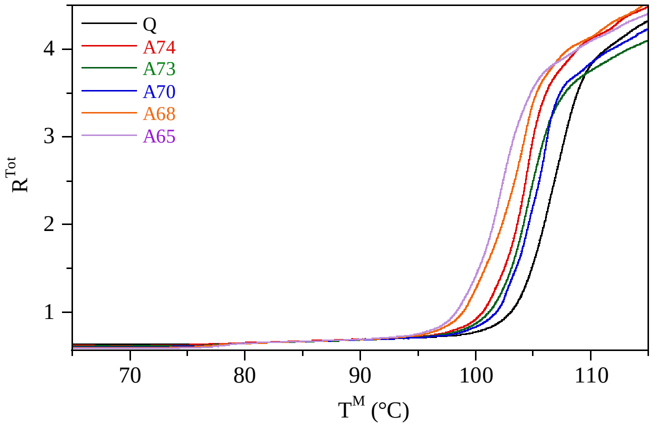

Figure 3.9. R total variation as function of the temperature for PET aged at different T_a.

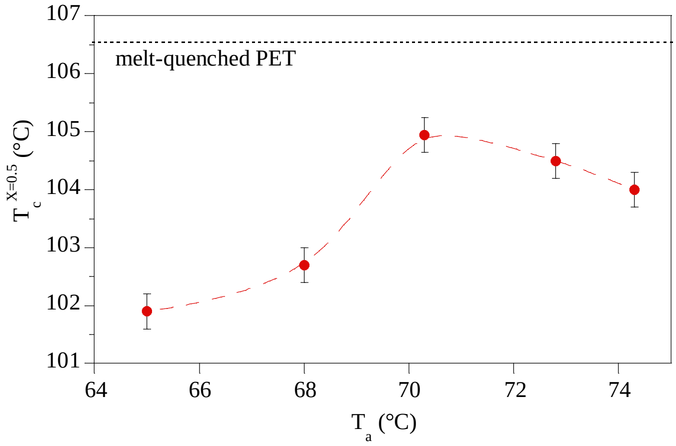

Figure 3.10. Crystallization temperature at half-conversion for PET samples as function of the aging temperature T_a. Short-dashed line at $T_c^{X=0.5}$ = 106.6 °C indicated the crystallization temperature for melt-quenched sample.

The results of Figure 3.10 showed a non-monotonic trend as function of the aging temperature. Although all aged samples (A65-68-70-73-74) had a lower crystallization temperature respect to the melt-quenched PET ($T_c^{X=0.5}$ = 106.6 °C), it was observed a maximum at $T_c^{X=0.5}$ =105.0 °C for PET aged at 70 °C (A70). Other aging treatments, both below and above this temperature, led to a further decrease of the crystallization temperature. From literature suggestions, the $T_c^{X=0.5}$ trend may be explained by a combination two phenomena occurring at different temperatures that bring about an early crystallization. The first is the formation of "cohesion entanglements" during the physical aging relaxation, hypothesized by Qian,[11,12] that persist above the glass transition and act as nuclei. A decrease of the aging temperature can lead to more intense aging, hence an increase of cohesion entanglements between PET chains. The second phenomenon that may facilitate the crystallization is the structural pre-ordering process proposed by Imai[23] and others.[28] This process was associated to the formation of stiff chain segments in *trans* conformation, 1-2 repeating units long, that can possibly order parallelly and form nuclei. This phenomenon requires a fair chain mobility for the rearrangement, hence the increase of the aging temperature brings about intense structural pre-ordering. Nevertheless, this kind of structural rearrangement has been observed only above the glass transition, starting from 90 °C.

In order to investigate on the relationship between the intensity of the relaxation during physical aging and the crystallization temperature behavior, the MTFTIR curves acquired on heating for the five different aged samples and the melt-quenched PET were analyzed. In particular, Figure 3.11 shows the variation of R total in the glass transition region (65-95 °C) and its reversing and non-reversing components as function of the mean temperature.

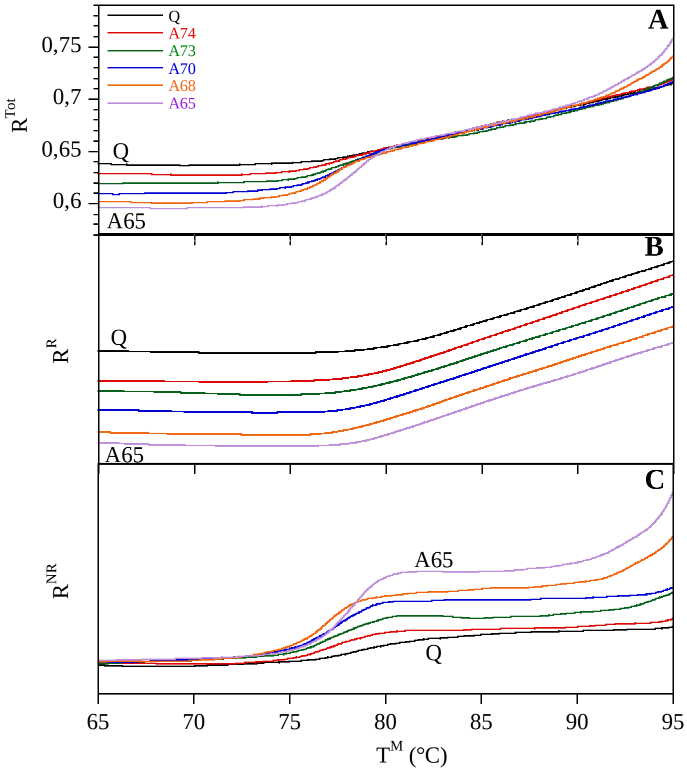

Figure 3.11. R total variation (A), reversing (B) and non-reversing (C) components as function of the mean temperature.

At the glassy state, from the start of experiment up to 75 °C, R^{Tot} showed a linear trend, almost parallel for all samples analyzed (Figure 3.11 A). Physical aging at different temperatures caused a decrease of the R^{Tot}, associated to the rearrangement from *trans* to *gauche* ethylenic forms to reach the extrapolated equilibrium concentrations. Hence, the R^{Tot} value at the start of the experiment was maximum for the unrelaxed glass (Q sample), and it decreased with decreasing the aging temperature, according to the fact that the lower the aging temperature the more is the relaxation. Between 75 °C and 82 °C, the relaxation recovery took place superimposed to the glass transition, with an increase of the R^{Tot}. The intensity of the recovery was maximum for the A65 sample and decreased by increasing the aging temperature, coinciding with the relaxation intensity of the physical aging. In fact, the R^{Tot} for all the samples returned to almost the same value above the glass transition, indicating that the equilibrium liquid condition was retrieved with the same *trans-gauche* concentrations irrespective to the glass history. In the liquid state, R^{Tot} increased with a linear trend as function of the mean temperature, almost coinciding for all sample up to the onset of the cold-crystallization. The MTFTIR analysis allowed to study separately the reversing and non-reversing processes occurring during the heating of PET with different thermal histories. In Figure 3.11 B, the reversing component of R (R^R) was plotted as function of the mean temperature. The curves of different samples were arbitrarily shifted on the ordinate axis to follow the order Q, A74, A73, A70, A68, A65 from up to down. As far as the reversing component, no differences were observed among samples. The overall trend was linear and parallel, with a slope change for all the aging treatments in the range 77-81 °C, associated to the glass transition. Hence, the different thermal behavior was ascribed to the non-reversing, or out-of-equilibrium, processes occurring during the heating. In fact, the relaxation recovery is a non-reversing transition, and could be seen clearly at about 80 °C in the R^{NR} component displayed in Figure 3.11 C. The increase of the ethylenic *trans* conformer relative amount respect to the stable *gauche*, proportional to the R ratio, followed the trend discussed for R^{Tot}. It could be noticed also the presence of a small recovery for the Q sample, indicating that in the cooling process below T_g at 2 °C/min, and in the subsequent slow modulated heating with linear heating rate at 0.2 °C/min, the material experienced a dynamic aging process less effective than isothermal aging for other samples.

To obtain a quantitative evaluation on the intensity of the relaxation process occurred in physical aging, the fictive temperature T_f of the aged and unaged glasses during heating were calculated by means of the modified Moynihan method discussed in the paragraph 2.1.7.

The fictive temperature calculated for the $R=I_{1340}/I_{1370}$ ratio can be defined as the temperature at which the glass ethylenic *trans-gauche* composition would be equal to that extrapolated for the liquid equilibrium. During the physical aging at a temperature T_a, the glass evolves toward the equilibrium condition. With the same evolution, also T_f approaches the aging temperature T_a. At the extrapolated equilibrium $T_f = T_a$, meanwhile the offset of T_f from T_a represents the departure from equilibrium. In Figure 3.12, the fictive temperature calculated from R^{Tot} and R^R values for the five different aging were plotted against the aging temperature T_a.

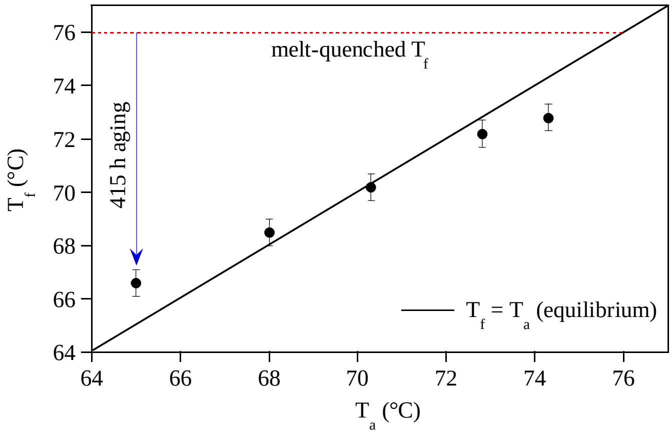

Figure 3.12. Fictive temperature vs. aging temperature for the A74 A73 A70 A68 and A65 PET samples. The solid line at $T_f = T_a$ represents the extrapolated liquid equilibrium in the glass

temperature region. Red dashed line at T_f = 76 °C represents the fictive temperature of the melt-quenched sample. The blue arrow indicates the fictive temperature evolution during the 415 h aging at 65 °C (A65 sample)

The melt-quenched sample showed a T_f = 76 °C, 3 °C less than the glass transition temperature, indicating that in the slow heating scan a dynamic aging occurred. From Figure 3.12 a decrease of the fictive temperature by decreasing the aging temperature was observed, being 72.8, 72.2, 70.2, 68.5, 66.5 ±0.5 °C for the A74, A73, A70, A68 and A65 samples respectively. The continuous decrease of T_f was in accordance with the trend obtained for the relaxation recovery reported in Figure 3.11. In fact, the plot highlighted that the intense relaxation of the A65 sample decreased gradually in magnitude with increasing the aging temperature. Furthermore, fictive temperature results allowed to investigate the departure of the relaxed glass from the equilibrium state, where $T_f = T_a$. For the aging at 65 °C, the equilibrium state was not reached ($T_f > T_a$). It suggests that the 415 h aging time was not enough for the material to relax completely, taking into account the low segmental mobility of the glass at the lower T_a. By increasing the aging temperature, the segmental mobility increases and, hence, the other samples were able to reach the equilibrium conditions. For A73 and A74 samples, a fictive temperature lower than the aging temperature was observed, because of the additional dynamic aging occurred in the slow heating scan that allowed the glass to relax further, such as the melt-quenched sample (Q) did.

Summarizing, the MTFTIR analysis on the heating of PET with different thermal histories highlighted that the cold-crystallization was affected by aging treatments at different temperatures (Figure 3.10). For the aging at 70 °C a minor effect on the cold-crystallization was observed, in accordance with McGonigle[13] and Zhao[15] DSC study, meanwhile the aging treatments below and above this temperature resulted to be more efficient for decreasing the cold-crystallization temperature. Two different mechanism at low and high temperature were hypothesized. The first concerns the formation of “cohesional entanglements”, as Quian suggested,[11] meanwhile in the second the onset of a pre-ordering process[23,28] can be involved. It is believed that these processes are responsible for the formation of stable nuclei that survive after the relaxation recovery and causes the early crystallization of PET. The study of the relaxation recovery (Figure 3.11) and the fictive temperature (Figure 3.12) of glasses aged at different temperatures highlighted more intense relaxation and lower fictive temperatures for low temperature aging, as expected, suggesting that the formation of “cohesional entanglements” could explain the decrease of the crystallization temperature at low aging temperatures. Although, the MTFTIR data acquired on heating did not allow to find any evidence on the conformational mechanism ruling the early crystallization at higher temperatures. However, the higher segmental mobility above 70 °C can be a clue to hypothesize that the pre-ordering process of PET, observed only above the glass transition temperature until nowadays[15,22,23,28], can start also at the glassy state. In order to find evidences on structural rearrangements occurring in PET during the physical aging that justify its effect of the subsequent cold-crystallization, in the next paragraph an extensive study on the relaxation kinetics carried out by combining infrared spectroscopy and differential scanning calorimetry was reported.

3.3.4 Kinetics study on the physical aging at different temperatures by FTIR, DSC and FSC

Time-resolved infrared spectroscopy is a useful technique to follow the evolution of chains conformational variation during the aging processes, being able to follow contemporarily different bands associated to the isomeric forms of different atomic groups. As an example, the investigation on the variation of *gauche* and *trans* concentrations of the ethylenic bond (CH_2-CH_2), and of the glycolic bond (O-CH_2) of PET is possible by following the time evolution of different absorption bands associated to the different conformational arrangement. Although the technique has been utilized to study the physical aging process of other polymers, such as PLLA,[29,30] in the literature there is a lack of time-resolved FTIR direct studies during the physical aging of PET, due principally to the small intensity changes involved in process. Qian[12] reported the evolution from *trans* to *gauche* ethylenic conformers after the aging at 67 °C of a quenched PET, by following the ratio between the band at 1340 and the band at 1370 cm^{-1}. From our knowledge, the evolution of other conformational bands was not studied during the aging process, in particular those associated to the glycolic bond *trans-gauche* isomers, centered at 973 and 1048 cm^{-1}.

As far as the calorimetric studies on the physical aging of amorphous PET, the evolution kinetics was not well characterized neither. In general, the kinetics study of physical aging by conventional DSC was carried out by following the time evolution of the endothermic peak superimposed to the glass transition, associated the enthalpic recovery. The kinetic of the enthalpy loss caused by the physical aging is too slow to be observed directly by differential analysis, hence the measure of the relaxation was performed on the effects on the subsequent heating. By this way, the study of relaxation kinetics requires repeated aging for a defined time, heating, and cooling again at the aging temperature to restart the procedure with a different aging time. Being the PET a crystallizable polymer, heating the sample above the glass transition could imply partial crystallization. Obtaining the amorphous PET sample after each cycle was not possible by cooling the melt at DSC conventional cooling rate, hence a further step of melt-quenching outside the instrument was required, with a repeatability and accuracy loss.

DSC study by Lu[9] and Aref-Azar[16,17] has evidenced that the relaxation during the aging occur by one-step mechanism that appears to follow an Arrhenius temperature dependence with a quite high activation energy, calculated 470 ± 20 kJ/mol by Lu, and 420 ± 70 kJ/mol [17] or 650 ± 100 kJ/mol [16] by Aref-Azar in two different papers. Furthermore, another study,[31] following the aging far below the Tg (50-60 °C) by dilatometry, DSC and element-specific o-positronium lifetime spectroscopy, have discovered two faster relaxation processes with lower activation energy, 20 and 36 kJ/mol, associated to the non-cooperative rearrangements of small chain segments below 1 nm persistent length that sum up to the slower cooperative α relaxation, that shows a Vogel-Tamman-Fulcher temperature dependence. Dynamic mechanical analysis studies[17] have showed two different processes of aging, the α cooperative rearrangement with an activation energy of 790 ± 70 kJ/mol and a fast β Arrhenius-type relaxation with 100 ± 20 kJ/mol activation energy. Hence, from the literature a very complex and unclear scenario emerged for the physical aging of PET. Although an extensive conformational analysis during the PET aging treatment was not performed yet, it is believed that both cooperative and non-cooperative relaxation processes toward the equilibrium state involve the conformational rearrangement of ethylene units from the *trans* to the *gauche* form, allowing a better packing of the amorphous chains.

In the following section the time evolution of the conformational distribution of PET was followed by time-resolved FTIR spectroscopy during the isothermal physical aging at different temperatures. In particular, the intensity ratio R ratio ($R= I_{1340}/I_{1370}$), already described, as well as the intensity of 1048 and 973 cm^{-1} bands were analyzed in order to follow contemporarily the conformational behavior of the ethylenic and glycolic bonds, the conformational degrees of freedom of the PET monomeric unit. Moreover, from the temperature dependence of the kinetics of aging, the activation energy was calculated for two different mechanism observed during the relaxation process. Finally, in collaboration with the tenured scientist PhD Daniele Cangialosi from Materials Physic Center of San Sebastian, the aging at different temperatures was studied by the new calorimetric technique Flash Scanning Calorimetry (FSC), highlighting some new results for the fast enthalpy relaxation of PET.

Time-resolved FTIR results for the A74, A73, A70, A68 and A65 samples were showed in Figures 3.9-3.10-3.11, in which the excess of the fictive temperature respect to the aging temperature (T_f -T_a) for the R ratio (Figure 3.13), the 1048 cm-1 (Figure 3.14) and the 973 cm-1 (Figure 3.15) intensities were reported as function of the aging time t_a.

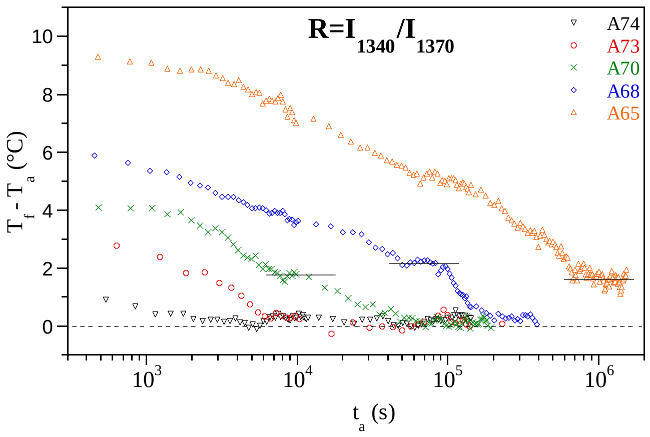

Figure 3.13. T_f -T_a relaxation curves calculated from $R=I_{1340}/I_{1370}$ ratio as function of the aging time (logarithmic scale) for samples aged at 74.3, 72.8, 70.3, 62.5 and 65.1 °C. Dashed line at T_f -T_a = 0 represents the extrapolated equilibrium liquid. Solid lines are a guide for the eye for highlight the intermediate plateau.

As stated previously, the fictive temperature is an intensive property that allows to follow the evolution of the glass state toward the equilibrium. During an isothermal relaxation, the T_f starts from the higher value of the unrelaxed glass and approaches equilibrium, represented by $T_f = T_a$. The value of T_f - T_a is proportional to the departure respect to the equilibrium extrapolated from the liquid, hence for an isothermal aging T_f - T_a starts from a positive value and approaches the zero value, decreasing as function of the time. In Figure 3.13, the T_f –T_a time evolution for physical aging at different temperatures were calculated from the R ratio, associated to the *trans* ethylenic abundance. It is worth to remind that the relaxation followed by the R ratio was associated to the conformational transition from the *trans* form to *gauche* form by rotation around the ethylene bond CH_2-CH_2.[12] For all the samples the fictive temperature calculated at the start of the aging was equal to that of the melt-quenched Q sample, between 75 and 76 °C, as expected. Hence, the T_f -T_a initial values, increasing with decreasing aging temperature, were proportional to the departure of the unrelaxed glass from the extrapolated equilibrium liquid. All glasses aged at different temperature relaxed toward the equilibrium value Tf – Ta = 0 with different kinetics, slowing down for lower aging temperatures. At the end of the isothermal aging, all samples reached the equilibrium *trans-gauche* ethylene concentration, except the A65 because of the too large time-scale of the relaxation process at 65 °C. Surprisingly, the kinetics of the aging process highlighted a complex time dependence, with a non-monotonic trend found at aging temperatures below 70 °C. In fact, for A70, A68 and A65 sample the relaxation stopped at an intermediate plateau and after a latency time continued until the reaching of the liquid equilibrium. The first plateau evidenced that the glassy state of PET possessed another unstable (metastable) *gauche-trans* equilibrium concentration other than that extrapolated by the liquid, with a higher content of ethylenic *trans* conformer, hence, presumably with an intermediate enthalpy between the unrelaxed glass and the extrapolated liquid equilibrium. These results were the first conformational evidences for PET of a double relaxation mechanism for the *trans (T)* to *gauche (G)* ethylenic relaxation, and agreed well with Cangialosi's observations of the double aging mechanism for poly(styrene) and poly(carbonate) obtained by DSC analysis.[33]

In order to complete the characterization of the conformational relaxation in the glassy state of PET, the evolution of the bands centered at 1048 cm^{-1} and 973 cm^{-1} were analyzed for different aging temperatures. Being these bands associated to the O-CH_2 stretching mode, the following analysis aimed to retrieve information on the conformational transition between *trans (t)* and *gauche (g)* isomers obtained by rotation around the glycolic bond O-CH_2. It gives flexibility to the PET chain together with the CH_2-CH_2 bond. In Figure 3.14, the T_f -T_a value calculated for the 1048 cm^{-1} band, assigned to the *gauche* conformers, were plotted as function of time for different aging temperatures.

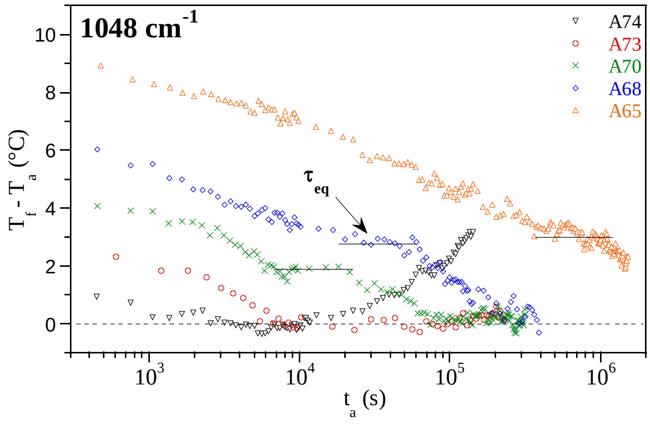

Figure 3.14. T_f -T_a relaxation curves calculated for the 1048 cm^{-1} absorption band as function of the aging time (logarithmic scale) for aging temperatures of 74.3, 72.8, 70.3, 62.5 and 65.1 °C. Dashed line at T_f -T_a = 0 represents the extrapolated equilibrium liquid. Solid lines is a guide for the eye for highlighting the intermediate plateau. τ_{eq} (equilibration time) is the time required for reaching the intermediate plateau.

Again, as seen for the R ratio results (Figure 3.13), the 1048 cm^{-1} band intensity showed an overall decreasing trend of the T_f -T_a parameter as function of the aging time, until the reach of the extrapolated liquid equilibrium. Moreover, the shape of the relaxation curves for all the aging temperatures, except for A74, gave the same results that those calculated for the R ratio, with the observation of two separated decays and an intermediate unstable equilibrium plateau for the A70, A68 and A65 samples. The equilibration time and the magnitude were the same for each relaxation, strongly indicating a correlation between the R and the 1048 cm^{-1} band. Unexpectedly, for the aging at 74.3 °C (A74, Figure 3.14), as soon as the T_f-T_a reached the equilibrium value, after 5000 s an abrupt increase of the T_f was observed until reaching a value of T_f -T_a = 3 °C at the end of the experiment.

The final part of the aging at 74.3 °C highlighted that in proximity of the T_g another conformational transition of different origin respect to the aging relaxation took place soon after the achievement of T_f -T_a = 0 °C. This conformational reproducible phenomenon caused the departure from the equilibrium and can be associated in first analysis to an ordering transition from the more stable *gauche* (*g*) in the amorphous phase to the ordered *trans* (*t*) glycolic conformation typical of crystalline order, in an opposite way respect to that occurred in the physical aging at lower temperatures. It is worth noticing that, except for the last part of the aging at 74.3 °C, the T_f – T_a curves calculated from the R ratio and the 1048 cm^{-1} band were almost superimposed for the all aging temperature. Hence, this strict relationship meant that the band at 1048 cm^{-1} is sensible to the conformational sequence *Gg* of the monomeric unit of PET, with adjacent glycolic *gauche* (*g*) and ethylenic *gauche* (*G*) forms.

Finally, in Figure 3.15 the T_f -T_a value calculated for the 973 cm^{-1} band, assigned to the O-CH$_2$ stretching of *trans* conformers (*t*), were plotted as function of time for different aging temperatures. For sake of clarity, the Tf- Ta were vertically shifted.

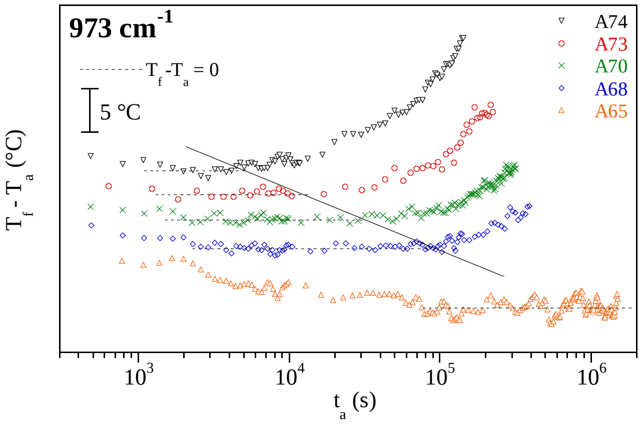

Figure 3.15. T_f -T_a relaxation curves calculated for the 973 cm^{-1} absorption band as function of the aging time (logarithmic scale) for aging temperatures of 74.3, 72.8, 70.3, 62.5 and 65.1 °C.

Dashed line represent the equilibrium at T_f -T_a = 0. Solid line is a guide for the eye for the onset of the departure from equilibrium.

The 973 cm^{-1} band showed a very unusual behavior respect to the R and 1048 cm^{-1} during the aging of PET. After an induction period in the first part of the aging, a slow intensity increase over time, associated to the increase of *trans* glycolic conformers was observed. Surprisingly, the $T_f – T_a$ value calculated for different aging showed an overall positive trend except for the A65 sample, in contrast to the other bands analyzed. T_f-T_a, after a latency time at the equilibrium value (short-dashed lines, Figure 3.15) increased abruptly, indicating the onset of the ordering phenomena involving the *gauche* to *trans* glycolic conformational transition. The onset of the transition shifted at lower aging time with increasing the aging temperature (solid line, Figure 3.15) The intensity of the conformational transition, proportional to the $T_f – T_a$ deviation, increased with increasing the temperature. Differently from other samples, in the aging at 65 °C (A65, Figure 3.15), the relaxation toward the equilibrium was observed in the first 10^5 s of the experiment, then the T_f -T_a value remained constant until the end of the experiment ($1.4x10^6$ s.).

These results highlighted that the conformational behavior of the glycolic O-CH_2 bond was different respect to the ethylene CH_2-CH_2 group. The latter was responsible of the glass evolution toward equilibrium with the transformation from *T* to *G* conformers. Meanwhile, the transition associated to the rotation around the glycolic bond remained inactive for a latency time, roughly corresponding to the time needed for the glassy system to equilibrate, and then activated in order to promote the formation of *trans* glycolic conformers. This process could be associated to the pre-ordering process observed by other authors[22,23,28] above the glass transition, that led to the formation of stiffer segment of the PET chain. Alternatively, it could be caused by the homogeneous nucleation already observed for other polymers after the cease of the enthalpy relaxation.[43-46]

The results obtained by analyzing the kinetics of relaxation for R ratio, 1048 and 973 cm^{-1} furnished solid evidences about the two different conformational transition associated to ethylenic and glycolic groups in the PET chain. Nevertheless, a poor correlation was observed between the relaxation behavior of 1048 cm^{-1} and 973 cm^{-1} bands, associated respectively to *gauche* and *trans* conformers of the same atomic group (see Figure 3.14-15). The explanation of such differences could be accomplished by considering the relationship of those absorption band to particular conformational sequences in the PET chain, and not only ascribed to one singular conformation.

In order to determine in a more precise way the assignment of the analyzed absorption bands to some peculiar conformational sequences of the glycol bond, ethylene bond and terephthalate unit, a study was performed by means of factorial analysis on the heating scan of Q and A70 samples (3.2.2 Factor analysis on the heating of quenched and aged PET). The results gave a more precise assignments to the absorption bands used for FTIR analysis, showed in Table 3.3.

Briefly, results confirmed that the band at 1048 cm^{-1} was associated to *Gg* sequences of adjacent ethylene and glycolic bonds. Moreover, the 1340 cm^{-1} band was assigned to both the isolated *trans* ethylenic *T* form in the amorphous phase of PET, and the ordered all-trans chain TtT_B in the crystalline phase. The 973 cm^{-1} band was assigned to a combination of *Gt* and *Tt* forms of the $O\text{-}CH_2\text{-}CH_2\text{-}O$ in the amorphous phase and was characterized by a weak absorption. The band shifts at 971 cm^{-1} and increases in absorptivity in the crystalline phase, being sensible to the all-trans form TtT_B.

On the basis of the new conformational assignment of the bands at 1048 cm^{-1} (*Gg*) and 973 cm^{-1} (*Tt* + *Gt*) as well as of the R ratio, proportional to the *T*/*G* ratio in the amorphous phase, it was possible to hypothesize the following scenario, concerning the conformational rearrangements of PET during the physical aging.

From experimental result showed in Figures 3.13/3.15, during the physical aging two different processes took place, concerning the ethylenic and the glycolic moiety of the PET monomeric unit. The first transition observed was the relaxation of the glass toward to the extrapolated liquid equilibrium, which was caused entirely by the *T* → *G* conformational rearrangement of the $CH_2\text{-}CH_2$ atomic group, as reported in literature[10-12]. A complex time dependence was observed for the *T*→*G* relaxation, characterized by a double process and the appearance of an intermediate unstable equilibrium at lower aging temperatures. The intensity of the relaxation increased with decreasing aging temperatures. This process was observed for both the R ratio, sensible to the *T/G* ratio, and the 1048 cm^{-1} band (Figures 3.13-3.14), sensible to *Gg* sequences. Hence, the $T_f - T_a$ trend over time for R and 1048 cm^{-1} associated to the *T* to *G* rearrangement was coincident (Figures 3.13 and 3.14).

The second relaxation mechanism involved the transformation of the glycolic moiety of the PET chain from the *gauche* (*g*) to the *trans* (*t*) form by rotation around the $O\text{-}CH_2$ bond. The driving force for this relaxation was not the offset from liquid equilibrium, but allowed the $O\text{-}CH_2$ bond to enter in the plane of the terephthalate unit, causing a stiffening of small chain segments. This phenomena could be associated to the pre-ordering process observed by Imai and others[22,23,28], involved the formation of ordered string sequences in the amorphous PET. On the other hand, studies performed with Fast Scanning Calorimetry of the relaxation of PLLA[45,46] and other polymers[43] highlighted a homogeneous nucleation occurring below the glass transition soon after the end of the enthalpy relaxation. The conformational behaviour of the chain during nucleation could be expected as a cluster formation of ordered segments in which both glycol and ethylenic groups order in trans forms, hence the conformational transition $G\rightarrow T$ and $g\rightarrow t$ must occur simultaneously. The behaviour of the bands associated to the glycolic moiety of PET chain, located at 1048 and 973 cm^{-1}, seem to be in accordance with the homogeneous nucleation mechanism. Indeed, the $g\rightarrow t$ transition of the glycolic bond started after the enthalpy relaxation, namely the equilibration of the $T\rightarrow G$ ethylenic distribution, and increased in intensity and kinetics with increasing the temperature. Nevertheless, the R ratio was insensible to this conformational rearrangement, confirming that the ethylenic transition $G\rightarrow T$ was inactive. The decoupling between the glycolic and ethylenic conformational ordering after the cease of the enthalpic relaxation could be addressed to a conformational glycolic pre-ordering process, at least in the limit of sensibility of current FTIR experiments. Hence, a concurrent homogeneous nucleation that causes a small intensity change below the detection limit of FTIR measurements can not be excluded.

For the 1048 and 973 cm^{-1} bands, related to *Gg* and *Gt* + *Tt* conformers, respectively, the conformational transition associated to the glycolic moiety was observed with different features. As far as the aging at temperatures in proximity of the glass transition, at 74.3 °C (A74, Figure 3.14-3.15), after the achievement of the equilibrium of the 1048 cm^{-1} band, it was observed a departure evidenced by the T_f-T_a that increase, and the 1048 cm^{-1} intensity decrease over time. With the same kinetics, the 973 cm^{-1} band increased. It is worth noticing that the two bands were correlated each other only at this aging temperature. Hence, it could be possible that during the aging at 74 °C, after the glass reached the liquid equilibrium, a pre-ordering involving the transformation of *Gg* sequences in *Gt* ones took place. At lower aging temperatures, below 74 °C, the $Gg\rightarrow Gt$ pre-ordering did not occur anymore, because of the stability of the 1048 cm^{-1} band after the approach of the liquid equilibrium. The *Gg* concentration is constant over time (Figure 3.14). Nevertheless, the variation of the 973 cm^{-1} band, associated to the *Gt* + *Tt* sequences in the O-CH_2-CH_2-O moiety, can infer the *trans* glycolic pre-ordering up to the aging at 68 °C. This indicates that a small quantity of *Tg* conformers, not associated to any absorption band so far, could presumably rearrange in ordered *Tt* sequences. The proposed scenario could explain all the experimental observation on conformational rearrangements observed by time-resolved FTIR during the physical aging of PET below the glass transition temperature. At this stage, it could be important to compare FTIR experimental results with those obtained by calorimetry. For this purpose, in order to verify the existence of the double relaxation mechanism, a DSC analysis was performed on the sample aged at 68 °C. Finally, PET isothermal aging in the temperature range between 65 and 80 °C were performed by means of the Fast Scanning Calorimetry (FSC) technique.

In order to compare the FTIR data with DSC results, the T_f -T_a curves calculated from R ratio and the 1048 cm^{-1} band for the aging at 68 °C were showed as a function of the aging time in Figure 3.16. Furthermore, a DSC analysis was performed on the aging at 68 °C for PET at the time-scale of the intermediate plateau. The results were reported together with those of FTIR analysis in Figure 3.16.

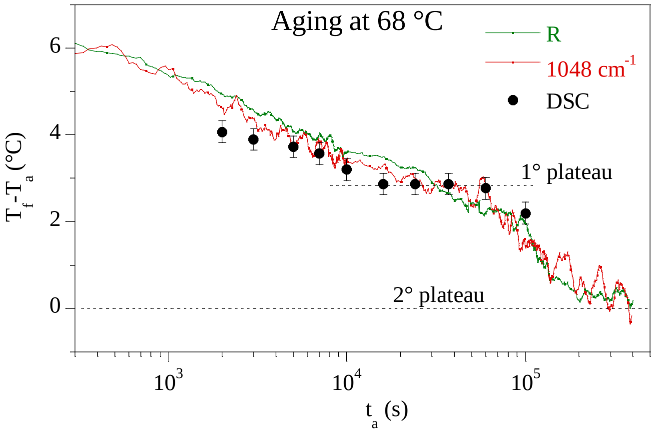

Figure 3.16. T_f –T_a relaxation curves calculated from the R ratio, the 1048 cm^{-1} band and from enthalpic recovery calculation (DSC) of PET aged at 68 °C. Short-dashed lines represents the two plateaus associated to the double relaxation mechanism.

The T_f -T_a curves calculated by FTIR and DSC were almost superimposed in the whole experiment time range. The double relaxation of the T_f-T_a curves, with an intermediate plateau between 20000 and 50000 s, was confirmed also by the elaboration based on the enthalpic recovery. Additionally, the almost coincident T_f-T_a curves from the aging at 68 °C of DSC and FTIR analysis strongly suggested that the ethylenic conformational transition $T \rightarrow G$ was responsible of the relaxation of the glass toward the extrapolated liquid equilibrium, being the major source of enthalpy loss during the aging in order to approach equilibrium.

Besides, the physical aging of PET was studied by FSC, in order to retrieve information on the short-time scales on the relaxation of glasses. FSC uses very high cooling and heating rates, up to 1000 °C/s, allowing the analysis of extremely fast relaxation mechanism starting from the first milliseconds. Figure 3.17 displayed the $T_f - T_a$ variation over aging time calculated by the enthalpic recovery on the subsequent heating for aging between 65 and 80 °C.

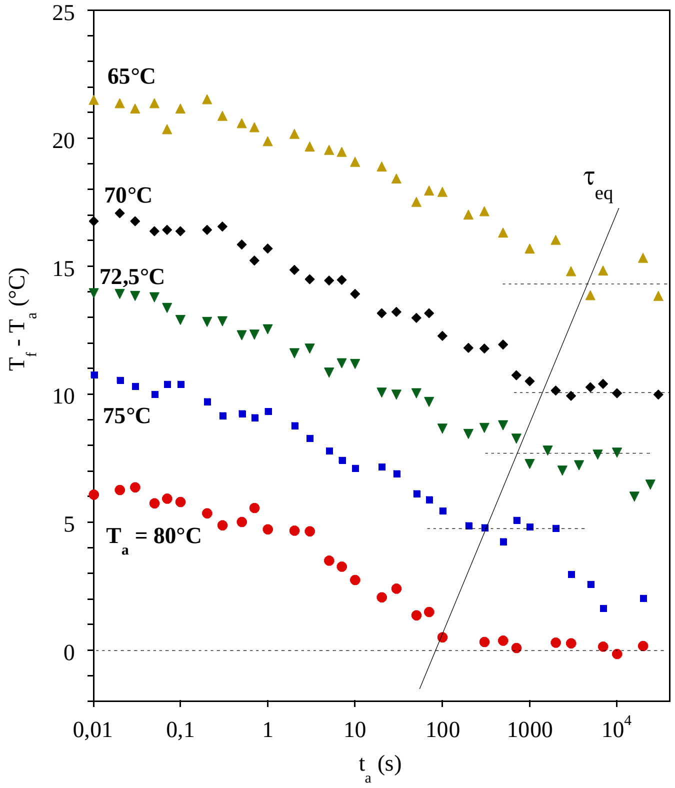

Figure 3.17. $T_f - T_a$ as a function of aging time calculated by the evolution of enthalpic recovery during the subsequent heating scan, for aging at different temperatures. Short-dashed lines represents the intermediate plateau reached by the relaxing glasses, meanwhile the solid line is a guide for the eye to evidence the shift of the equilibration time (τ_{eq}).

The $T_f - T_a$ showed an overall decrease over time, sign of the enthalpic relaxation of the glass toward the extrapolated liquid equilibrium. All the PET samples cooled at 1000 °C/s showed an initial $T_{f\,(t=0)}$ = 86 °C, 10 °C higher than the fictive temperature of 76 °C measured at the start of the FTIR aging. This discrepancy was simply attributed to the kinetic nature of the glass transition, that shift at higher temperatures with increasing the cooling rates, being 3000 times faster for the FSC analysis compared to the FTIR (60000 °C/min vs 2 °C/min). The glasses obtained in this way had a higher content of excess quantity of the thermodynamic properties that those obtained by slow cooling, hence a higher driving force of sample transformation and lower stability. The evolution of $T_f - T_a$ over time, proportional to the driving force, showed also in this case a non-monotonic trend of the relaxation phenomena and the presence of an intermediate plateau.[33-35] Only the sample aged at 80 °C reached the extrapolated liquid equilibrium with a singular relaxation, meanwhile the others could not reach the liquid equilibrium in the relatively short time-scale of the experiment. Hence, the time required to reach the equilibrium increases (2° plateau) and the intermediate plateau (1° plateau) shift to higher aging times by decreasing the temperature, as seen by time-resolved FTIR analysis previously.

For the understanding of the two-decay equilibration mechanisms, linked to the existence of two different plateaus in the relaxation kinetics for both FTIR and FSC analysis, some thermodynamic and kinetic characterization was made. Firstly, the thermodynamic aspect of the intermediate plateau appearing during the glassy relaxation could be evidenced by plotting the fictive temperature calculated at the first equilibration and, if present, at the second step as function of the aging temperature (Figure 3.18).

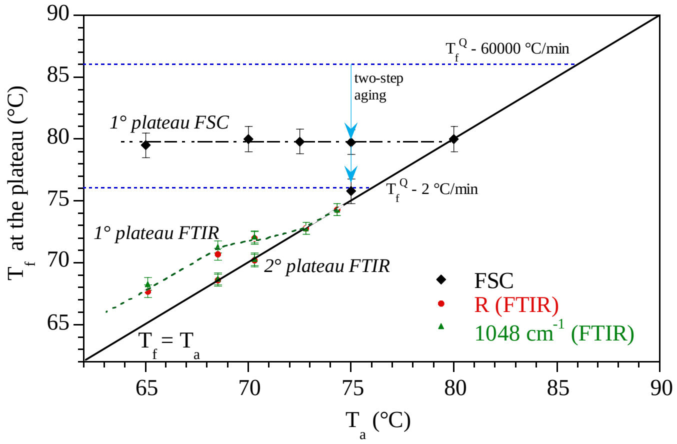

Figure 3.18. Fictive temperature calculated at the intermediate and, if present, at the final equilibration obtained from FSC data and from time-resolved FTIR analysis (R and 1048 cm^{-1}) as function of the aging temperature. Tf = Ta solid line indicates the liquid equilibrium, T_f^Q is the fictive temperature of the unrelaxed glass cooled at 60000 °C/min (FSC) and at 2 °C/min (FTIR). The arrows indicate schematically the double-step aging.

From the fictive temperature data of the intermediate plateau a complex scenario emerged for the relaxation of the glassy state. As for as the FSC data, the fictive temperature of the unrelaxed glass started from the highest temperature of 86 °C. The first equilibration mechanism led to a partial relaxation up to a fictive temperature of 80 °C independently from the aging temperature (black diamonds, Figure 3.18). After the first relaxation step, in the time-scale of the FSC experiment only the sample aged at 75 °C showed the second relaxation and reached the extrapolated liquid equilibrium. As for the FTIR analysis, the T_f of the slowly cooled glass started from 76 °C, below the 1° plateau observed by FSC data. In the aging evolution, by decreasing the aging temperature, the R and 1048 cm^{-1} experienced a change of the relaxation behavior from a single plateau (A74 and A73 samples) to a double-step decay with the appearance of an intermediate equilibrium (A70, A68 and A65 samples). The first FTIR plateau was characterized by a fictive temperature much lower than that observed for FSC analysis. Being ruled by the same conformational transition, namely the ethylene *T* to *G* rearrangement, both R and 1048 cm^{-1} highlighted at lower temperature a common 1° plateau and the last equilibration mechanism that led to the 2° plateau, coinciding with liquid equilibrium.

Hence, the analysis of the fictive temperatures characterizing the enthalpic states of the metastable equilibria in the energy landscape of glassy PET delineated a scenario in which three different metastable equilibria were possible. From higher to low energy content, the first at T_f = 80 °C was highlighted by the analysis of unstable PET glasses by FSC, the second was observed below 70 °C from FTIR analysis and finally the third corresponding to the energy minimum of the liquid equilibrium. The interpretation of the experimental results is not straightforward, and at this point of the research, some hypothesis could be proposed, taking in mind that further experiments should be done to have a clearer picture of the described phenomena. However, the kinetics analysis for the three different mechanisms associated to three different metastable equilibria could help the interpretation. As characteristic kinetics parameter, the equilibration time τ_{eq}, defined as the time needed for the system to reach the equilibrium, was calculated for the FSC 1° plateau and for the 1048 cm^{-1} and R 1° and 2° plateaus. The logarithm of the equilibration times for each of the three mechanism were plotted against the inverse temperature, in the Arrhenius plot of Figure 3.19.

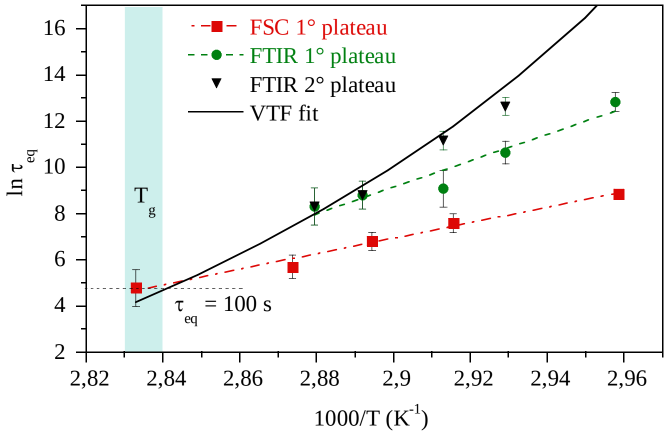

Figure 3.19. Arrhenius plot for the three mechanisms seen in FSC and time-resolved FTIR analysis. Blue shaded area defined the standard glass transition region with characteristic equilibration time of 100 s.

Being the equilibration times of the two relaxation mechanisms nearly coincident for the R ratio and the 1048 cm^{-1} band, it was chosen to plot the average between the two, labeled generically as “FTIR”. The Arrhenius plot of the equilibration time showed different temperature dependence for the three mechanisms. As expected, FSC analysis highlighted the fastest relaxation process of PET in the glassy state. The fast mechanism follows an Arrhenius relationship with a constant activation energy of 280 ± 20 kJ/mol. Concerning the other two relaxation mechanisms revealed by time-resolved FTIR, the two equilibration times merge at higher temperature, meanwhile they split below 70 °C. The equilibration time of the two processes, associated to the first (intermediate) and second (liquid equilibrium) plateaus, seemed to have a linear temperature dependence in the Arrhenius plot, with higher activation energies respect to the FSC relaxation. In fact, for the relaxation associated to the FTIR first plateau we calculated an activation energy of 480 ± 80 kJ/mol, meanwhile, for the slower mechanism associated to the relaxation toward the liquid equilibrium, a 760 ± 70 kJ/mol activation energy was found, in agreement with the 790 kJ/mol value obtained by DMA studies.[17] In the case of the slower relaxation, a fitting using the empirical VFT relationship was performed, showed in equation 3.6, and the VFT parameters were compared with those reported in literature from dielectric spectroscopy measures.[36-38]

$$\ln \tau_{eq} = 2.303(A + B/(T - T_{\infty})) \qquad \text{Eq. 3.6}$$

where A is the preexponential factor, B is the Vogel activation energy and T_{∞} is the temperature at which the relaxation time diverges. In Table 3.4 the fitting parameters used for the VTF fit in Figure 3.19 was reported and compared with two set of parameters used to fit the dielectric alfa relaxation.

Table 3.4. VFT fitting parameters comparison between experimental data and calculated by dielectric spectroscopy

	A	B (K)	T_{∞} (K)
Experimental	-8.12	397	313 (T_g – 40 °C)
Dielectric spectroscopy [Ref 36]	-11.3	397.7	315.6
Dielectric spectroscopy [Ref 37]	-11.07	404	318

The good accordance between the experimental VTF parameters for the slower FTIR relaxation and the fitting parameters for the dielectric alpha relaxation highlighted that the equilibration time had the same temperature dependence. Hence, the relaxation phenomena seen for the R ratio and the 1048 cm^{-1} band, which bring about to the extrapolated liquid equilibrium, could be related to the PET alpha process.

In conclusion, a tentative explanation was given for the three different mechanisms observed in the PET glassy state relaxation toward the equilibrium. As far as the FTIR measurements for the R ratio and 1048 cm^{-1} band, an ethylenic conformational rearrangements from *T* to *G* forms was observed, causing the major part of the enthalpy loss measured by calorimetry. This rearrangement, nevertheless, showed a complex relaxation kinetics, exhibiting two different mechanisms with different temperature dependency. The first, faster process with lower activation energy (Ea = 480 ± 80 kJ/mol) led the glassy PET to an intermediate metastable equilibrium, characterized by a higher concentration of *T* conformers and higher enthalpic content. The second slow process was associated to the $T \rightarrow G$ ethylenic rearrangement toward the extrapolated liquid equilibrium. This relaxation led to a completely relaxed glass, with structural and thermodynamic properties equal to that of the liquid. The temperature dependence of such relaxation showed a higher activation energy (Ea = 760 ± 70 kJ/mol) in accordance to that calculated for the alpha relaxation by DMA measurements.[17] Moreover, the temperature dependence followed the VTF law of the alpha relaxation calculated by dielectric measurements.[36,37] This results strongly indicated that the conformational rearrangement of the ethylenic units from the *Trans* to the *Gauche* forms plays a substantial role during the physical aging of PET. The overall relaxation is characterized by a rapid non-cooperative process, characterized by a lower activation energy and a linear Arrhenius temperature dependence, followed by a delayed slow cooperative transformation associated to the alpha relaxation, characterized by a non-linear VTF temperature dependence, a typical of the glass transition, involving a cooperative rearranging region, 2.5 ± 1 nm length.[38] Moreover, by FSC measurements, another very rapid non-cooperative relaxation was highlighted in the higher energy landscape of the glassy PET. It was probable that also this process could originate from the ethylenic $T \rightarrow G$ non-cooperative transition, because of the high enthalpy loss associated to it.

Ultimately, time-resolved FTIR measurements highlighted another kinetically slow transition of different nature that took place in proximity of the glass transition, namely the conformational rearrangements from the *gauche* to the *trans* form of the glycolic unit, by rotation around the O-CH_2 bond. The transformation increased in intensity by increasing the aging temperature, and occurred as soon as the glassy PET approached the extrapolated liquid equilibrium by mean of the other mechanisms previously described. This process could be considered as a segmental chains pre-ordering that occurs prior to the crystallization, already hypothesized or observed. Such stiff chain segments may favor the formation of crystalline nuclei, that can not be observed directly, and promote the early cold-crystallization. This phenomenon explains the depression of the crystallization temperature of samples aged in proximity to the T_g, as shown by the A73 and A74 PET samples in Figure 3.10.

3.3.5 Annealing above the glass transition: study of the pre-ordering process by FTIR and DSC

In the following section the conformational rearrangements occurring during the annealing above the glass transition region are discussed. A set of PET samples were annealed isothermally at different temperatures in a range between 76 and 84 °C. The intensity variation of conformational bands centered at 1370, 1340, 1048, 973 and 841 cm^{-1} were followed over time by means of time-resolved FTIR. For the higher annealing temperature, at 84 °C, a DSC study was performed on the effect of the annealing on PET cold-crystallization kinetics. Finally, from the characteristic time of relaxation calculated by the glycolic *gauche-trans* sensible bands, an activation energy for the pre-ordering process was determined.

From the comparison of WAXD, SAXS and SANS measurements of a PET sample annealed just above the glass transition temperature, Imai[22,23] theorized that an ordering phenomena occurred prior to the cold-crystallization, involving two steps. Firstly, a conformational rearrangement, due to the high segmental mobility of the liquid phase, brings about the formation of *all-trans* glycolic units $O\text{-}CH_2\text{-}CH_2\text{-}O$ that increased the stiffness of chain segments. Reached a critical length, a spinoidal decomposition took place comprising the parallel ordering between the rod-like chain segment, that could eventually form crystalline nuclei. The pre-ordering of PET chain segments was measured also by NMR,[28] that confirmed an increase of *trans* conformers in the glycolic unit prior to the onset of cold-crystallization. However, it is important to remark that such sample evolution up to the crystallization, which excludes the typical nucleation and growth mechanism, has been source of a hard debate among the scientific community. Another mechanism was proposed by Androsh,[44] performing experiments with FSC and applying the Tamman two-stage protocol (see Paragraph 1.3.5). The temperature program involved a stage of nucleation slight above T_g for different times followed by a rapid heating up to the growth stage. This procedure allows the nuclei eventually formed in the nucleation stage to grow, and successively record in a subsequent heating scan an appreciable heat flow signal generated by the melting of the crystalline phase. FSC results highlighted that by heating the system the nuclei formed during the nucleation stage did not survived, but a melting/disordering−reorganization process with continuously increasing size and stability of the nuclei on heating took place.

Alternatively, the idea of the presence of a preordering step before the three-dimensional crystalline structure formation, have been partially proposed again by Strobl. He had argued that in all polymer crystallization process, a mesophase precursor phase is first formed before the crystalline phase.[39,40]

In order to study the sequential conformational ordering of the PET chain, an isothermal annealing at 84 °C, about 5 °C above the T_g , was followed by time-resolved FTIR. This annealing temperature, slight above the T_g, was chosen to have a long induction period prior to the cold-crystallization, allowing to study the conformational rearrangement that could eventually occur in this latency time. Figure 3.20 reports the relative intensity variation as a function of annealing time of R ratio, the 1048, 973 and 841 cm^{-1} absorption bands, normalized for the value at the start of the annealing for the value at the start of the annealing.

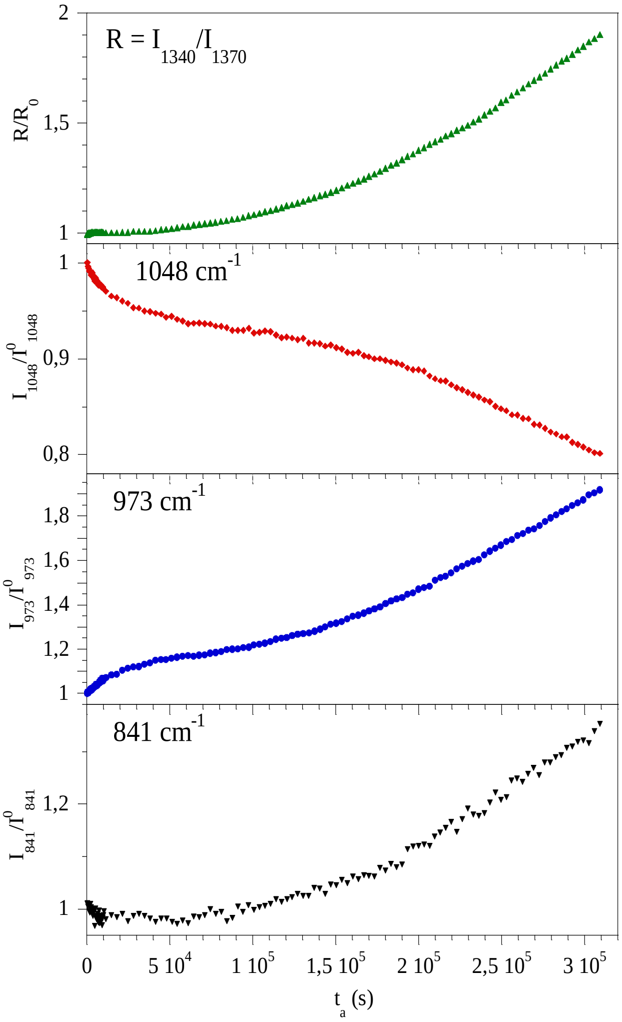

Figure 3.20. R ratio, 1048, 973 and 841 cm^{-1} variation over time for a PET annealed at 84 °C.

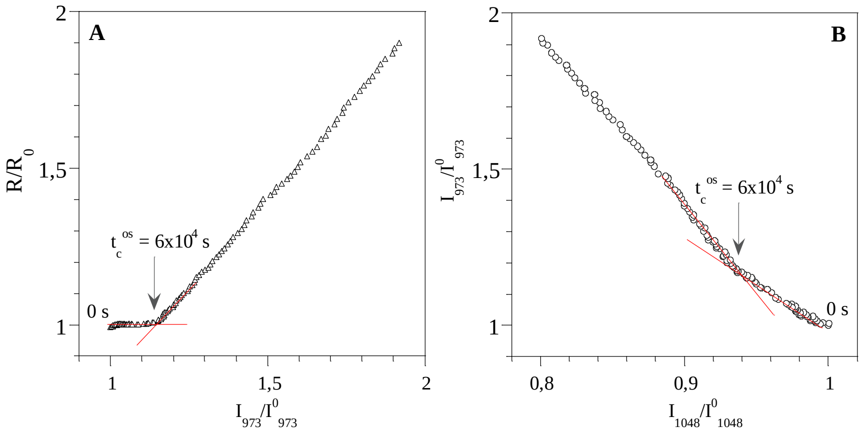

Figure 3.21 Correlation plot R/R_0 vs I_{973}/I^0_{973} (A) and I_{973}/I^0_{973} vs I_{1048}/I^0_{1048} (B)

In order to better understand the different kinetics between absorption bands, it is worth to remind the different assignment to absorption bands and their differences between the amorphous and crystalline phases of PET, studied by factorial analysis (see Table 3.3). For the amorphous phase, the R ratio is proportional to the *trans*/*gauche* ratio of the ethylene units (*T/G*), meanwhile the 1048 cm^{-1} and the 973 cm^{-1} bands are associated to the combination of ethylene and glycolic conformational sequences *Gg* (1048) and *Gt* + *Tt* (973). The crystalline phase of PET is characterized by ordered string-like segments in all-trans conformation (TtT_B), namely the ordering of the terephthalate unit with the O-CH2-CH2-O glycolic unit on the same plane. The 1340, 973 and 841 cm^{-1} conformational bands are sensible to this peculiar ordered conformation, leading to a sharper and more intense bands respect to those relative to the amorphous phase. Furthermore, the band centered at 841 cm^{-1} is related only to the crystalline phase.

From the Figure 3.20, a clear discrepancy for the time evolution of different bands emerges, with the possibility to distinguish two different transformations. The R ratio and the relative intensity of the 841 cm^{-1} band seemed to possess a common kinetics. At the first stages of the experiment, both R and 841 cm^{-1} remained constant up to about 60000 s, at which an abrupt increase took place. Nevertheless, the relative intensities for 973 and 1048 cm^{-1} bands began to variate immediately from the start of the experiment, showing an initial conformational rearrangement that continued similarly to the late process already highlighted by the R ratio and the 841 cm^{-1} relative intensities.

For sake of comparison, correlation plots were performed between the R and the 973 cm^{-1} band relative intensity variations, and between the 973 cm^{-1} and 1048 cm^{-1} bands during the annealing at 84 °C, showed in Figure 3.21. In the R vs. 973 plot (Figure 3.21 A), a double trend was observed. At the start to the experiment (point t = 0 s) there was no correlation between the relative intensity of 973 cm^{-1} that began to increase immediately, meanwhile the R ratio remained constant (vertical line, Figure 3.21 A). From 60000 s up to the end of the experiment, a positive linear correlation between the two relative intensities was observed, indicating at 60000 s the onset of the cold-crystallization (t_c^{os}, Figure 3.21 A) with the increasing of ordered PET segments in all-trans conformation (TtT_B). Regarding the correlation between the 973 cm^{-1} band (*Gt*+*Tt* amorphous, TtT_B crystalline) and the 1048 cm^{-1} band (*Gg*), two different linear regimes were observed. Below 60000 s, the first regime was associated to the transformation Gg→Gt , involving the increase of 973 cm^{-1} intensity at the expense of the 1048 cm^{-1}. At 60000 s (t_c^{os}, Figure 3.21 B), like the 973 vs R correlation plot, an abrupt change of the slope was observed, indicating an increase of the absorptivity of the 973 cm^{-1} band probably due to the intense absorption of ordered sequences TtT_B.

Hence, from the kinetics data of the annealing at 84 °C a probable scenario was proposed, involving two distinct processes. In figure 3.22, the scheme of the evolution of a portion of the PET chain is reported.

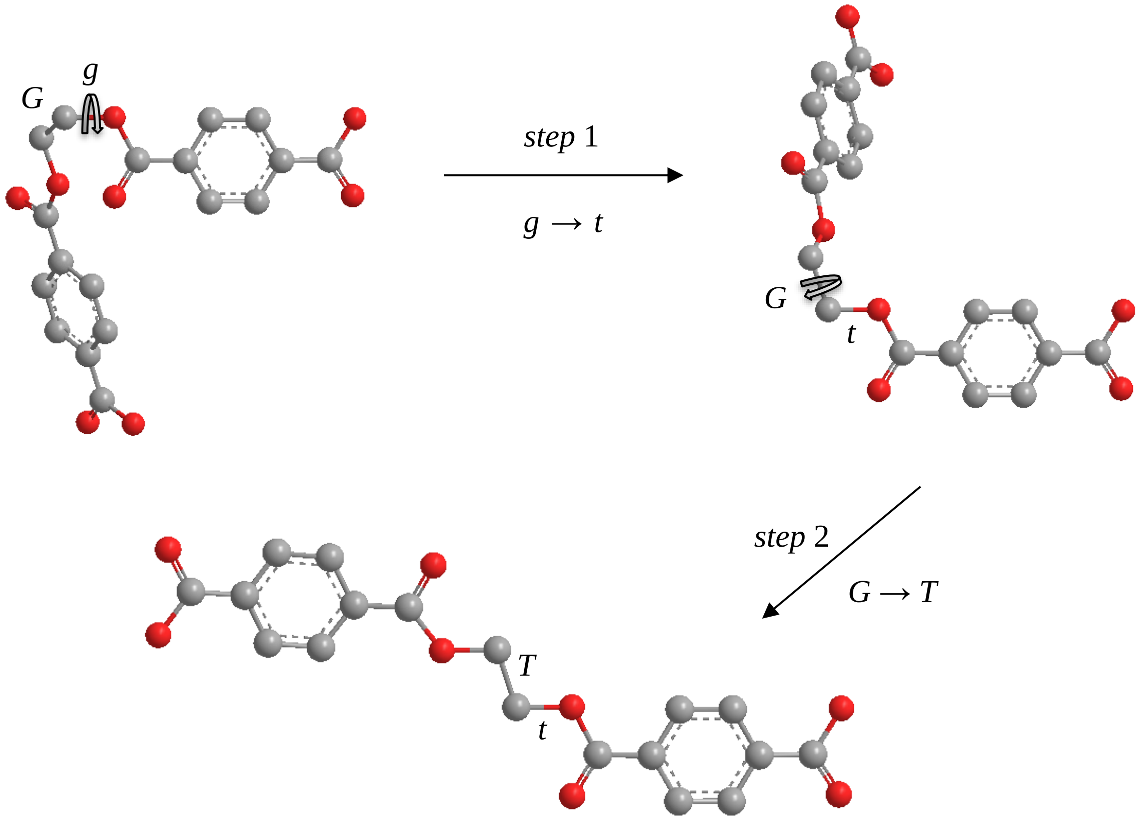

Figure 3.22. Scheme of the evolution of a portion of the PET chain during the annealing at $T>T_g$.

The polymer chains, being above the glass transition, had the segmental mobility needed to conformationally and spatially ordering to form crystalline nuclei and eventually small crystals. In a preliminary phase of the annealing, corresponding to the induction period of the crystallization, the conformational rearrangements of the glycolic units $O\text{-}CH_2$ from the gauche (g) to the trans (t) form took place (step 1 in figure 3.22). The rotation around the glycolic bond, defined as “pre-ordering” process, allows the ethylenic group ($CH_2\text{-}CH_2$), both in trans or gauche conformation, to arrange in the same plane of the adjacent terephthalic unit. In the second phase of the annealing, at the onset of the cold-crystallization, the strand chain segments formed during the pre-ordering process starts to order sequentially along the chain (step 2 in figure 3.22). The rotation around the ethylenic bond $CH_2\text{-}CH_2$ allows the *gauche* ethylene units (G) to transform into the *trans* form (T), causing the formation of an all-trans chain segment (TtT_B) that lies on the same plane. Finally, the conformational ordering in string sequences allow the chains to order parallelly and form the crystalline structure (see Introduction, Figure 1.9).

The hypothesis of the pre-ordering process prior to the crystallization was confirmed by the factor analysis performed on the PET spectral variations during the annealing at 84 °C. For the analysis, the same experimental conditions were used respect to that performed on the heating scan of quenched and aged samples (2.3.2 Factor analysis on the heating of quenched and aged PET). Figure 3.23 displays the variation of the relative fraction of the G, TX and TC phases of PET as function of the annealing time at 84 °C.

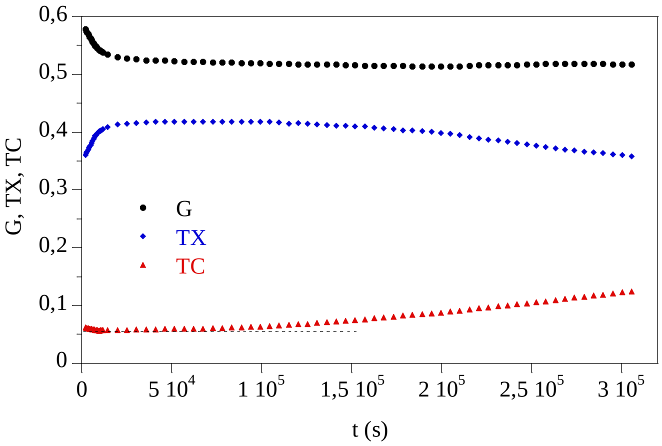

Figure 3.23. Variation of the relative content of G (gauche-rich amorphous phase), TX (trans-rich amorphous phase) and TC (crystalline phase) of PET as function of the annealing time at 84 °C.

As far as the factor analysis of the heating scan (Figure 3.7), the *gauche*-rich amorphous phase of PET was the principal component at the start of the annealing at 84 °C. In the liquid phase, also a small fraction of crystallinity was highlighted, corresponding to about 6 % of the total. In the first stage of the annealing, as expected, the pre-ordering process took place, with an abrupt increase of the *trans*-rich phase (TX) at the expense of the *gauche*-rich amorphous (G) fraction. The crystalline fraction TC remained almost constant up to about $6 \cdot 10^4$ s, at which the cold-crystallization took place with an abrupt increase of the crystalline fraction. It was interesting to note that the pre-ordering process ceased at about 4-$5 \cdot 10^4$ s, and sequentially the cold-crystallization took place, involving the transformation of the *trans*-rich amorphous (TX) in crystalline fraction (TC), meanwhile the G fraction remained unchanged up to the end of the annealing.

In order to investigate the effects of the pre-ordering process on the kinetics of the subsequent cold-crystallization of PET, a DSC analysis was performed on PET samples annealed for different times at 84 °C. Figure 3.24 shows some thermograms recorded on heating at 10 °C/min after an annealing at 84 °C for different times.

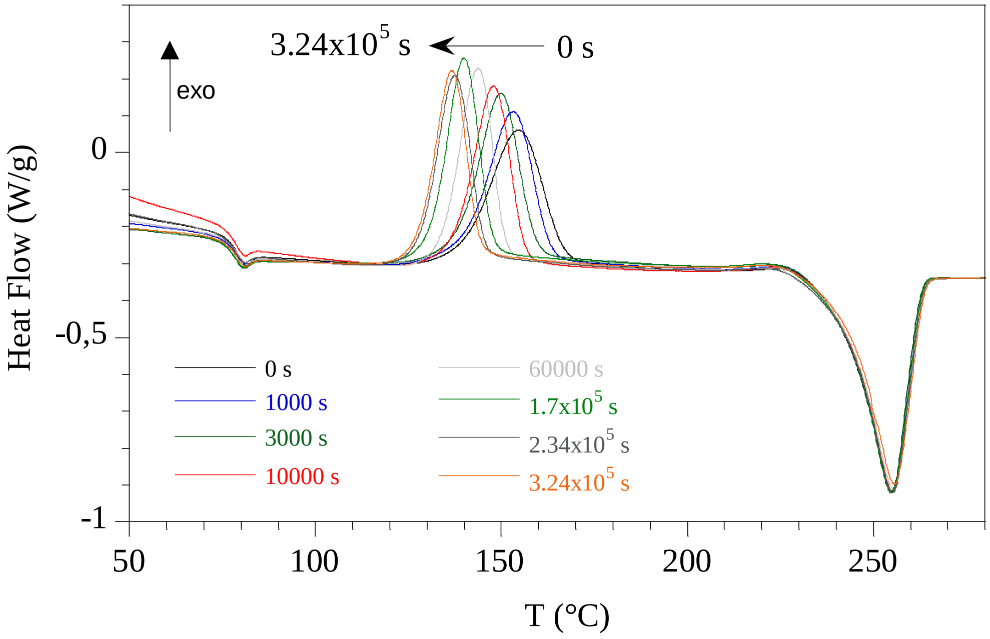

Figure 3.24. DSC thermograms during the heating at 10 °C/min of PET sampled annealed for different times at 84 °C.

DSC curves of Figure 3.24 displays for all the PET samples the glass transition at 77.0 ± 0.5 °C, calculated at the midpoint of the c_p change, the cold-crystallization as an exothermic peak in the range 120-170 °C and the endothermic melting peak at 255 ± 0.5 °C. The glass transition and the melting of PET were independent from the annealing time at 84 °C, meanwhile the cold-crystallization showed an increase of the kinetics and a shift to lower temperature by increasing the annealing time. A clearer picture of the change in the crystallization behavior was displayed in Figure 3.25, where the crystalline conversion X_c, calculated from the exothermic peak of the cold-crystallization, was plotted as function of the temperature for different annealing times.

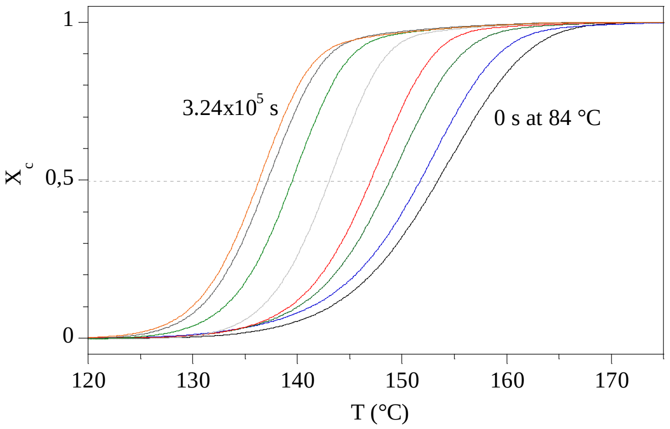

Figure 3.25. Crystalline conversion of the non-isothermal crystallization of melt-quenched PET annealed for different times at 84 °C.

From Figure 3.25, the crystallization temperature at half-conversion $T_c^{0.5}$ and the crystallization rate at half conversion $v^{0.5}$ were calculated as parameters characterizing the crystallization kinetics. Moreover, the crystalline fraction W_c as function of the annealing time was evaluated by the excess between the enthalpy of fusion ΔH_f and the enthalpy of cold-crystallization ΔH_c, normalized for the enthalpy of fusion of the 100% crystalline PET ΔH_f^0. The following the relationship was used:

$$W_c = \frac{\Delta H_f - \Delta H_c}{\Delta H_f^0} \qquad \text{Eq. 3.7}$$

where ΔH_f^0 = 140 J/g, from Ref. 41.

The crystallization temperature and the crystallization rate at half conversion, as well as the crystalline fraction calculated by DSC (W_c) and by FTIR factor analysis (TC) were showed in Figure 3.26 as function of the annealing time at 84 °C.

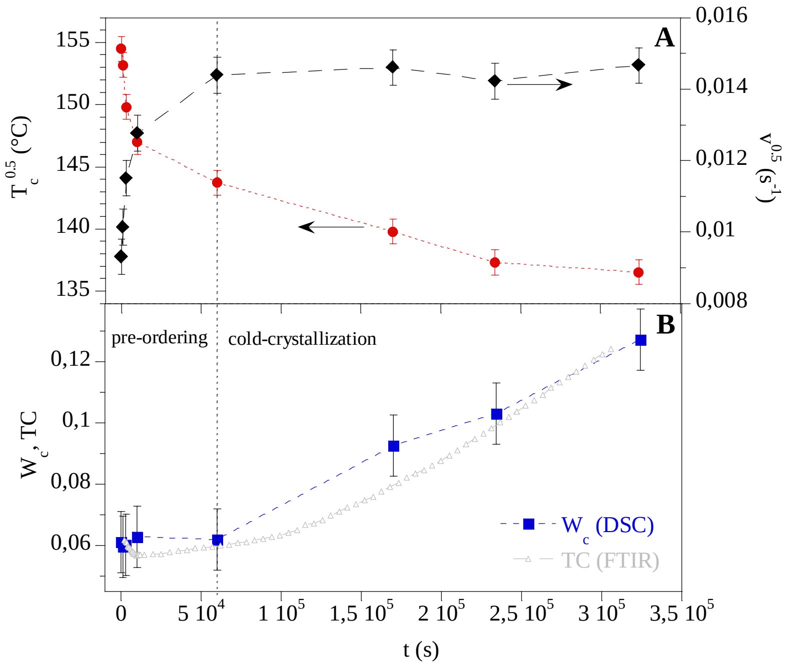

Figure 3.26. Crystallization temperature ($T_c^{0.5}$) and crystallization rate ($v^{0.5}$) at half conversion (upper panel, A); crystalline fraction calculated by DSC (W_c) and by the factor analysis of FTIR spectra (TC) (lower panel B) as function of the annealing time at 84 °C.

For sake of clarity, the vertical dashed line at t_c^{os} = 60000 s was drawn for separating the pre-ordering process from the cold-crystallization. The cold-crystallization temperature at half conversion decreased without any clear discontinuity by increasing the annealing time in the whole range of the experiment. On the other hand, the crystallization rate at half conversion showed an increase during the pre-ordering process and a stabilization at 60000 s, the onset time of the cold-crystallization (Figure 3.26 A). Moreover, the crystalline content of the amorphous PET annealed at 84 °C remained constant at 6 ± 1% up to the onset of the cold-crystallization, time at which an abrupt increase was observed, up to reach a crystalline fraction of 13 ± 1% for the longest annealing. It was interesting to highlight the similar evolution over time of the PET crystalline fraction obtained by independent techniques, namely DSC measurements (filled squares, Figure 3.26 B) and factorial analysis performed on FTIR spectra during the annealing (open triangles, Figure 3.26 B).

Interesting effects were highlighted concerning the crystallization rate and the crystallization temperature at half conversion. The evolution over time of the pre-ordering process, associated to the conformational rearrangement from the *gauche* to the *trans* form by rotation around the glycolic bond O-CH_2, was the main source of the increased kinetics of the subsequent cold-crystallization.

3.3.6 Kinetics study of the pre-ordering process of PET

In the previous section the pre-ordering process occurring on amorphous PET prior to the cold-crystallization was characterized and associated to the *gauche* to *trans* glycolic conformational rearrangement. In order to investigate the kinetics and the temperature dependence of this process, isothermal annealing in a temperature range between 76 and 84 °C, that is in PET liquid phase slight above the glass transition temperature, were followed by time-resolved FTIR. Two glycolic sensible bands, namely the 1048 cm^{-1} (Gg) and the 973 cm^{-1} ($Gt + Tt$), together with the crystalline sensible band at 841 cm^{-1} (TtT_B) were followed as function of annealing time. In particular, Figure 3.27 shows the relative intensity of these three bands over time for the A76, A80, A81, A82, A84 PET samples.

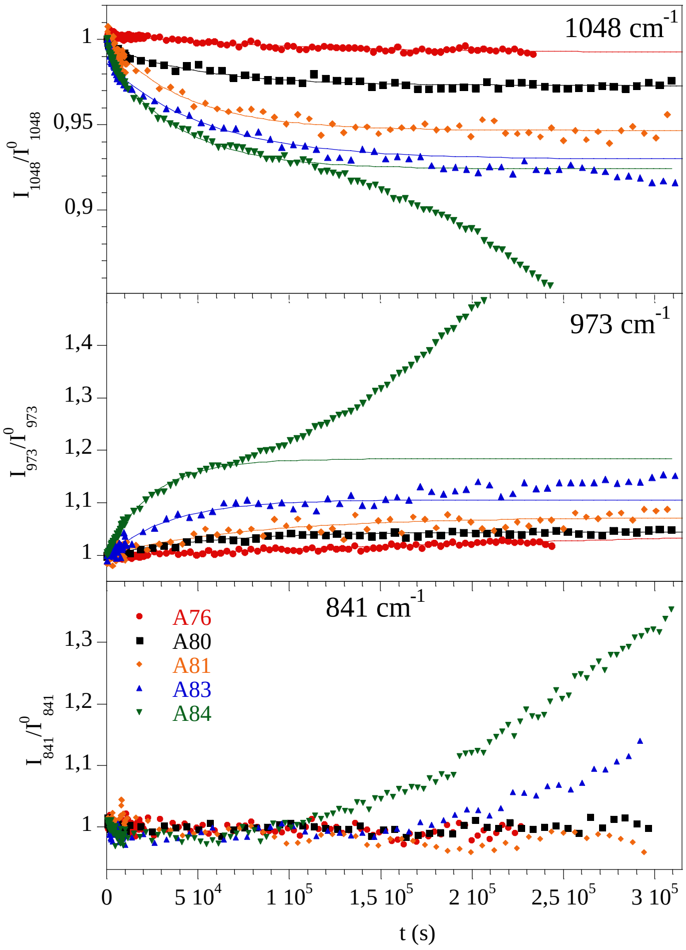

Figure 3.27 Relative intensity calculated for the 1048, 973 and 841 cm^{-1} bands as function of the annealing time at different temperatures: at 76 °C (circle), 80 °C (square), 81°C (diamond), 82.5 °C (up triangle), 84 °C (down triangle). Solid lines represent the best fit of the pre-ordering process, fitted by a Debye function (pure exponential).

For the 1048 cm^{-1} band, the pre-ordering process was observed as a decay of the intensity over time from the early stages of the annealing, meanwhile the correlated 973 cm^{-1} band increased. The intensity of the 841 cm^{-1} band, correlated to the ordered sequences *TtT$_B$*, was not affected by the pre-ordering process, hence, it was sensible only to the crystallization. For the low temperature annealing A76, A80 and A81, in the glass transition region, the cold-crystallization process was not observed in the explored annealing time period. For the annealing at 82.5 °C (A83) and at 84 °C (A84) the onset of the crystallization was calculated by the first departure of the 841 cm^{-1} relative intensity. The start of the cold-crystallization was found at t_c^{os} of $1.5\cdot10^5$ s for A83 and $6\cdot10^4$ s for the A84 sample.

As far as the kinetics of the pre-ordering process, it was observed an exponential relationship for the 1048 cm^{-1} and the 973 cm^{-1} bands. The pre-ordering time region of the relative intensities for these two bands were fitted by a Debye function[42] (solid lines, Figure 3.26), characterized a unique characteristic time τ, hence, a pure exponential decay (Equations 3.8 and 3.9)

$$\frac{I_{1048}}{I^0_{1048}} = A + B \cdot exp\left(-\frac{t}{\tau}\right) \qquad \text{Eq 3.8}$$

$$\frac{I_{973}}{I^0_{973}} = A + B\left(1 - exp\left(-\frac{t}{\tau}\right)\right) \qquad \text{Eq 3.9}$$

where A is the offset, B in the decay intensity and τ is the characteristic time of the decay.

By increasing the annealing temperature, it was observed an increase in the intensity of the decay and a decrease of the characteristic time for both the absorption bands. Moreover, for the 973 and 1048 cm^{-1} bands of the A83 and A84 PET samples, the incipient cold-crystallization occurred at the last stages of the pre-ordering process causing the departure from the Debye's decay fitting.

The temperature dependence of the pre-ordering process was investigated by plotting in an Arrhenius plot the natural logarithm of the characteristic time for the decay as function of the inverse temperature, as showed in Figure 3.28. It is worth noticing that the characteristic times calculated for the 973 and 1048 cm^{-1} were almost coincident for each annealing temperature, being the bands correlated and, hence, the average characteristic time was showed in Figure 3.28.

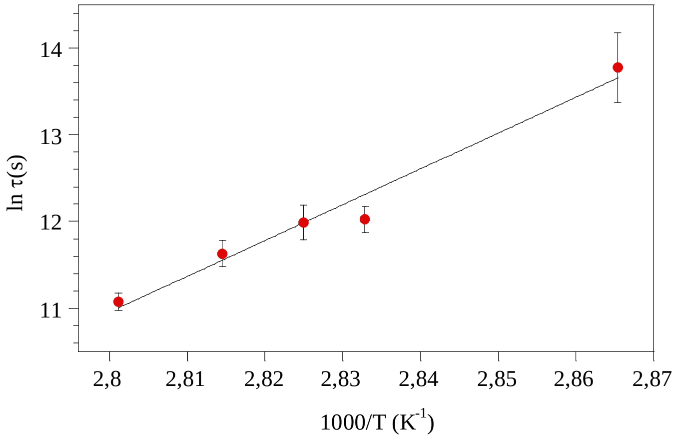

Figure 3.28. Arrhenius plot of the pre-ordering process of PET. The characteristic time was calculated as the average of the values derived from of the 1048 and 973 cm^{-1} bands.

The temperature dependence of the preordering process appeared to follow an Arrhenius relationship, with constant activation energy of 340 ± 40 kJ/mol. As far as the author knowledge, this is the first direct FTIR measurement of the time evolution during the annealing slight above T_g of absorption bands correlated to the *gauche* and *trans* glycolic conformers. The transformation of the glycolic *gauche* form to the *trans* could be associated definitively to the pre-ordering phenomenon of PET, observed also by Imai[22,23] and Chang[28]. This process forms stiffer and more ordered chain segments, that favors the kinetics of the cold-crystallization. It was interesting to note that the pre-ordering process at temperatures slight above the glass transition occurs in the induction period of the crystallization, with a kinetics evolution that was described accurately by an exponential decay function. Indeed, the glycolic *gauche* to *trans* rearrangement could be characterized by a unique relaxation time, differently to the relaxation processes below the glass transition temperature that occurs generally with a distribution of relaxation times, following a KWW decay[42], given by the heterogeneity of the glassy system. Hence, the pre-ordering process occurs in a homogeneous system characteristic of the liquid state. Ultimately, the Arrhenius-like temperature dependence highlighted the non-cooperative nature of this phenomenon.

3.4 CONCLUSION

In the present research the conformational behavior of the amorphous PET in the glass transition region was studies by a combination of the new MTFTIR technique, time-resolved FTIR, factor analysis of infrared spectra, DSC and FSC analysis. Firstly, the Modulated Temperature FTIR allowed to study separately the reversing and non-reversing transition of PET during the glass transition and the cold-crystallization. The technique highlighted and separated superimposed transition of different nature. In the glass phase, the unaged glass may undergo *dynamic aging*, an out-of-equilibrium phenomenon (non-reversing) assigned to the ethylenic $T \rightarrow G$ transition, that allow a better packing of polymer chains in disordered structure. The reversing devitrification at the glass transition was separated to the superimposed non-reversing relaxation recovery, caused by the retrieve of equilibrium concentration of the *gauche-trans* ethylenic conformation. Prior to the non-reversing cold-crystallization, the MTFTIR allowed to separate from the equilibrium conformational rearrangements of ethylenic *gauche-trans* (reversing) a kinetic pre-ordering process involving the formation of *trans* sequences, that could favor the early cold-crystallization. These results were the first insights of an extensive investigation on the conformational transition occurring during the physical aging and the pre-ordering phenomenon of PET in glassy and liquid state. By means of factor analysis, infrared absorption bands were associated more precisely to peculiar conformers, or conformational sequences in the chain of PET. The effects of physical aging below the glass transition on the kinetics of the cold-crystallization was studied by MTFTIR. It was observed that two phenomena contribute to the depression of the crystallization temperature during the aging below the glass transition, namely the physical aging with concomitant formation of "cohesional entanglements"[11,12] and the pre-ordering process, responsible to the formation of ordered chain segments.

In order to characterize the relaxation below and above the glass transition of PET, an extensive kinetic study was performed by means of time-resolved FTIR, DSC and FSC. The time evolution of the intensity of infrared absorption bands, and of the endothermic peak of enthalpic recovery (DSC and FSC), were followed. Two principal mechanisms of relaxation were highlighted, concerning the relaxation of the glass toward the metastable liquid equilibrium and the formation of ordered *trans* segments that are favored by the stable crystalline equilibrium. The first was associated to the ethylenic *T*→*G* transformation, occurring in the glassy state, that allow a better packing of the amorphous chain. FTIR, DSC and FSC combined kinetics study highlighted three consecutive relaxation processes associated to this conformational rearrangement, possessing different time-scales[33-35]:

- Very fast non-cooperative *T*→*G* relaxation, occurring in unstable glasses (analyzed by FSC), allowing the glass to reach a high enthalpy equilibrium state.
- Fast non-cooperative *T*→*G* relaxation, allowing the glass to relax up to an intermediate equilibrium.
- Slow cooperative α process, up to the reach of the liquid equilibrium.

The second mechanism was associated to the rearrangement from the glycolic *gauche* to the *trans* form (*g*→*t* transition). This process, assigned to the pre-ordering process observed by Imai and others[22,23,28] involves the rotation of the chain around the glycolic bond O-CH_2, allowing to the ethylene bond and the adjacent terephthalate unit to lie on the same plane. Hence, chain segments become stiffer, allowing the subsequent parallel ordering in order to form crystalline nuclei and eventually crystallization. The pre-ordering process was observed mostly in the liquid state, occurring during the induction period of the cold-crystallization. Here, time-resolved FTIR allowed to characterize for the first time the kinetics of the pre-ordering of PET, highlighting a Debye-like relaxation and an Arrhenius-like temperature dependence with an activation energy of 340 ± 40 kJ/mol. Moreover, the *g*→*t* transition was observed also in the glassy state of PET. As soon as the physical aging, namely *T*→*G* conformational transition of ethylenic group CH_2-CH_2 ceases and the liquid equilibrium was retrieved, the conformational rearrangement of glycolic group activates.

Ultimately, the research on PET showed the potentiality of the MTFTIR technique in acquiring new information at a molecular level. Merging the potentiality of a spectroscopic analysis with the ability to separate reversible from non-reversible processes occurring in polymers reveals new useful thermodynamic information on the conformational state of the system. Another key advantage showed in this research was the strength of combining DSC with FTIR analysis, giving new insights at a molecular level on the transformations occurring in PET, not only during the main phase transitions, as the cold-crystallization and the glass transition, but also during the permanence in the glassy and in the liquid state.

3.5 REFERENCES

(1) Riga, A. T., & Judovits, L. (2001, June). Materials characterization by dynamic and modulated thermal analytical techniques. ASTM. Haines, P. J. (2012). Thermal methods of analysis: principles, applications and problems. Springer Science & Business Media.B

(2) Reading, M., Elliott, D., & Hill, V. (1993). A new approach to the calorimetric investigation of physical and chemical transitions. *Journal of thermal analysis and calorimetry*, *40*(3), 949-955.

(3) Blaine, R. L., & Hahn, B. K. (1998). Obtaining kinetic parameters by modulated thermogravimetry. *Journal of thermal analysis and calorimetry*, *54*(2), 695-704.

(4) Efremov, M. Y., Kiyanova, A. V., Last, J., Soofi, S. S., Thode, C., & Nealey, P. F. (2012). Glass transition in thin supported polystyrene films probed by temperature-modulated ellipsometry in vacuum. *Physical Review E*, *86*(2), 021501.

(5) Pan, P., Zhu, B., Kai, W., Dong, T., & Inoue, Y. (2008). Polymorphic transition in disordered poly (L-lactide) crystals induced by annealing at elevated temperatures. *Macromolecules*, *41*(12), 4296-4304. Turi, E. (Ed.). (2012). Thermal characterization of polymeric materials. Elsevier.

(6) Reddy, K. R., Tashiro, K., Sakurai, T., Yamaguchi, N., Sasaki, S., Masunaga, H., & Takata, M. (2009). Isothermal crystallization behavior of isotactic polypropylene H/D blends as viewed from time-resolved FTIR and synchrotron SAXS/WAXD measurements. *Macromolecules*, *42*(12), 4191-4199.

(7) Caminiti, R., D'Ilario, L., Martinelli, A., Piozzi, A., & Sadun, C. (1997). DSC, FT-IR, and energy dispersive X-ray diffraction applied to the study of the glass transition of poly (p-phenylene sulfide). *Macromolecules*, *30*(25), 7970-7976.

(8) Caminiti, R., D'Ilario, L., Martinelli, A., & Piozzi, A. (2001). Poly (p-phenylene sulfide) Isothermal Cold Crystallization Investigated by Usual and Unusual Methods. *Macromolecular Chemistry and Physics*, *202*(14), 2902-2914.

(9) Lu, X., & Hay, J. N. (2000). The effect of physical aging on the rates of cold crystallization of poly (ethylene terephthalate). Polymer, 41(20), 7427-7436.

(10) Atkinson, J. R., Biddlestone, F., & Hay, J. N. (2000). An investigation of glass formation and physical ageing in poly (ethylene terephthalate) by FT-IR spectroscopy. Polymer, 41(18), 6965-6968.

(11) Qian, R., Shen, D., Sun, F., & Wu, L. (1996). The effects of physical ageing on conformational changes of poly (ethylene terephthalate) in the glass transition region. Macromolecular Chemistry and Physics, 197(4), 1485-1493.

(12) Wang, Y., Shen, D., & Qian, R. (1998). Subglass-transition-temperature annealing of poly (ethylene terephthalate) studied by FTIR. Journal of Polymer Science Part B: Polymer Physics, 36(5), 783-788.

(13) McGonigle, E. A., Daly, J. H., Gallagher, S., Jenkins, S. D., Liggat, J. J., Olsson, I., & Pethrick, R. A. (1999). Physical ageing in poly (ethylene terephthalate)—its influence on cold crystallisation. Polymer, 40(17), 4977-4982.

(14) Zhang, W., & Shen, D. (1998). The effects of thermal histories on crystallization of poly (ethylene terephthalate). Polymer journal, 30(4), 311.

(15) Zhao, J., Yang, J., Song, R., Linghu, X., & Fan, Q. (2002). The effect of annealing on the subsequent cold crystallization of amorphous poly (ethylene terephthalate). European polymer journal, 38(4), 645-648.

(16) Aref-Azar, A., Biddlestone, F., Hay, J. N., & Haward, R. N. (1983). The effect of physical ageing on the properties of poly (ethylene terephthalate). Polymer, 24(10), 1245-1251.

(17) Aref-Azar, A., Arnoux, F., Biddlestone, F., & Hay, J. N. (1996). Physical ageing in amorphous and crystalline polymers. Part 2. Polyethylene terephthalate. Thermochimica Acta, 273, 217-229.

(18) Štokr, J., Schneider, B., Doskočilová, D., Lövy, J., & Sedláček, P. (1982). Conformational structure of poly (ethylene terephthalate). Infra-red, Raman and nmr spectra. Polymer, 23(5), 714-721.

(19) Djebara, M., Stoquert, J. P., Abdesselam, M., Muller, D., & Chami, A. C. (2012). FTIR analysis of polyethylene terephthalate irradiated by MeV He+. Nuclear Instruments and Methods in Physics Research Section B: Beam Interactions with Materials and Atoms, 274, 70-77.D'esposito, L., & Koenig, J. L. (1976). Application of Fourier transform infrared spectroscopy to the study of semicrystalline polymers: poly (ethylene terephthalate). Journal of Polymer Science: Polymer Physics Edition, 14(10), 1731-1741.

(20) Snyder, R. G., Maroncelli, M., Strauss, H. L., & Hallmark, V. M. (1986). Temperature and phase behavior of infrared intensities: the poly (methylene) chain. *The Journal of Physical Chemistry*, *90*(22), 5623-5630.

(21) Lin, S. B., & Koenig, J. L. (1982). Spectroscopic characterization of the rotational conformations in the disordered phase of poly (ethylene terephthalate). Journal of Polymer Science: Polymer Physics Edition, 20(12), 2277-2295.

(22) Imai, M., Mori, K., Mizukami, T., Kaji, K., & Kanaya, T. (1992). Structural formation of poly (ethylene terephthalate) during the induction period of crystallization: 1. Ordered structure appearing before crystal nucleation. Polymer, 33(21), 4451-4456.

(23) Imai, M., Kaji, K., Kanaya, T., & Sakai, Y. (1995). Ordering process in the induction period of crystallization of poly (ethylene terephthalate). Physical Review B, 52(17), 12696.

(24) Cole, K. C., Ajji, A., & Pellerin, E. (2002). New insights into the development of ordered structure in poly (ethylene terephthalate). 1. Results from external reflection infrared spectroscopy. Macromolecules, 35(3), 770-784.

(25) Daubeny, R. D. P., Bunn, C. W., & Brown, C. J. (1954). The crystal structure of polyethylene terephthalate. Proc. R. Soc. Lond. A, 226(1167), 531-542.

(26) Fakirov, S., Fischer, E. W., & Schmidt, G. F. (1975). Unit cell dimensions of poly (ethylene terephthalate). Die Makromolekulare Chemie: Macromolecular Chemistry and Physics, 176(8), 2459-2465.

(27) Boyd, S. U., & Boyd, R. H. (2001). Chain dynamics and relaxation in amorphous poly (ethylene terephthalate): A molecular dynamics simulation study. Macromolecules, 34(20), 7219-7229.

(28) Huang, J. M., Chu, P. P., & Chang, F. C. (2000). Conformational changes and molecular motion of poly (ethylene terephthalate) annealed above glass transition temperature. Polymer, 41(5), 1741-1748.

(29) Pan, P., Liang, Z., Zhu, B., Dong, T., & Inoue, Y. (2008). Roles of physical aging on crystallization kinetics and induction period of poly (L-lactide). *Macromolecules*, *41*(21), 8011-8019.

(30) Pan, P., Zhu, B., Dong, T., Yazawa, K., Shimizu, T., Tansho, M., & Inoue, Y. (2008). Conformational and microstructural characteristics of poly (L-lactide) during glass transition and physical aging. *The Journal of chemical physics*, *129*(18), 184902.

(31) Sato, K., & Sprengel, W. (2012). Element-specific study of local segmental dynamics of polyethylene terephthalate upon physical aging. *The journal of chemical physics*, *137*(10), 104906.

(32) Illers, K. H., & Breuer, H. (1963). Molecular motions in polyethylene terephthalate. *Journal of Colloid science*, *18*(1), 1-31.

(33) Cangialosi, D., Boucher, V. M., Alegría, A., & Colmenero, J. (2013). Direct evidence of two equilibration mechanisms in glassy polymers. Physical review letters, 111(9), 095701.

(34) Cangialosi, D. (2018). Glass Transition and Physical Aging of Confined Polymers Investigated by Calorimetric Techniques. Handbook of Thermal Analysis and Calorimetry, 6, 301-337.

(35) Perez-De Eulate, N. G., & Cangialosi, D. (2018). The very long-term physical aging of glassy polymers. Physical Chemistry Chemical Physics, 20(18), 12356-12361.

(36) Ezquerra, T. A., Balta-Calleja, F. J., & Zachmann, H. G. (1993). Dielectric relaxation of amorphous random copolymers of poly (ethylene terephthalate) and poly (ethylene-2, 6-naphthalene dicarboxylate). *Acta polymerica*, *44*(1), 18-24.

(37) Bravard, S. P., & Boyd, R. H. (2003). Dielectric relaxation in amorphous poly (ethylene terephthalate) and poly (ethylene 2, 6-naphthalene dicarboxylate) and their copolymers. *Macromolecules*, *36*(3), 741-748.

(38) Dobbertin, J., Hensel, A., & Schick, C. (1996). Dielectric spectroscopy and calorimetry in the glass transition region of semi-crystalline poly (ethylene terephthalate). *Journal of Thermal Analysis and Calorimetry*, *47*(4), 1027-1040.

(39) Reiter, G., & Strobl, G. R. (Eds.). (2007). *Progress in understanding of polymer crystallization* (Vol. 714). Springer.

(40) Strobl, G. (2000). From the melt via mesomorphic and granular crystalline layers to lamellar crystallites: A major route followed in polymer crystallization?. *The European Physical Journal E*, *3*(2), 165-183.

(41) Blaine, R.L.. Polymer Heats of Fusion. THERMAL APPLICATION NOTES. T.A. Instruments

(42) Palmer, R. G., Stein, D. L., Abrahams, E., & Anderson, P. W. (1984). Models of hierarchically constrained dynamics for glassy relaxation. *Physical Review Letters*, *53*(10), 958.

(43) Androsch, R., Zhuravlev, E., Schmelzer, J. W., & Schick, C. (2018). Relaxation and crystal nucleation in polymer glasses. European Polymer Journal, 102, 195-208.

(44) Androsch, R., Schick, C., & Rhoades, A. M. (2015). Application of Tammann's two-stage crystal nuclei development method for analysis of the thermal stability of homogeneous crystal nuclei of poly (ethylene terephthalate). Macromolecules, 48(22), 8082-8089.

(45) Androsch, R., Di Lorenzo, M. L., & Schick, C. (2016). Crystal nucleation in random l/d-lactide copolymers. European Polymer Journal, 75, 474-485.

(46) Androsch, R., Di Lorenzo, M. L., & Schick, C. (2017). Effect of molar mass on enthalpy relaxation and crystal nucleation of poly (l-lactic acid). European Polymer Journal, 96, 361-369.

4. EFFECTS OF ANNEALING ABOVE T_g ON THE PHYSICAL AGING OF QUENCHED PLLA BY MTFTIR

4.1 INTRODUCTION

Amorphous glassy polymers characterized by an operating temperature not far below the glass transition temperature undergo bulk property changes over time, including embrittlement, stiffness and hardness increase, gas permeability decrease as well as size changes.[1-4] This process, called physical aging, is due to the occurrence of local structural relaxations driven by the attempt of the macromolecules to cancel out the excess thermodynamic quantities, such as enthalpy, entropy and specific volume, accumulated during the departure from the liquid equilibrium in the vitrification process. The relaxation occurred in physical aging can be recovered by heating the sample trough the T_g where, because of the increased macromolecular mobility, the amorphous phase regains the liquid equilibrium state. This process is defined thermal rejuvenation or de-aging because the sample loses almost all the memory of its previous sub-T_g thermal history. Then, a new and structurally defined glassy state can be obtained by cooling the de-aged sample in controlled conditions.[3,5,6] Indeed, a choice of a standard amorphous state is mandatory for the study and model of sub-T_g relaxation, its kinetics depending not only on the actual sample temperature, but also from the amount of excess thermodynamic quantities of the glass.[7] Moreover, annealing above the glass transition has an applicative and technological relevance. It was observed, in fact, that this thermal treatment has great effects on the mechanical properties of glassy materials and that can be exploited to increase material performances.[8,9] In addition, the phenomena occurring during physical aging and de-aging could affect the behaviour of semi-crystalline polymers. In fact, it was observed that, according to the cooling conditions and annealing both above and below T_g, "locally ordered structures" can be formed in the glassy amorphous phase.[10,11] Although they are not or hardly observed directly, they have a clear effect on the cold crystallization process. In fact, acting as nuclei, they increase the crystallization rate, decrease the crystallization temperature and the induction crystallization period as well as modify the sample morphology. The rejuvenation experiments were also used to evaluate the stability of the ordered structures according to different cooling or aging condition.[12] However, although the sample equilibration above T_g is a fundamental phase in sub-T_g relaxation studies it is not always applied. Moreover, to the authors' knowledge, no experiments dealing with the effects of the de-aging on polymer liquid state and on physical aging are reported in literature. In this paper, the effects of annealing below and above T_g, on the amorphous structure of quenched poly(L-lactide) (PLLA) were investigated. PLLA is a degradable thermoplastic characterized by mechanical properties comparable with those of petroleum-derived commodities. The hydrolytic degradation in non-toxic products and the biocompatibility make PLLA one of the most studied polymer in relation to its use in biomedical applications, including system for controlled drug or antigen delivery, scaffolds for tissue engineering or surgical devices.[13,14] On the other hand, PLLA presents some technical drawbacks related to the slow crystallization from the melt which implies the necessity to use nucleating additives and/or to face the problem of final high amorphous fraction. In fact, it can be obtained in completely amorphous or in amorphous-rich semi-crystalline state in the transformation operations and processing. Then, at the operating temperature, it is subject aging and properties evolution. Besides the applicative concerns, these features made PLLA one of the polymer of choice for fundamental studies on relaxation phenomena occurring below T_g and their effects on the relaxation recovery and cold-crystallization above T_g.[3,15-19]

In figure 4.1, a scheme of the repeating unit of PLLA is reported.

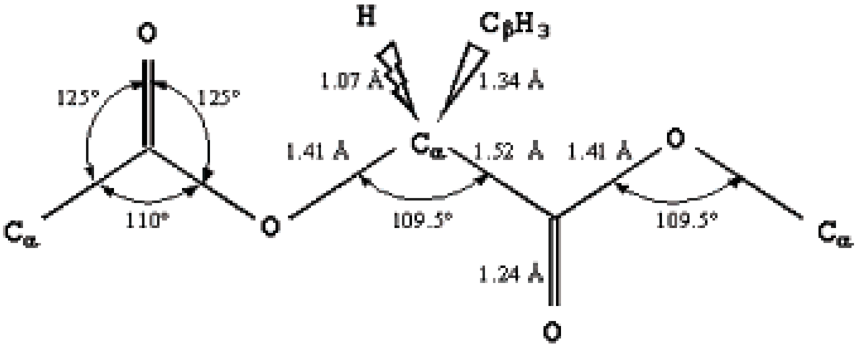

Figure 4.1. Repeating unit of PLLA.

It is assumed that the C-O bonds (ester) are locked in a trans-planar conformation due to conjugation with the next carbonyl group.[20]

The O-C_α bond has two energetic minima at about -160 ° and -48 ° while the C_α-C bond has two minima at about 160 ° and -73 °. The minima at -160 ° are called trans (*t*) and the two minima at -48 ° and -73 ° are called gauche (*g*). The combination of the energetic minima originates 4 distinct conformations for the O-C_α and C_α-C bonds shown below:

- *tt* (-160°, 160°)
- *tg* (-160°,-48°)
- *gt* (-73°, 160°)
- *gg* (-73°, -48°)

In the table 4.1, the characteristics of the conformation are reported.[21]

Table 4.1. Characteristics of the four possible conformation of PLLA

Conformation	**Torsion angle (°)**	**Energy (kcal/mol)**	**Relative abundance (25°C)**	**Helix**
tt	-160, -160	1,40	4,2	2_1
tg	-160, -48	1,52	4,0	5_1
gt	**-73, 160**	**0,0**	**55**	$\mathbf{3_1}$
gg	-73, -48	0,08	37	4_1

The conformation *gt* has the lowest energy and is specific to the helix 10_3 or 3_1 typical of the crystalline phase. From research reported in literature, it has been defined that about 55 % of the chains at 25 ° C assumes this conformation.[22] The second energy minimum is represented by the conformation *gg*, which has an energy content of 0.08 kcal/mol higher than the conformer *gt* and corresponds to about 37 % of the conformations of the polymer chains at 25 ° C. The remaining configurations, *tt* and *tg*, have an energy equal to 1.40 and 1.52 kcal / mol, respectively, and are the remaining 8 % of the conformations.[21] Then, it may be considered that the glassy PLLA consists mainly of chains in conformation *gg* or *gt*.

FTIR spectroscopy is able to follow at the molecular level the local structure of the amorphous phase, providing information on the conformer distribution in the disordered phase and its evolution as a function of temperature and time. Accordingly, it was widely employed in physical aging investigation.[23-25] As far as amorphous PLLA, variable temperature FTIR (VTFTIR) has been used to enlighten the glass transition and the recovery of sub-T_g relaxation of quenched and physical aged samples by following the evolution of the absorption bands related to high energy *gg* and low energy *gt* conformers.[23] In particular, in proximity to the *Tg*, a distinct change in the slope of spectral intensity versus temperature plot has been detected (figure 4.2, from ref. 19).

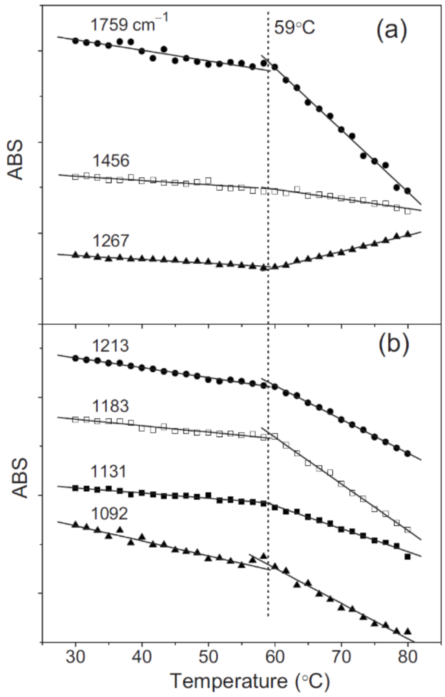

FIG. 2 Intensity changes in the indicated bands as a function of temperature for unaged PLLA during heating from 30 to 80 °C at 5 °C/min. The full lines represent the linear least-square fit to the data collected at the temperatures below and above T_g.

Figure 4.2. From ref. 19

FTIR results suggest that the energy-favourable *gauche-trans (gt*) conformers rearrange into the less energy-favourable *gauche-gauche (gg)* counterparts with heating over the glass transition region. The 1267 cm^{-1} band, which shows different trends of variation from the other bands upon heating, has been assigned to be more sensitive to the n_{as} (C–O–C)+d (CH) vibration mode of the less energy-favourable *gg* conformers in PLLA. By comparing the FTIR spectra of the aged and de-aged PLLA, it has been demonstrated that the rearrangement from the high- to low-energy conformers, i.e., *gg* to *gt*, occurs with physical aging (figure 4.3, from ref. 23).

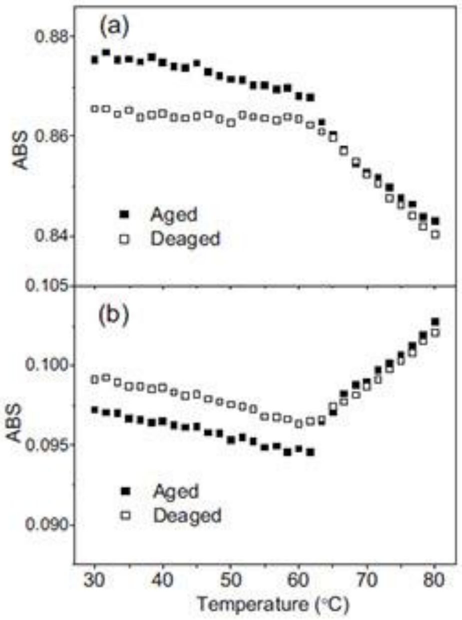

Fig. 3 Comparison between the temperature-dependent intensities of (a) 1759 and (b) 1267 cm^{-1} bands for aged (at 40 °C for 360 h) and deaged PLLAs during heating from 30 to 80 °C at 5 °C/min.

Figure 4.3. from ref. 23

VTFTIR has been employed to evidenced also the formation of an ordered structure during sub-T_g annealing and its partial melting at T_g.[17]

According to Zhang et al., such local ordered structure showed the same characteristic band at 918 cm^{-1} as that of the mesomorphic structure formed during the uniaxially drawn process of PLLA from the glassy state (Figure 4.4).

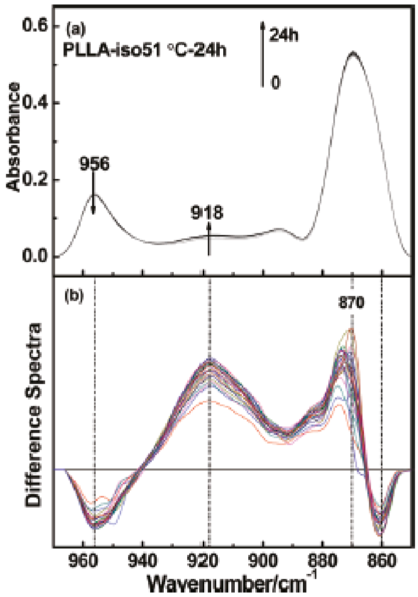

Figure 2. Time-resolved IR spectra (a) and difference spectra in the 970−850 cm^{-1} range (b) for PLLA aged at 51 °C for 24 h. These spectra were collected with a 1 h interval.

Figure 4.4. from Ref. 17

On the basis of spectroscopic evidence, the authors had inferred that the so-called local ordered structure formed during physical aging can be ascribed to a kind of mesophase of PLLA. Moreover, it has been found that a very small amount of mesophase already exists in the initial state of melt quenched PLLA sample and that the local ordered structure formed during the physical aging process were partially molten in the temperature region corresponding to the physical aging peak of aged PLLA (Figure 4.5)

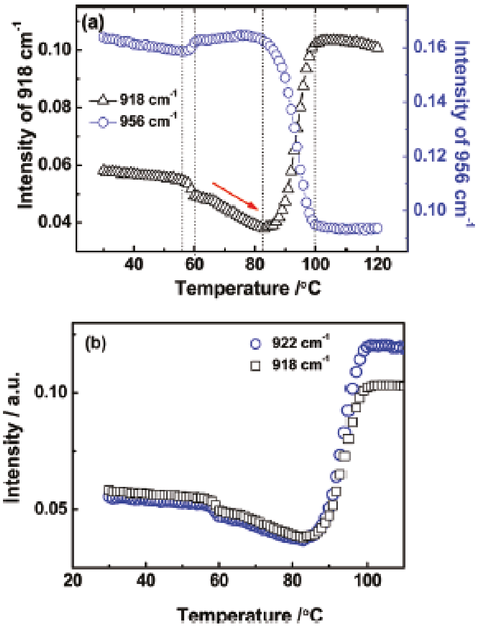

Figure 7. Intensity changes of the characteristic bands at 918 and 956 cm^{-1} as a function of temperature (a) and the intensity changes of the band at 918 cm^{-1} and the crystalline band at 922 cm^{-1} (b) during the heating processes of the PLLA sample aged at 51 °C for 24 h.

Figure 4.5. From ref. 17

Such an observation could be the cause of enhanced cold crystallization rate observed after the physical aging.

On the other hand, a different approach was used by Androsh et al.[27,29-31] to study the effect of the annealing in the glass transition region of PLLA to the kinetics of crystallization. FSC measurements were performed using the Tamman two-stage protocol, which allow to retrieve information on the nucleation of the system during the annealing. In order to suppress nucleation phenomena during heating or cooling ramps, 60000 °C/min rates were used. These studies highlighted that a homogeneous nucleation in PLLA took place soon after the end of the enthalpy relaxation at 60 °C, few degrees below the T_g, that is 66 °C at 60000 °C/min. Hence, the enhancement of cold-crystallization rate was addresses to the increase of stable nuclei in PLLA, that can occur both in liquid and glassy state.

Conventional VTFTIR can not give a clear description of possible complex or subtle sample transformation originate from the superimposition of reversing and non-reversing processes occurring in the same temperature range. Taking into account this limitation, in the present research the amorphous PLLA thermal behavior was investigated by collecting FTIR spectra sequentially during a modulated temperature ramp (modulated temperature FTIR, MTFTIR). The main result obtained by the MTFTIR deals with the presence of a non-reversible transformation occurring in the quenched PLLA in the temperature range between the glass transition and the onset of cold crystallization. Such transition of the liquid phase was erased by annealing the quenched sample above T_g (rejuvenation or de-aging), just few degrees to avoid crystallization. Moreover, it was observed that the subsequent physical aging of the vitrified polymer was affected by the rejuvenation. The obtained results evidenced that MTFTIR is able to give new insights on polymer transformations otherwise not accessible by other conventional thermal analyses.

4.2 EXPERIMENTAL PART

Poly(L-lactide) (PLLA, Purasorb PL 38, inherent viscosity in $CHCl_3$, 0.1 g/dl at 25 C: 3.9 dl g^{-1}; $[\alpha]_D^{25} = -157.7°$ 0.1 g dl^{-1} in chloroform) M_w = 600000 Da was kindly supplied by Corbion Purac. Chloroform and spectroscopy grade KBr were purchased from Sigma-Aldrich and used without purification.

Polymer films were obtained by casting on KBr disk a chloroform PLLA solution (2.5 wt/v %). After drying under vacuum, the thickness of the films was about 6-10 μm. In order to have PLLA in the amorphous state, the films were melted at 200 °C for 2 min and rapidly quenched in liquid nitrogen.

Then, four thermal treatments were imposed:

1. a quenched sample was brought at 45 °C and then subjected to the modulated temperature heating ramp (sample Q);
2. a quenched sample was annealed for 19 h at T_{pa}=51 °C (physical aging temperature), cooled at 2 °C min^{-1} to 45 °C and then heated with the modulated temperature ramp (sample A51);

3. a quenched sample was heated from room temperature at 2 °C min^{-1} to T_{da}=62 °C (de-aging temperature) and kept at this temperature for 19 h, cooled at 2 °C min^{-1} to 45 °C and then heated with the modulated temperature ramp (sample A62);
4. a quenched sample was heated to T_{da} = 62 °C for 19 h, cooled at 2 °C min^{-1} to T_{pa}=51 °C, held at this temperature for 19 h, cooled at 45 °C and, then, heated with the modulated temperature ramp (A62-51).

The scheme of Figure 4.6 shows the programs and the used sample codes.

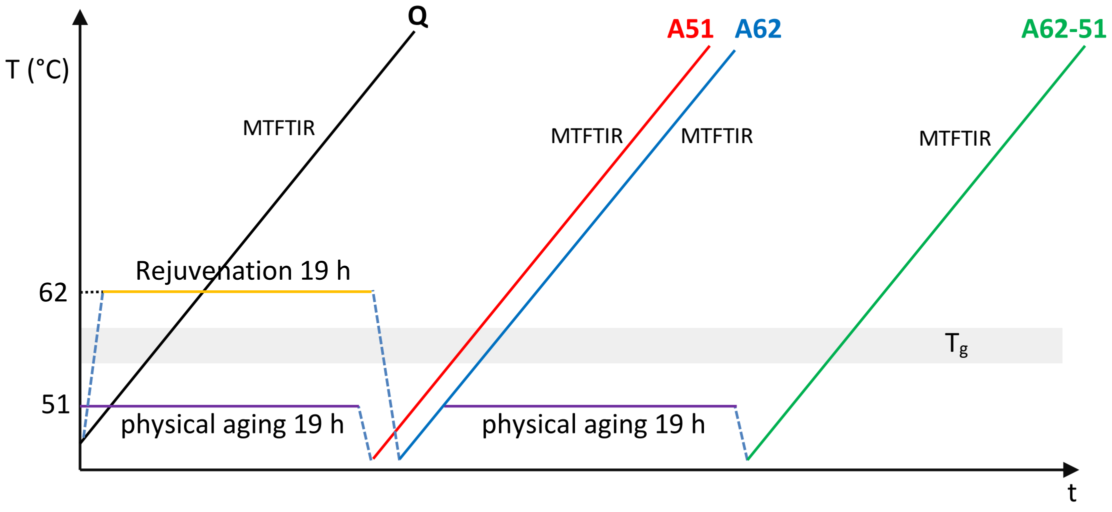

Figure 4.6. Scheme of the temperature programs and sample code.

The modulated temperature ramp comprised a linear heating at 0.2 K min^{-1} superimposed to a periodic modulation characterized by an amplitude of 2.5 °C and a period of 480 s. During the heating, FTIR spectra were acquired sequentially, co-adding 40 scans per spectrum at a resolution of 4 cm^{-1} by using a Nicolet^{TM} 6700 FTIR with a SPECAC variable temperature cell. Temperature program was executed by a HELLMA temperature controller. In these conditions, each spectrum was acquired every 30 seconds.

At the end of the acquisition, the absorbance intensity of the selected bands per each spectrum was recorded, given a local baseline. The detailed signal transformation used to obtain the total band intensity variation and the reversing and non-reversing components as a function of the mean temperature is reported in dedicated section of this thesis.

For DSC measurements a PLLA amorphous film of about 500 μm thickness was prepared by compression-mold at 200 °C. The film was cut in pieces of about 4 mg each and placed in sealed

40 μl aluminium pans. DSC samples were heated at 200 °C for 2 minutes and quenched in liquid nitrogen. Then, four different thermal treatments were imposed, as described for FTIR measurements, by using a Linkam HFS 91 hot stage driven by a Linkam TP 92 temperature controller. The Q, A62, A51 and A62-51 samples were obtained. Ultimately, standard DSC were performed from 25 to 200 °C with a linear heating rate of 10 °C/min. From DSC traces the enthalpy of crystallization, enthalpy of fusion and the fictive temperature of the glass were calculated. The method to determine the fictive temperature was described in Paragraph 2.2.3.

4.3 RESULTS AND DISCUSSION

Infrared spectroscopy is able to characterize materials at microstructural level, being specific absorption bands influenced by the local conformation of the polymer chain. In the present research the attention was focused on the bands at 1265 cm^{-1}, relative to the ν_{as} C–O–C +δ CH vibration mode of the high energy *gg* conformation, and 1183 cm^{-1}, assigned to the ν_{as} (COC) + $r_{as}(CH3)$ vibration of low energy *gt* conformation, respectively.[23,25] According with the elaboration, the intensities of these absorption bands as a function of acquisition time were transformed in the total intensity variation as a function of mean temperature as well as in their reversible and non-reversible components. As an example, the 1265 cm^{-1} band intensity row data of the Q sample and temperature recorded as a function of the acquisition time were reported in Figure 4.7 A. After the data elaboration, the total intensity and the reversing and non-reversing components as a function of the mean temperature were obtained (Figure 4.7 B, the R values reported in the ordinate are referred only to the total component). At a first glance, the main features of the graph of Figure 4.7 B are the slope change of the total and reversing intensities at 58 °C, indicative of the glass transition, and the abrupt absorption variation of total and non-reversing intensity between 75 and 85 °C, due to the cold crystallization. For sake of comparison, the total intensity of the two selected bands (I^{Tot}_{1265}, I^{Tot}_{1185}) vs T^M are reported in Figure 4.7 C. The plot is equal to that obtained by using a linear temperature ramp at the same mean heating rate. The intensity chances of the two bands of the *gg* and *gt* conformers are nearly symmetric, being strictly related each other. Hence, in order to compare of the results obtained in the other experiments and to avoid effects due to the different sample thickness, in the following analysis the intensity ratio R between the band at 1183 cm^{-1} and 1265 cm^{-1}, indicative of the relative *gg/gt* conformer concentration, will be reported. The total R ($R^{Tot}=I^{Tot}_{1183}/I^{Tot}_{1265}$) variation of all the sample as a function of T^M are shown in Figure 4.8 A, while in the panel B is displayed the change of $R(t)$ of the A62-51 sample recorded as a function of annealing time at T_{da}=62 °C and T_{pa}=51 °C for the de-aging and physical aging processes, respectively.

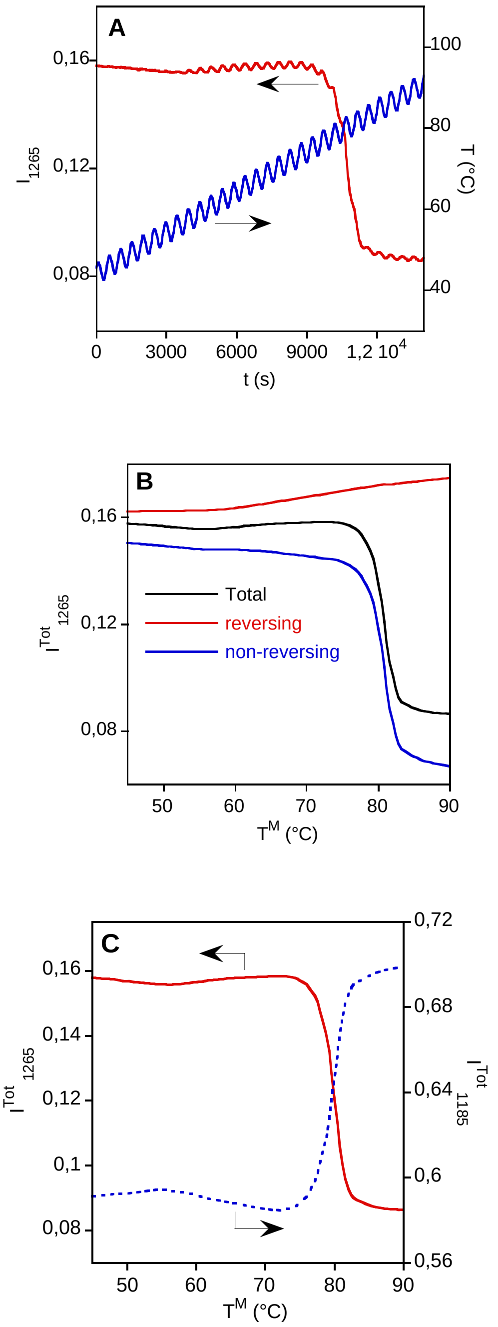

Figure 4.7. Intensity variation of the band at 1265 cm^{-1} (I_{1265}) and modulated temperature recorded as a function of time (A). Total intensity of the band at 1265 cm^{-1} (I^{Tot}_{1265}) as well as its reversing (I^{R}_{1265}) and non-reversing (I^{NR}_{1265}) components as a function of mean temperature (T^M) (B). Total intensity variation of the bands at 1265 cm^{-1} (I^{Tot}_{1265}) and 1183 cm^{-1} (I^{Tot}_{1183}) of the Q sample as a function of the mean temperature T^M (C).

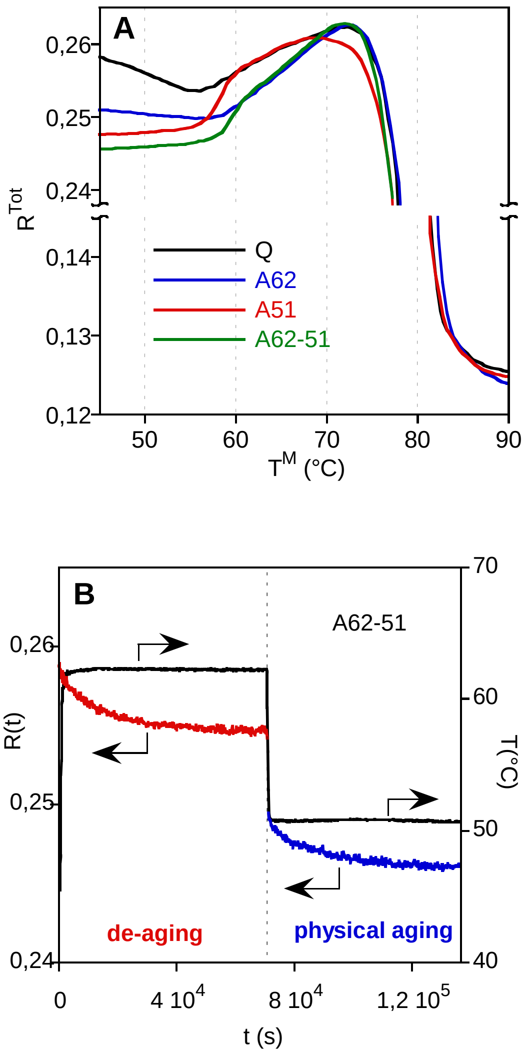

Figure 4.8. Comparison of the total relative intensity variation ($R^{Tot}=I^{Tot}_{1183}/ I^{Tot}_{1265}$) of all the samples as a function of the mean temperature (T^M) (A). Variation of R(t) of the A62-51 sample recorded as a function of annealing time at T_{da}=62 °C and T_{pa}=51 °C for the de-aging and physical aging processes, respectively (B).

The figure 4.8 A shows that the cold crystallization did not display a significant difference among the samples. As reported in literature, the physical aging favours the crystallization kinetics trough the formation of nuclei[10,26] but the overall thermal history of samples, that is the slow cooling and heating steps as well prolonged annealing, levelled off this process. Proper experiments dedicated to the study of nucleation kinetics have been carried out by using heating and cooling rate well above to that employed in this research.[26,27] Actually, the samples behaved very differently before the crystallization, according to their thermal treatments. In general, it can be observed that at the initial temperature T=45 °C, the Q sample showed the highest R^{Tot} value due to the large *gg* conformer content as obtained from the quenching and that it decreased by the annealing at 51 °C. Furthermore, the increase of R^{Tot} of the A51 and A62-51 samples in the

55-60 °C temperature range is indicative of the recovery of the relaxation occurred at T_{pa}=51 °C. The interpretation of the other differences is not straightforward. However, the MTFTIR technique offers the possibility to separate the reversible transformation from the non-reversible one and, then, the opportunity to give a more detailed analysis of the sample evolution. The reversing and non-reversing transformations that occur during sample heating are strictly related to the equilibrium or out-of-equilibrium conformational rearrangement of disordered chains, respectively. To better appreciate the different sample behaviour in the temperature range before the crystallization, the total variation ($R^{Tot}=I^{Tot}_{1265}/I^{Tot}_{1183}$) as well as the reversible ($R^{R}=I^{R}_{1265}/I^{R}_{1183}$) and non-reversible ($R^{NR}=R^{Tot}-R^{R}$) components of the band intensity ratio R of the four samples as a function of mean temperature T^{M} are reported up to 70 °C separately in figure 4.9. The y axes of the plots are referred to R^{Tot}, while the R^{R} and R^{NR} are arbitrary shifted for convenience. In particular, the reversing component values were arranged so as to coincide with R^{Tot} above the glass transition, where the sample should be a liquid in equilibrium state. The glass transition, being a reversible transformation, appears as a clear slope change of R^{R} vs temperature. The T_g values were taken at the in correspondence of the intersection point of the two straight lines interpolating the reversible data before and after the transition and are indicated by the vertical bars in figure 4.9.

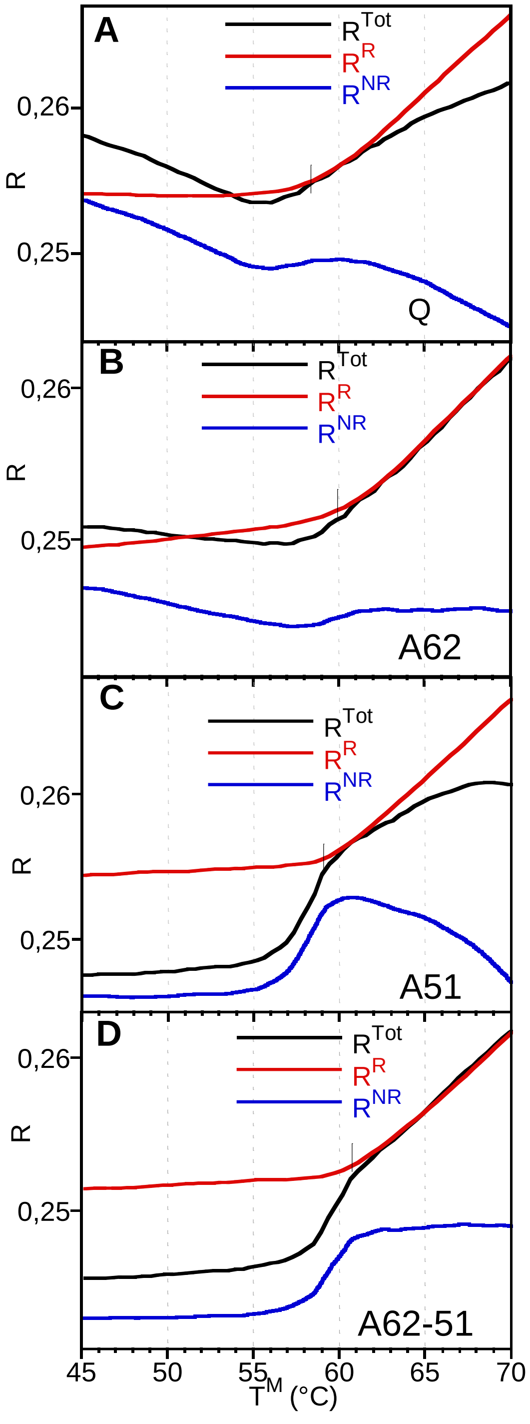

Figure 4.9. Variation of $R^{Tot}=I^{Tot}_{1265}/ I^{Tot}_{1183}$, $R^R=I^R_{1265}/I^R_{1183}$ and $R^{NR}=R^{Tot}-R^R$ of Q (A), A62 (B), A51 (C) and A62-51 (D) samples as a function of the mean temperature T^M (A). The vertical bars indicate the glass transition temperature.

From the reversing component R^R of the four samples the glass transition temperature was calculated. For all samples the glass transition, calculated at a linear heating rate of 0.2 °C/min lies around 60 °C. The detailed results were reported in Table 4.1.

Table 4.1. Glass transition temperature for PLLA samples

Sample	T_g (± 1 °C)
Q	58
A62	60
A51	59
A62-51	61

Above the T_g, besides the effect of the variation of the absorption coefficient with temperature ($d\varepsilon/dT$), the reversible component variation is indicative of the relative conformer concentration change, which, in turn, depends on sample temperature and on the potential energy difference between the conformers. It is important to remark that the straight lines interpolating the R^R above T_g of all the sample are parallel.

In addition, figure 4.9 helps to interpret the complex transformation occurring before the crystallization onset, different for each sample. In particular, it can be observed that R^{NR} of Q sample initially decreased up to T_g, levelled off and, then, decreases again. The great non-reversing variation up to the T_g is indicative of an extended non-isothermal relaxation of the glassy polymer chains, characterized by a high *gg* content, towards the more stable *gt* conformation during the heating, that is a dynamic physical aging. The relaxation could has begun also into the time period soon after the quenching, not analysed. The further decrease R^{NR} from T_g to the onset of the cold crystallization is unexpected. In fact, the devitrified amorphous phase should show only a reversible transformation, generally being it considered a liquid in equilibrium state. The phenomena can not be ascribed to an incipient crystallization because the spectra did not show the formation of the regularity band at 922 cm^{-1} of 10_3 helices up to about 70 °C.[25] In order to interpret the phenomenon, the non-reversing process was forced to occur by an isothermal annealing of quenched sample at T_{da}=62 °C for 19 h (de-aging, A62 sample), only few degrees above the glass transition, to avoid any crystallization. The slow *R(t)* variation during the de-aging is reported in the left side of figure 4.8 B. Indeed, in PLLA the temperature range for the de-aging is very narrow since it was observed that thermal treatment few degrees above the glass transition brought about a partial polymer crystallization, possibly favoured by the formation in the physical aging of ordered structures that acts as crystallization nuclei.[3,27] In fact, it has been observed that annealing at 75 °C for 2 min or at 78 °C for 5 min have brought about partial crystallization. By VTFTIR analysis, Zhuo et al. have observed that that a critical cold crystallization temperature is located between 63 and 68 °C.[28] An incipient crystallization has been also observed in the present research at temperature of 67 °C. In Figure 4.10 the evolution of R ratio and of the intensity of the band at 922 cm^{-1} were reported as function of the annealing time at two different temperatures, 62 °C and 67 °C.

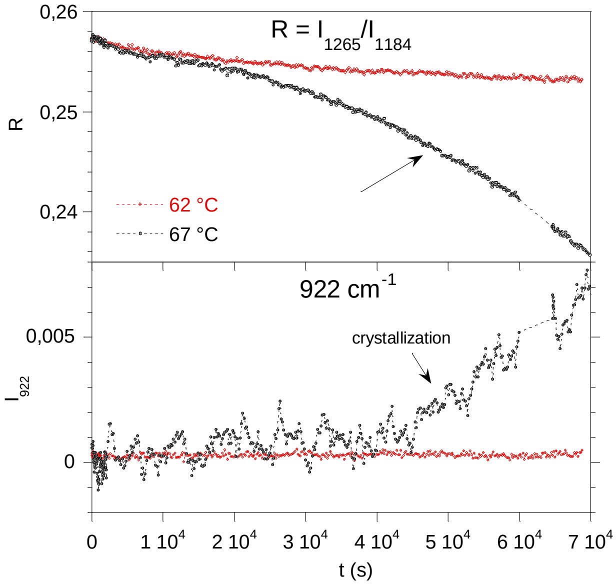

Figure 4.10. Evolution of R ratio and 922 cm^{-1} band intensity (I_{922}) during the isothermal annealing treatment at 62 °C and 67 °C. Arrows indicate the effect of the incipient cold-crystallization at 67 °C.

From Figure 4.10 it is possible to highlight the incipient cold-crystallization of the PLLA sample aged at 67 °C for 19 h by an abrupt intensity increase of the 922 cm^{-1} band at 40000 s, nor present in the sample annealed at 62 °C (A62). Furthermore, the sample annealed at 67 °C shows a more pronounced R decrease.

The spectroscopic results obtained in the modulated temperature heating ramp are reported in figure 4.9 B (A62 sample). After the annealing at T_{da}=62 °C, the sample behaviour is quite different from that of Q sample. Now, from T_g to the cold crystallization onset, the total and non-reversible components showed the same linear variation. It means that the relative concentration of the conformers reached the equilibrium and that the non-reversible transformation of the devitrified amorphous phase completely vanished, R^{NR} levelling off from 62 °C. Moreover, a small but clear relaxation recovery can be observed in the R^{NR} trace between 57 °C and 63 °C, superimposed to the glass transition at 60 °C. It is the result of the glass physical aging occurred in the overall sample thermal history below T_g. In the Q sample, the same phenomenon was partially hidden by the simultaneous non-reversible transformation. In order to verify the effects of the liquid phase relaxation (de-aging) on the glass physical aging, the quenched and de-aged samples were annealed below T_g at T_{pa}=51 °C for 19 h (A51 and A62-51 samples, figure 4.9 C and D). The *R(t)* variation of A62-51 sample in the de-aging and physical aging processes is reported in the left and right side of figure 4.8 B, respectively.

Figure 4.9 C and D display that, before the glass transition, the A51 and A62-51 samples had a null R^{NR} variation because the long relaxation at T_{pa} completely wiped out the non-isothermal physical aging during the heating ramp. Then, a large recovery of the sub-T_g relaxation took place between 55 °C and 60 °C. The intensity of non-reversible transformation of the A62-51 sample was lower than that of A51 and occurred at higher temperature. At temperature above the recovery, the non-reversible process in the liquid phase of A51 sample, already observed in the quenched sample, persisted. Then, this transformation merged with the cold crystallization. Vice versa, the A62-51 sample shows no non-reversing variation between the recovery and the crystallization, the liquid having already relaxed at T_{da}=62 °C (figure 4.9 D). A number of researches have reported that annealing below or above T_g causes the formation of ordered structures in the amorphous phase which, acting as nuclei, favour the cold crystallization at higher temperature. FTIR investigation on PLLA had suggested that such structures, appearing during physical aging, are constituted by a mesophase, analogues to that found in drawn glassy polymer, and characterized by a IR band at 918 cm^{-1}.[17] The mesophase formation, hence, could change the conformer distribution and cause the non-reversing R variation observed above the T_g. In figure 4.11, the total band intensity variation (I_{918}^{Tot}) and its non-reversible component (I_{918}^{NR}) is reported as a function of T^M up to 70 °C because, at higher temperature, the absorption overlaps with the tail of the adjacent regularity band at 922 cm^{-1}, whose formation and intensity increase are indicative of the crystallization process. No absorption intensity normalization was applied to the data of figure 4.11, being here interested just in the band evolution with temperature. Because of the low intensity of the band at 918 cm^{-1}, the I_{918}^{Tot} and I_{918}^{NR} profiles resulted more irregular than those previously analysed. However, the figure 4.11 B clearly shows that the mesophase fraction increased during the heating of Q sample and that it was pre-existent in the other samples at the beginning of the experiment. The I_{918}^{Tot} intensity rapid drop in the temperature range from 57 to 62 °C, common in all the samples, has been attributed to the melting of the mesophase. Moreover, the I_{918}^{NR} variation of Q sample evidences that the band intensity decreases at 57 °C was lower than its previous increase at low temperature, that is the melting process is partial, as suggested by Zhang et al..[17]

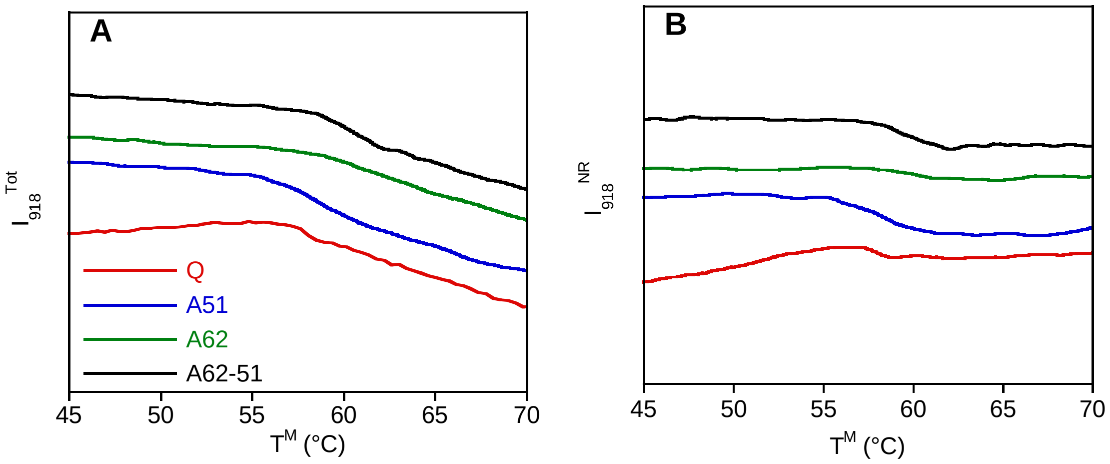

Figure 4.11. Intensity variation of the total (A) and non-reversible (B) component the band at 918 cm^{-1} as a function of the mean temperature T^M.

In addition, at T>62 °C the I_{918}^{NR} value of all the samples was constant and, therefore, the non-reversing process is null after the relaxation recovery, independently from the sample thermal histories. Hence, the R non-reversible change observed in Q and A51 samples at $T > T_g$ involves only the amorphous liquid phase and any variation of conformer distribution due to the formation of mesophase is be excluded.

In order to give a wider picture of the sample behaviours described until now, the R^{Tot} of all the samples are compared in figure 4.12 A and B. The dashed lines, tangent to the curves above the relaxation recovery, are parallel to the reversible component recorded at $T>T_g$. They represent the equilibrium variation of the relative conformers concentration (*gg/gt*) with temperature of the non-rejuvenated and rejuvenated liquids (liquid 1 for Q and A51 samples, liquid 2 for A62 and A62-51 samples). These data are available exclusively by the MTFTIR technique.

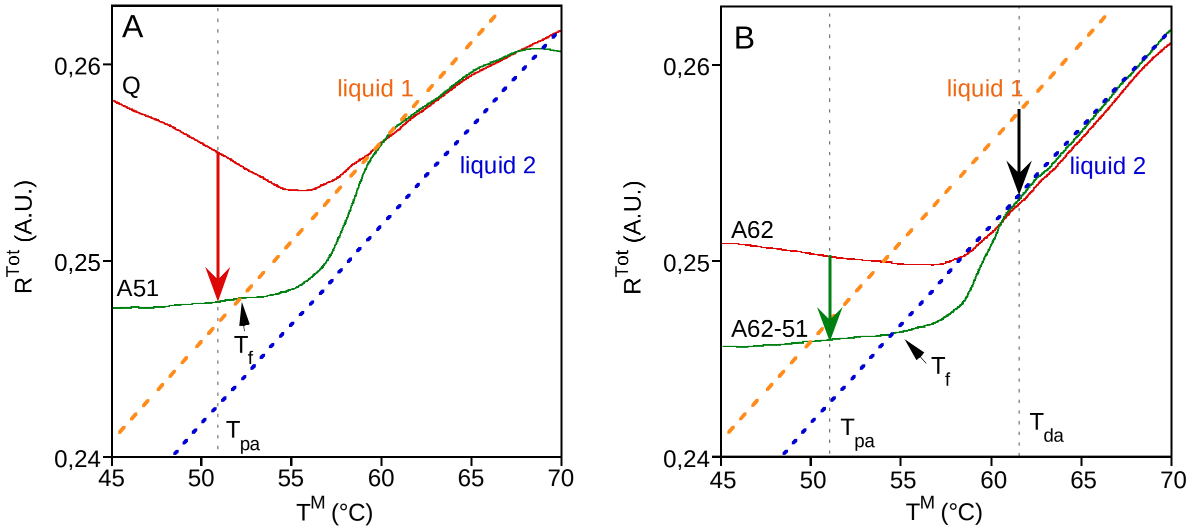

Figure 4.12. Comparison of the total R variation of all the sample as a function of mean temperature. Orange and blue dotted lines are parallel to the reversible component of the non-rejuvenated (Q and A51 samples, liquid 1) and rejuvenated (A62 and A62-41 samples, liquid 2) liquids.

The Q and A51 samples, quenched from the melt, during the heating underwent a non-reversible transformation from about 60 °C, soon after the glass transition. These non-rejuvenated glasses, annealed in the liquid state at T_{da}=62 °C, undergo a slow relaxation towards a more stable state, characterized by a higher content of the lower energy *gt* conformation (figure 4.9 B and black arrow in figure 4.12 B). The relaxation kinetic at 62 °C has been shown in Figure 4.8.

The parameter generally used to describe univocally the departure of the glassy state from the equilibrium is the fictive temperature T_f. It represents the temperature at which the equilibrium liquid structure would be identical to that actually existing in the glass. In the present investigation, the T_f is referred to the glass structure as defined by the relative *gg/gt* conformer concentration. During the relaxation at T_{pa}, and also during the slow heating scans at 0,2 °C/min, the T_f of the glass moves from the initial value towards the equilibrium T_f=T_{pa}, assuming all the intermediate values. The intersection of the R^{Tot} curves with the R^R equilibrium straight line, extrapolated at lower temperature, correspond to the fictive temperature T_f reached by A51 and A62-51 samples during a physical aging of 19 h at T_{pa}=51 °C and is an indication of the extent of the sub-T_g glass relaxation.

During physical aging at T_{pa}, the Q and A62 glasses evolved towards their own liquid state (red and green arrows in figure 4.12), retaining the memory of their original condition before the vitrification. In the sub-T_g relaxation, the A51 sample reached in 19 h a T_f=52 °C, very close to

T_{pa}, that is the relaxation was near the completion. Differently, the physical aged sample vitrified from the rejuvenated liquid (A62-51) reached a higher T_f=54,5 °C after the same annealing time. Although the A62-51 glass had a smaller offset from the equilibrium line than that of Q sample (figure 4.12), it relaxed slower. This is also reflected in the larger recovery at the T_g of A51 sample than that of A62-51 sample. Hence, the prolonged rejuvenation not only erased the previous sample thermal history below the T_g, but also brought about a more stable liquid, characterized by a higher content of the low-energy conformer. This implies that the PLLA glasses vitrified from different liquid states relaxed differently not only because of their different structure (namely enthalpy, specific volume or entropy excess content) but also because the process was driven by different equilibrium target.

Besides the conformer relative concentration, in the present research the thermal properties evolution was investigated by calorimetry in order to verify the observed different physical aging. DSC measurements were performed on PLLA samples with similar thermal histories respect to those used for FTIR measurements. In Figure 4.13, DSC traces of the Q, A51, A62 and A62-51 samples were shown between 25 and 200 °C, with a linear heating rate of 10 °C/min.

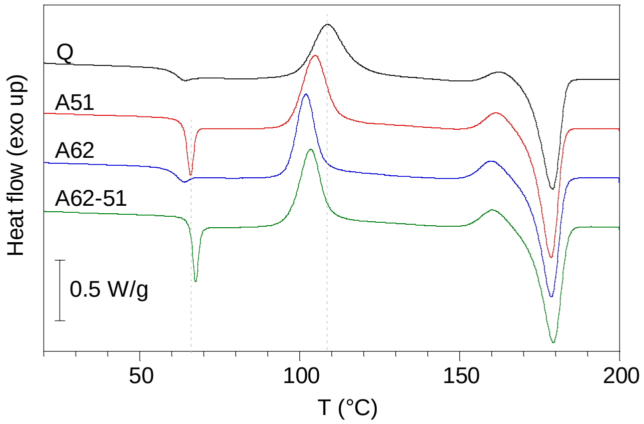

Figure 4.13. DSC traces of Q, A51, A62 and A62-51 samples as function of the temperature. Dashed lines, from left to right, indicates the overshoot peak of the A51 sample and the maximum crystallization temperature of the Q sample.

The DSC thermogram of the quenched PLLA (Q) displays the glass transition at 60,5 ± 0,5 °C, calculated at the midpoint of the heat flow step, the cold-crystallization as an exothermic peak at 109 °C and the endothermic melting peak at 178 °C. By aging the quenched sample at 51 °C for 19 h (A51), an endothermic peak (overshoot) appears superimposed to the glass transition, that is the enthalpy recovery, with its maximum at 66 °C. The sub-Tg annealing treatment caused the shift of the cold-crystallization to lower temperatures (T_c^{A51} = 105 °C) with increased kinetics. Concerning the de-aging process (T_{da} =62 °C) slight above the glass transition, it caused a greater anticipation of the cold-crystallization process (T_c^{A62}=102 °C) and a faster kinetics than other thermal treatments. Moreover, the glass transition temperature was not affected by the de-aging process, at 60,5 °C, and the overshoot peak was nearly absent, sign of the slight dynamic physical aging occurred during the cooling of the de-aged sample to room temperature prior to the start of the DSC scan. The A62-51 sample, instead, shows the enthalpy recovery at 67, 5 °C, shifted at higher temperature respect to the A51 sample, as seen from FTIR measurements. Similar cold-crystallization of aged samples A51 and A62-51 were observed. Ultimately, the fictive temperatures of the glass formed with the A51 and the A62-51 aging treatments were performed. Interestingly, the FTIR and DSC measurements gave similar results, with a higher fictive temperature for the rejuvenated sample before the aging at 51 °C $T_f^{A62\text{-}51}$= 54,3 °C respect to T_f^{A51}= 51,8 °C (Table 4.2). From DSC results, the effect of the aging and de-aging treatments on crystallization kinetics could be clearly seen, both lead to an anticipate and higher-rates cold-crystallization. Unfortunately, no differences in the supercooled liquid regions of quenched (Q and A51) and rejuvenated (A62 and A62-51) samples were found.

Table 4.2. Fictive temperatures calculated by FTIR and DSC measurements of the quenched sample aged at 51 °C for 19 h (A51) and the rejuvenated samples aged at the same temperature and same aging time (A62-51)

Sample	*T_f (FTIR) (°C)*	*T_f (DSC) (°C)*
A51	52 ± 0,5	51,8 ± 0,2
A62-51	54,5 ± 0,5	54,3 ± 0,2

By the comparison between DSC and FTIR experiments, it could be observed that the annealing treatment of glassy or undercooled liquid PLLA promoted the increase of the most stable conformer concentration, a process probably driven by the lowest energy crystalline state, leading to faster and anticipated crystallization. It is important to remember that above T_g, the lines interpolating R^R vs T^M of all the samples had the same slope (figure 4.12, liquid 1 and 2). This is indicative that the interconversion of the two conformers was a fast process and that, at least in the employed heating rate (0.2 °C/min), their relative concentrations rapidly reached the equilibrium. The variation of the equilibrium liquid line (Figure 4.11) after the annealing above the glass transition temperature at T_{da}=62 °C and the non-reversible transformation of non-rejuvenated liquids could be accounted to two different phenomena, namely the liquid-liquid phase transition of PLLA related to polyamorphism and the homogeneous nucleation. Firstly, polyamorphism is the ability of a substance of forming two different liquid phases, and it was observed only in extensively hydrogen-bonded systems, in water[33] and recently in D-mannitol.[32] The transition from two different liquid states occurs slight above the glass transition, and was classified as a first-order transition, involving a volume expansion and a heat release (exothermic). For the PLLA supercooled liquid system, it was observed an increase of *gt* conformers if treated at 62 °C, slight above the glass transition temperature. Hence, before and after the rejuvenation treatment, two liquids with different *gg*-*gt* equilibrium concentrations were found. More interestingly, the *gg*-*gt* equilibrium concentrations achieved during the rejuvenation treatment was preserved after aging in PLLA glassy state (Figure 4.12). Then, both the annealing above and below the glass transition favoured the increase of lower energy conformers which have an influence in the following cold-crystallization.

On the other hand, the investigation on the nucleation kinetics needs selected experimental procedure, not applied in the present research. However, the reported phenomena could be related also to the results presented by Androsch and Di Lorenzo according to which both the annealing below and above T_g favoured an homogeneous nucleation mechanism and that, most importantly, the nucleation rate varied without any discontinuity at the glass transition (Figure 4.14).[27]

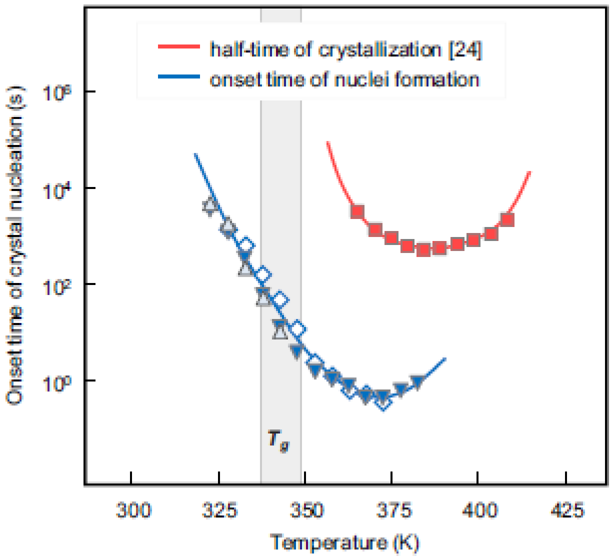

Fig. 4. Onset time of crystal nucleation (blue symbols) and half-time of crystallization (red symbols) of PLLA as a function of temperature. The temperature range of the glass transition is indicated with the gray shaded bar. (For interpretation of the references to colour in this figure legend, the reader is referred to the web version of this article.)

Figure 4.14. From ref. 27

4.4 CONCLUSION

MTFTIR analysis has given the possibility to deeply investigate the physical aging and de-aging process of the quenched amorphous PLLA from the molecular point of view and to enlightened phenomena otherwise hard to detect. The new technique, in fact, allowed the direct observation of a non-reversing transformation occurring above T_g and before the crystallization, suggesting the possible evolution of the polymer in the liquid state towards a more stable structure, characterized by a higher low-energy *gt* conformer concentration. The relaxation of the initial liquid towards the new state was forced to occur by an isothermal annealing treatment, few degrees above the T_g. The subsequent vitrification brought about a glass which behave differently from that obtained from unrelaxed liquid. In fact, it was observed that the sub-T_g relaxation phenomena did not depend only on the temperature and on the structure of the glass but also from the structure of the liquid from whom it originated. The results hereafter reported indicate that the fictive temperature can not describe univocally the glassy structure, at least as far as the conformer distribution is concerned and for semi-crystalline polymers. These finding would imply a great attention in adopting a controlled and verified procedure to attain a standard liquid state to have reliable results in physical aging experiments, not always applied.

4.5 REFERENCES

(1) J. Verdu, *J. Macromol. Sci., Part A: Pure Appl. Chem.* **1994**, *31*, 1383.

(2) H. Cai, V. Dave, R. A. Gross, S. P. McCarthy, *J. Polym. Sci. Part B: Polym. Phys.* **1996**, *34*, 2701.

(3) P. Pan, B. Zhu, Y. Inoue, *Macromolecules* **2007**, *40*, 9664.

(4) M. Kwon, S. C. Lee, Y. G. Jeong, *Macromol. Res.* **2010**, *18*, 346.

(5) H. M. Naeem Iqbal, C. Sungkapreecha, R. Androsch, *Polym. Bull.* **2016**, *74*, 2565.

(6) J. L. Gomez Ribelles, M. Monleon Pradas, *Macromolecules*, **1995**, *28*, 5867.

(7) J. M. Hutchinson, *Prog. Polym. Sci.* **1995**, *20*, 703.

(8) G. J. M. de Koning, A. H. C. Scheeren, P. J. Lemstra, M. Peeters, H. Reynaers, *Polymer* **1994**, *35*, 4598.

(9) T. Huang, M. Miura, S. Nobukawa, M. Yamaguchi, B*iomacromolecules,* **2015**, *16*, 1660.

(10) F. Hernandez Sanchez, J. Molina Mateo, F. J. Romero Colomer, M. Salmeron Sanchez, *J. Phys. Chem. B* **2011**, *115*, 10844.

(11) J. Zhao, J. Yang, R. Song, X. Linghu, Q. Fan, *Eur. Polym. J.* **2002**, *38*, 645.

(12) S. Piccarolo, E. Vassileva, Z. Kiflie, In Polymer Crystallization: Observations, J. U. Sommer and G. Reiter, Eds.; Springer: Heidelberg, **2008**; Chapter 18, pp 326-342

(13) L. Pellegrino, R. Cocchiola, I. Francolini, M. Lopreiato, A. Piozzi, R. Zanoni, A. Scotto d'Abusco, A. Martinelli, *Colloids Surf.*, *B* **2017**, *158*, 643

(14) P. Di Bonito, L. Petrone, G. Casini, I. Francolini, M. G. Ammendolia, L. Accardi, A. Piozzi, L. D'Ilario, A. Martinelli, *Int. J. Nanomed.*, **2015**, *10*, 3447

(15) K. Aou, S. L. Hsu, L. W. Kleiner, F.-W. Tang, *J. Phys. Chem. B* **2007**, *111*, 12322

(16) X. Monnier, A. Saiter, E. Dargent, *Thermochim. Acta* **2017**, *648*, 13.

(17) T. Zhang, J. Hu, Y. Duan, F. Pi, J. Zhang, *J. Phys. Chem. B* **2011**, *115*, 13835.

(18) J.F. Mano, J. L. Gomez Ribelles, N. M. Alvesa, M. Salmeron Sanchez, *Polymer* **2005**, *46*, 8258.

(19) R. Androsch, M. L. Di Lorenzo, C. Schick, *Eur. Polym. J.* **2017**, *96*, 361

(20) P. De Santis, A. J. Kovacs, *Biopolymers*, **1968**, *6*, 299

(21) S. Kang, S. L. Hsu, H. D. Stidham, P. B. Smith, M. A. Leugers, X. Yang, *Macromolecules* **2001**, *34*, 4542

(22) D. A. Brant, A. E. Tonelli, P. J. Flory, *Macromolecules* **1969**, *2*, 228

(23) P. Pan, B. Zhu, T. Dong, K. Yazawa, T. Shimizu, M. Tansho, Y. Inoue, *J. Chem. Phys.* **2008**, *129*, 184902.

(24) B. Na, R. Lv, S. Zou, Z. Li, N. Tian, Macromolecules 2010, 43, 1702.

(25) P. Pan, J. Yang, G. Shan, Y. Bao, Z. Weng, A. Cao, K. Yazawa, Y. Inoue Macromolecules 2012, 45, 189.

(26) R. Androsch, M. L. Di Lorenzo, Polymer 2013, 54,6882.

(27) R. Androsch, M. L. Di Lorenzo, C. Schick, Eur. Polym. J. 2017, 96, 361

(28) R. Zhuo, Y. Zhang, G. Li, C. Shao, Y. Wang, C. Liu, Q. Li, W. Cao, C. Shen, Vibr. Spect. 2016, 86, 262

(29) Androsch, R., Zhuravlev, E., Schmelzer, J. W., & Schick, C. (2018). European Polymer Journal, 102, 195-208.

(30) Androsch, R., & Schick, C. (2016). The Journal of Physical Chemistry B, 120(19), 4522-4528.

(31) Androsch, R., Di Lorenzo, M. L., & Schick, C. (2016). European Polymer Journal, 75, 474-485.

(32) Zhu, M., & Yu, L. (2017). Polyamorphism of D-mannitol. The Journal of chemical physics, 146(24), 244503.

(33) Winkel, K., Elsaesser, M. S., Mayer, E., & Loerting, T. (2008). The Journal of chemical physics, 128(4), 044510.

5. MOLECULAR MECHANISMS OF REVERSIBLE CRYSTALLIZATION AND MELTING OF ISOTACTIC POLYPROPYLENE INVESTIGATED BY MTFTIR, QUASI-ISOTHERMAL FTIR AND DSC

Modulated temperature FTIR (MTFTIR) analysis allowed the description at molecular level of the reversing and non-reversing tranformations occurring during the isotactic polypropylene non-isothermal melt crystallization. The intensity of regularity absorption bands, assigned to conformation sequences arranged in 3_1 helix of different length, were acquired in MTFTIR experiments. The data elaboration gave the band intensity total variation as well as its reversing and non-reversing components as a function of mean temperature. The results revealed that a reversing variation of helix concentration occurred from few degrees below the crystallization onset to lower temperature, when the primary transition ceased, and that the extent of the transformation depended on helix length. The comparison between Quasi-isothermal FTIR and Quasi-isothermal DSC results highlighted that the reversible crystallization of isotactic polypropylene was ascribed to the molecular mechanism of formation-disruption of longer helices principally. Moreover, two different regimes of reversible crystallization were observed. The first more intense phenomenon, defined as *regime II*, was associated to a reversible formation-disruption of the overall helix population in iPP , taking place from the formation of the crystalline phase up to 96 °C, and occurring on the lateral edge of lamellar crystals. Below this temperature, until reaching 30 °C, the *regime I* of the reversible crystallization took place, ascribed only to the reversible formation and disruption of intermediate helix lengths. This lower intensity phenomenon affected in minor way the sample crystallinity.

5.1 INTRODUCTION

By the late 1900s, the very early experiments carried out by temperature modulated DSC (TMDSC) on semi-crystalline polymers, have evidenced the presence of reversible melting processes occurring during sample heating over a wide temperature range[1]. The transformation, observed in several polymers, resulted as an apparent reversible heat capacity in excess respect to the thermodynamic vibrational heat capacity[2-5]. In general, the molecular origin of the reversible process can not be directly identified but inferred from some issues concerning non-reversible polymer transitions. In the heating cycle of a temperature modulation, the melting of the polymer crystalline phase occurs via detachment of ordered stems from crystalline substrate. In the subsequent cooling process, the crystallization can occur only by molecular nucleation: there must be long chain segments, only partially melted, which leave molecular nuclei on the remaining crystal that permit reversibility. On the other hand, by cooling the melt, crystallization takes place at temperatures well below the equilibrium melting temperature and the macromolecule stems, longer than a critical length,[30] irreversibly attach on crystalline substrate. Accordingly, both the melting of the solid phase on heating and the crystallization of the molten phase on cooling are non-reversible processes. However, the observed spreading of reversibility over a wide temperature region implies the existence of a continuous distribution of local equilibria between the crystalline and molten states, well below the equilibrium melting point.

Therefore, reversible melting and crystallization cannot be an activated process and does not occur in absence of primary or molecular nucleation. Various are the molecular mechanisms proposed which fulfil these conditions, depending on experimental results interpretations and on polymer properties. It has been suggested that the reversible transition of polymers characterized by low sliding diffusion within the crystalline phase and for which a contribution of the fold surface is excluded, is mainly due to the local removal-deposition process of macromolecular segments, which can move independently from the rest of the molecule, already in the crystalline phase.[6-10] A microstructural model for the reversible crystallization ad melting phenomena has been proposed by Wurm et al.[10] who explored the isothermal crystallization experiments of various polymers by using calorimetric and dynamo mechanical temperature modulated techniques (TMDSC and TMDMA). They have suggested that the reversible crystallization and melting originated at the lateral surfaces of lamellae, where chain segments in the adjacent amorphous phase are driven by the undercooling to arrange in the crystalline array, but, contemporary, an opposite elastic force due to topological constrictions can humper the formation of new crystalline stems. The balance of the two opposite forces generates a dynamic "local equilibrium", which favours the stem deposition at lower temperature. The reversibility is maintained on condition that pre-existing, thermally stable molecular nuclei are present on crystalline substrate. It means that the melting temperature of macromolecule segments involved in the reversible crystallization should be lower than that of the portion in the crystalline phase. This model has been also confirmed for isotactic polypropylene by the evidence that the lower is the order or the lateral dimensions of the crystallites the higher is the amount of reversible melting[4].

However, other temperature modulated investigation techniques, able to observe the sample structural transformation, have been profitably combined with the calorimetric results, in order to interpret the origin of the reversible crystallization-melting process. In this contest, the reversible melting of linear PE was, although partially, associated also to the reversible lamellar thickness variation, by the combined use of TMDSC and time resolved temperature modulated SAXS and WAXD[6,11].

Variable temperature vibrational techniques, namely FTIR and Raman spectroscopy could be other powerful techniques, able to investigate at detailed microstructural level the thermal transition of materials[12]. Differently from a conventional DSC or MTDSC analysis, it is more detailed inasmuch it can distinguish the local variation of the conformations and specific inter- or intramolecular interactions involved in the sample transitions. Moreover, they allow the analysis of athermal or slow processes, which cannot be studied by calorimetric analysis, because of the null or low heat flux involved in the transformation[13].

As far as investigations on isotactic polypropylene thermal transitions are concerned, variable temperature FTIR and Raman spectroscopy have been successfully applied to the study of the time and temperature dependent evolution of characteristic regularity bands of the iPP mid infrared and Raman spectrum. They originate from the intramolecular coupling of conformation sequences arranged in 3_1 helix of different minimum length,[35,17,16,22,34] generally referred to the number of repetitive units in helical structure (*n*). The latter have been employed to characterize the iPP melting process[16], the melt crystallization[17,33,35,22] and the transformation of mesomorphic phase of quenched sample into crystalline monoclinic phase during sample heating[18,19]. Concerning the melt-crystallization mechanism, FTIR and Raman studies have highlighted a complex equilibrium distribution between the conformationally disordered chain and the 3_1 helix structure, that depends on temperature and helical length. According to the Doi's theory[30] on nematic phase separation prior to the melt-crystallization, the iPP helices are in equilibrium with the melt if their length does not exceed a critical value, set to 11 repetitive units in helix structure.[17,33,35] Helices longer than this value are unstable thermodynamically and, as soon as they form, they begin to orientate themselves parallelly to develop crystalline nuclei. A multistage growth model[31] for the crystallization has been proposed by Strobl, based on the observation of the sequential formation from shorter to longer helix structures.[17,22]

Moreover, spatial resolved FTIR have been used to study the conformational preordering on spherulite growth front in isothermal melt-crystallization.[14,15] The experimental results obtained by Cong et al. have evidenced a conformationally ordered phase, enriched of 3_1 helix structures with length of 10 repetitive units, at the growing front of spherulites (GFL). It have been observed that GFL could reach 30 μm thickness.

VTFTIR has been also used to highlight and interpret a subtle transition occurring in semi-crystalline samples at about 135 °C, initially described by Hanna et al.[20] and further analysed in detail by Zhu et al.[21]. Experiments on semi-crystalline undrawn and drawn iPP, as well as on chlorinated iPP, have led to suggest that the transition was due to the disordering of the helices in the partially ordered non-crystalline phase. Moreover, being the transformation reversible in successive cooling and heating scans in a wide temperature range, its relationship to a premelting process has been excluded. Anyway, the employed experimental set up could not have given any direct information on reversing processes, occurring in a small temperature range.

In the present study the reversing crystallization and melting of isotactic polypropylene was investigated in dynamic cooling condition, by using a modified variable temperature FTIR analysis. For this purpose, VTFTIR was implemented by sequentially recording the spectra during a temperature program comprised of a constant cooling rate superimposed to a temperature periodic oscillation (modulated temperature FTIR, MTFTIR). By processing selected spectral signals (here in specific, the absorption band intensities) as a function of the acquisition time, it has been possible to obtain their total variation, as well as the reversing and non-reversing components as a function of the mean temperature. In order to estimate the influence of non-reversing crystallization on the reversing crystallization and melting, different crystallization conditions were used. Two fast crystallizations, occurring in a small temperature range between about 120-135 °C, were achieved by cooling at different rates a homogeneous molten sample, obtained by keeping the polymer at 185 °C for 60 min. Conversely, a slow crystallization process was achieved by cooling a partially molten sample, in which the ordered structures, survived in the melt, acted as heterogeneous nuclei and favoured the crystallization at higher temperatures (130-160 °C). Independently from the crystallization rate and temperature, the MTFTIR analyses highlighted a reversing transformation starting few degrees below to the non-reversing crystallization onset and partially superimposed to it. Ultimately, a Quasi-isothermal FTIR experiment was performed to investigate the dependence of the reversible crystallization and melting of iPP as function of the length of helical structures. By comparing the spectroscopic results with those obtained by Quasi-isothermal DSC, according to the two distinct reversibility regimes depending on helix lenght were highlighted in the 30-130 °C temperature region.

5.2 EXPERIMENTAL PART

The isotactic polypropylene (iPP) used in this study was purchased from Sigma-Aldrich (M_w=340000, M_n=97000, MFI=4 g/10 min). In order to minimize oxidation reaction at high temperature, the iPP films (thickness about 20 μm) were compressed between two KBr disks. Mid-infrared spectra were acquired in transmission by a Nicolet 6700 FTIR equipped with a SPECAC variable temperature cell driven by a HELLMA temperature controller. Each spectrum was obtained by co-adding 40 scans at a resolution of 4 cm^{-1}. The temperature programs, directly applied into the cell sample holder, comprised of a linear heating ramp at 5 °C min^{-1} up to the polymer melting at 185 °C. The samples were kept at this temperature for 60 min and then cooled at two different rates. The slow temperature program (iPPs experiment) comprised of a linear cooling at 0.18 °C min^{-1} superimposed to a sinusoidal temperature modulation, characterized by an amplitude of 2.5 °C and a period of 480 s. The fast program (iPPf1 experiment) comprised of a linear cooling ramp at 0.51 °C min^{-1} superimposed to a sinusoidal temperature modulation, characterized by an amplitude of 2.7 °C and a period of 480 s. One non-isothermal crystallization experiment was also carried out by keeping the sample 5 min at 185 °C and by using the fast cooling program (iPPf2 experiment).

Quasi-isothermal measurements (QI-iPPs experiments) were performed within a 30-130 °C temperature range on the iPPs sample cooled at RT. A sawtooth modulation with constant mean temperature, an amplitude of 2.5 °C and 480 s period was used. For each temperature the modulation was kept for at least 1.5 hours to allow the achievement of stationary condition.

The summary of the temperature modulated experiments and their code are reported in Table 5.1.

Table 5.1. Experiment codes defining the different conditions employed in iPP melt crystallization as well as crystallization (T_C^{os}) and reversing (T_R^{os}) transitions onset temperature recorded in the three different experiments.

Experiment	Mean cooling rate (K min^{-1})	Time at 185 °C (min)	T_C^{os} (°C)	T_R^{os}
iPPs (slow)	0.18	60	138	129
QI-iPPs (quasi-iso)	0	-	-	-
iPPf1 (fast)	0.51	60	135	126

iPPf2 (fast)	0.51	5	166	136

At the end of the acquisition, the integrated intensity of selected absorption bands per each spectrum was recorded, given a suitable baseline. The detailed signal transformation used to obtain the total band intensity variation and the reversing and non-reversing components as a function of the mean temperature (T^M) is reported in the Supporting Information. Briefly, the modulated temperature and the integrated intensities recorded as a function of acquisition time were averaged over a modulation period to obtain the mean total intensity ($I_{\bar{\nu}}^{Tot}$) of band at wavenumber $\bar{\nu}$ as a function mean temperature. Then, by a deconvolution procedure, based on Sliding Fourier Transform, the complex intensity ($I_{\bar{\nu}}^{*}$) per each band and complex temperature (T^*) as function of the mean temperature were calculated. The reversing component of the intensity ($I_{\bar{\nu}}^{R}$) was given by integrating the ratio between the real part of the complex intensity $I_{\bar{\nu}}'$, and the modulus of the complex temperature$|T^*|$.The non-reversible component ($I_{\bar{\nu}}^{NR}$) was obtained by subtracting $I_{\bar{\nu}}^{R}$ from $I_{\bar{\nu}}^{Tot}$. It is important to remark that $I_{\bar{\nu}}^{R}$ is evaluated by considering only the real part of the complex intensity in order to exclude kinetics temperature-dependent contributions, characteristic of non-reversible phenomena. For quasi-isothermal FTIR measurement the prime derivative of the reversible intensity $\frac{dI^R}{dT}$ was calculated by the ratio $\frac{I_{\bar{\nu}}'}{|T^*|}$ as function of time and temperature. It's important to remark that the difference between reversing and reversible component was used for indicating the result obtained by quasi isothermal and temperature modulated experiments, respectively.

The spectroscopic degree of reversibility $R_{\bar{\nu}}^{FTIR}$ was determined for band at wavenumber $\bar{\nu}$ from quasi-isothermal FTIR by Equation 5.1:

$$R_{\bar{\nu}}^{FTIR}(T) = \frac{\left|\frac{dI_{\bar{\nu}}^{R}}{dT}(T) - \frac{d\varepsilon}{dT}_{(30\,°C)}\right|}{I_{\bar{\nu}\ (30\,°C)}} \cdot 100 \qquad \text{Eq 5.1}$$

Where $\frac{dI_{\bar{\nu}}^{R}}{dT}$ is the temperature dependent prime derivative of the reversible intensity, $\frac{d\varepsilon}{dT}$ is the variation of the absorption coefficient with temperature and $I_{\bar{\nu}}$ is the band intensity, both calculated at T = 30 °C. It's important to remark that the $\frac{dI_{\bar{\nu}}^{R}}{dT}$ value was taken after the equilibration period for each temperature, to exclude kinetic phenomena. The spectroscopic reversibility $R_{\bar{\nu}}^{FTIR}$, given in % $°C^{-1}$, is the percentage variation with temperature of the reversible intensity normalized to the total intensity.

Standard Differential Scanning Calorimetry (DSC) and quasi-isothermal DSC were performed using a Mettler Toledo DSC 822e equipped with a ceramic sensor FRS 5 and a liquid nitrogen cooler. Dry nitrogen at a flow rate of 30 ml min^{-1} was used to purge the furnace. Calibrations for the temperature, the heat flow and the tau lag were performed using indium and zinc. An iPP film of about 500 μm thickness was placed in a 40 μl aluminium pan, melted at 185 °C for 60 min and non-isothermally crystallized by cooling it at 0.18 K min^{-1} (iPPs temperature program without modulation) by using a Linkam HFS 91 hot stage driven by a Linkam TP 92 temperature controller. Standard DSC thermograms were recorded from 0 to 200 °C with a linear heating rate of 10 °C min^{-1}. The temperature dependent enthalpy-based crystallinity was determined by calculating the apparent total specific heat from experimental heat flow curves, and by a stepwise integration of the apparent total specific heat corrected for the thermodynamic specific heat[4]. Thermodynamic vibrational specific heat, temperature and enthalpy of fusion, were referred to the ATHAS database.[36]

For quasi isothermal DSC measurement, a sawtooth modulation was used with amplitude of 1 °C, 240 s period and 1.5 h equilibration time for each temperature step. The investigated temperature range was 25-130 °C. Temperature and time dependent apparent reversing specific heat c_p^{rev} was calculated by the ratio between the amplitudes of heat flow and heating rate, evaluated as the first harmonic of the Fourier series. Furthermore, the average specific reversibility R^{DSC} as function of the temperature was calculated by means of Equation 5.2, as reported by Androsh et al.[37]:

$$R^{DSC}(T) = \frac{c_p^{rev,\infty}(T) - c_p^{vib}(T, X_c)}{X_c(T) \cdot \Delta H_f^0(T)} \cdot 100 \qquad \text{Eq 5.2}$$

Where $c_p^{rev,\infty}$ is the reversible specific heat obtained after the equilibration period, c_p^{vib} the thermodynamic vibrational specific heat of the semi crystalline material, X_c the enthalpy-based crystallinity and ΔH_f^0 the temperature dependent enthalpy of fusion.

The average specific reversibility R^{DSC}, given in % °C^{-1}, is the percentage variation of the excess reversible specific heat respect to the thermodynamic specific heat, normalized for the temperature dependent heat of fusion and for the crystalline fraction.

5.3 RESULTS

5.3.1 Non-isothermal melt crystallization of iPP by MTFTIR

In order to study the non-isothermal crystallization of iPP samples cooled from the melt, three MTFTIR experiments, characterized by different residence time of polymer in the melt and modulated temperature cooling program, were carried out. For each experiment, three regularity bands at 998, 841 and 1220 cm^{-1} were followed. The bands are assigned to the coupling between C–C stretching, CH_2 rocking and CH_3 rocking for a characteristic helical length of n=10, n=12 and n>15 repeating units, respectively[17,20,22].

As an example, in Figure 5.1 A, the integrated intensity of the peak at 998 cm^{-1}(I_{998}, n=10) and the modulated temperature profile obtained in the slow cooling experiment (iPPs) was reported as a function of spectra acquisition time. The elaboration of the oscillating raw data of Figure 5.1 A gave the total intensity (I^{Tot}_{998}) and its reversing (I^{R}_{998}) and non-reversing (I^{NR}_{998}) components as a function of the mean temperature (T^M) (Figure 5.1 B). The starting intensity value at high temperature is not null because, as it is well known, this regularity band exists also in the molten state, indicating that sequences of ordered conformers can survive in the iPP liquid phase[17].

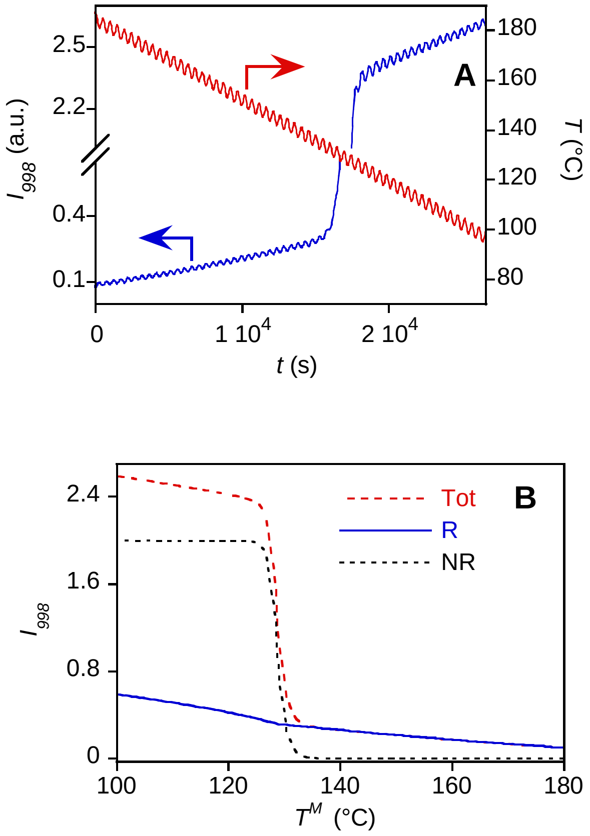

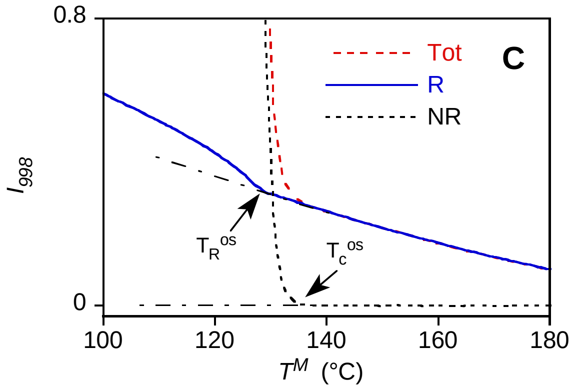

Figure 5.1. MTFTIR results of iPPs experiment. (A) Oscillating raw intensity variation of the band at 998 cm^{-1} (I_{998}) and modulated temperature as a function of the spectra acquisition time. (B) Variation of the total intensity (I^{Tot}_{998}) and the reversing (I^{R}_{998}) and non-reversing (I^{NR}_{998}) components of the band at 998 cm^{-1} as a function of the mean temperature (T^M). (C) Enlargement of Figure 5.1B. The arrows indicate the onset of non-reversing crystallization (T_c^{os}) and the onset of the reversible transition (T_R^{os}). The dash-dot lines are a guide for the eyes to indicate the nearly linear variation of I^{NR}_{998} and I^{R}_{998} before the transitions.

The total intensity variation of the 998 cm^{-1} band I^{Tot}_{998} in Figure 5.1 B shows an almost linear increase by cooling the sample, in the temperature range between 185 and 138 °C. In this region, corresponding to the iPP melt, the total intensity evolution I^{Tot}_{998} was caused exclusively by the variation of the reversing component I^{R}_{998}, being null the non-reversing I^{NR}_{998} component. Hence, according to the Lambert-Beer law, the reversing intensity variation as a function of temperature was due to the combination of three contributes, namely the reversing change of the absorption coefficient, of the sample density and of the n=10 helix equilibrium concentration. At 138 °C, the abrupt increase of the non-reversing component highlighted the crystallization onset. For sake of clarity, in Figure 5.1 C, the enlargement of Figure 5.1 B is displayed, where the onset of non-reversing crystallization T_c^{os} (Figure 5.1 C, Table 1) was displayed by an arrow in correspondence of the first departure of I^{NR}_{998}. Despite the start of the melt crystallization, the reversing component I^{R}_{998} showed a linear trend up to 129 °C, where a sharp positive inflection occurred (T_R^{os}, marked by the arrow in Figure 5.1 C and reported in Table 1). The same data analysis was carried out for the other absorptions associated to different helix lengths. The results of the reversing (I^R) and non-reversing (I^{NR}) components for the selected regularity bands, located at 998 cm^{-1} (n=10), 841 cm^{-1} (n=12) and 1220 cm^{-1} (n>15), are reported in Figure 5.2. Because the absolute band intensities were very different, for sake of comparison, the non-reversing components (I^{NR}) of each band were normalized respect to the value reached at 100 °C (Figure 5.2 A). The values of the reversing components were normalized by the same factor (Figure 5.2 B).

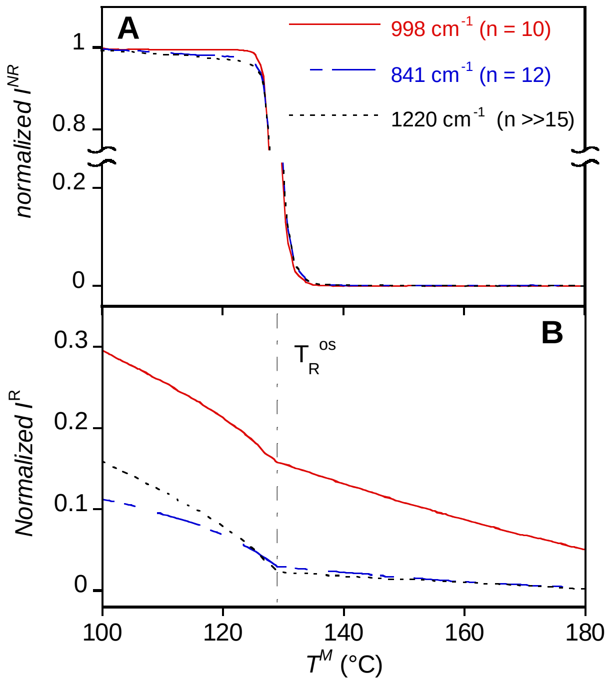

Figure 5.2. Normalized band intensity variation as a function of mean temperature recorded in iPPs experiment. Non-reversing (A) and reversing (B) components. The vertical dash-dot line indicates the onset temperature of the reversing transition.

Figure 5.2 A clearly shows that the non-reversing crystallization started at the same temperature, irrespective of the helix length, and that a different behavior can be observed only at the last stages of the transition. In fact, the concentration of the n=10 helix (998 cm^{-1}) suddenly levelled off at the end of the primary crystallization (125°C), while longer helices with n=12 (841 cm^{-1}) and n>15 (1220 cm^{-1}) continued to increase up to the end of the experiment. This process could be considered as a secondary non-reversing crystallization or order perfection favoured at the lower temperature.

As far as reversing components I^R are concerned, Figure 5.2 B shows that in the melt, up to the onset of the reversing transition T_R^{os}, only the n=10 helix (998 cm^{-1}) was present in appreciable concentration, while the n=12 and n>>15 helices were nearly absent. At T^M=T_R^{os} the reversing transition took place at the same temperature for all helix lengths, with a temperature delay respect to the non-reversing crystallization onset.

The melt crystallization was repeated by using a faster cooling rate (iPPf1 experiment) and a different residence time at 185 °C (iPPf2 experiment, Table 5.1). The total integrated intensity of the band at 1220 cm^{-1} (n>15), recorded in the three experiments, was reported in Figure 5.3. To consider the different thickness of the samples, the I^{Tot}_{1220} values of the three experiments were normalized respect to the band intensity at 1151 cm^{-1}, recorded at 185 °C (I^{0}_{1151}). It was assigned to vibrational mode coupling between C–C stretching, CH_2 rocking and CH_3 rocking in a disordered chain conformation.

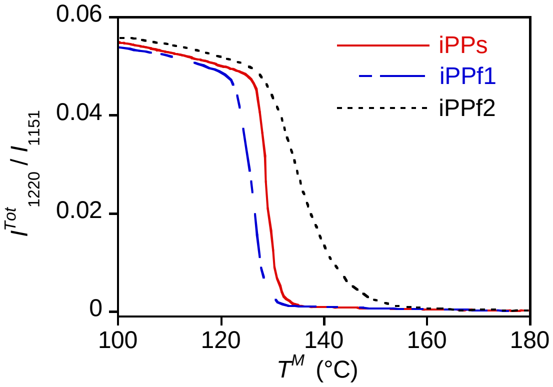

Figure 5.3. Normalized total intensity variation $I^{Tot}_{1220}/I^{0}_{1151}$ as a function of the mean temperature recorded in the three different experiments.

Figure 5.3 shows that the crystallization onset temperature of iPPf2 sample (T_c^{os}=166 °C) was much higher than that observed in the other experiments (Table 1). The shorter period of the sample into molten state, brought about an incomplete disruption of the previous crystalline state and the ordered structures survived in the melt acted as heterogeneous nuclei, favouring the crystallization at higher temperature. Therefore, the self-seeding crystallization was slow. Differently, the crystallization of iPPs and iPPf1 samples occurred without the presence of memory effects due to the previous crystalline state. The crystallization temperature of such samples was lightly influenced by the different cooling rate (Table 1).

The similar normalized intensities reached at low temperature indicate a nearly equal order degree of the crystallized samples.

The 998 cm^{-1} band intensity variation during the crystallization at low undercooling (iPPf2) is reported in Figure 5.4 A, meanwhile Figure 5.4 B shows a detail of the crystallization region.

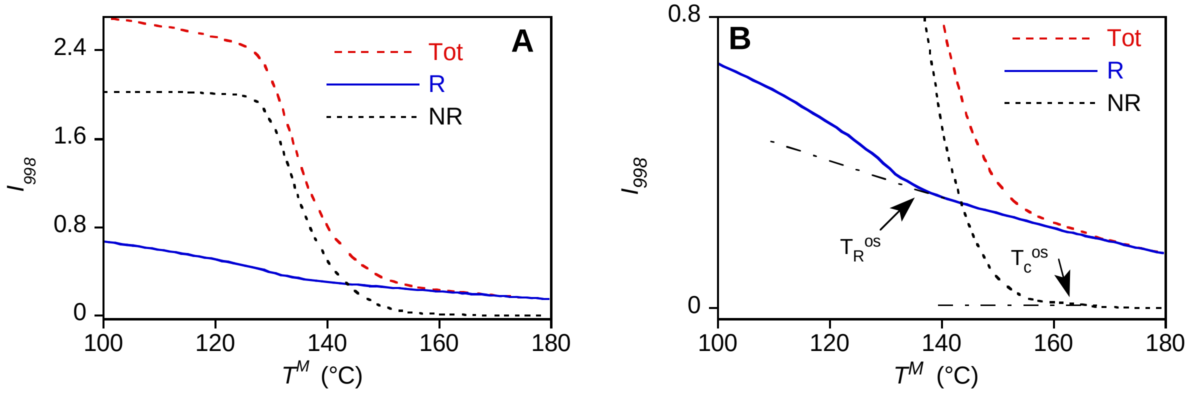

Figure 5.4. MTFTIR results of the iPPf2 experiment. (A) Variation of the total intensity (I^{tot}_{998}) and reversing (I^{R}_{998}) and non-reversing (I^{NR}_{998}) component of the band at 998 cm^{-1} as a function of the mean temperature (T^M). (B) Enlargement of Figure 5.4A. The arrows indicate the onset of non-reversing crystallization (T_c^{os}) and the onset of the reversible transition (T_R^{os}). The dash-dot lines are a guide for the eyes to indicate the nearly linear variation of I^{R}_{998} before the transition.

The enlargement of the Figure 5.4 A, displayed in Figure 5.4 B, shows the same features observed in the experiment at higher undercooling (iPPs), already discussed. The onset temperature of the non-reversing crystallization can be observed at T_c^{os}=166 °C and the deviation from linearity of the reversing component I^{R}_{998} at about T_R^{os}=136 °C (Figure 5.4 B). Again, as found in the iPPs and iPPf1 experiments, the reversible transition occurred after the start of the crystallization process.

The normalized non-reversing and reversing components for all analysed regularity bands are reported in Figure 5.5.

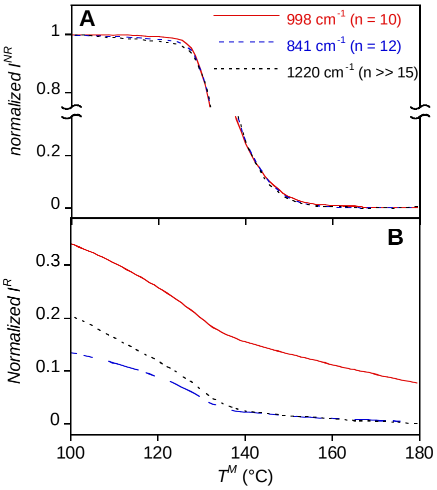

Figure 5.5. Normalized band intensity variation as a function of mean temperature recorded in iPPf2 experiment. Non-reversing (A) and reversing components (B).

Like in iPPs experiment (Figure 5.2), also in the iPPf2 cooling condition T_c^{os} and T_R^{os}, as well as the crystallization kinetics, did not depend on the analysed regularity bands. Moreover, the comparison among the three experiments highlights that the reversing process onset was strictly related to the non-reversing crystallization.

The results on the non-isothermal melt crystallization of isotactic polypropylene obtained by MTFTIR allowed to follow separately the occurrence of reversing and non-reversing processes in the melt phase and in the crystallization region of isotactic polypropylene. Regularity bands followed in this part of the research were the 998, 841 and 1220 cm^{-1} , assigned respectively to the intramolecular coupling of 10, 12 and more than 15 repeating units arranged in 3_1 helical structures. The results (Figures 5.2 and 5.5) highlighted that the non-reversing crystallization, involving the increase of the overall helix population, was followed by a reversing transition that started at the last stages of the crystallization, independently from the experimental conditions.

The reversing and non-reversing intensity variations occurring during the dynamic cooling were strictly related, respectively, to the equilibrium or out-of-equilibrium conformational rearrangement of disordered chain segments into helix structures of different length. In particular, the comparison between the reversing and non-reversing components showed that, on cooling the molten iPP, a reversing increase of helical structures took place few degrees below the non-reversing crystallization onset. At lower temperature, where the non-reversing transition almost ceased, the reversing process continued to the experiment end, without any clear discontinuity. The reversing process onset did not strictly depend on the temperature per se, but was tightly related to the non-reversing crystallization onset.

Hence, the crystallization proceeds trough formation of longer helices from the growth front layer (GFL) and their deposition on primary or branched lamellae. In the non-reversing crystallization, the growing lamellae select the thickness established by the supercooling in respect to the melting temperature.[32] During this period, the amorphous phase begins to experience mobility restriction because of the constraints of the adjiacent crystalline phase. The mobility reduction can originate from the formation of tie molecules, entanglements or loose folds. Then, when the amorphous phase can no longer supply chain portions of the proper length for the deposition on crystalline substrate, the non-reversing primary crystallization ceases. As a straightforward consequence of the crystallization mechanism, the resulted phase at the end of the crystallization is formed by primary and subsidiary lamellae surrounded by an amorphous interlamellar region that preserves the conformational and spatial order of the GFL.[14,15]

At the end of the primary non-reversing crystallization, a reversing increase of the overall helix population was observed by decreasing the temperature. The reversing phenomena has been ascribed to the reversing formation and disruption of helix structures of different length, and it was associated to the reversing crystallization and melting observed by means of modulated DSC.[4] These results support the idea that the helix-enriched interlamellar region is still present at the end of the primary crystallization, in which topological constrains generates “local equilibria” at the lamellar edge between disordered chain and helix structure.[10] At the same time, while the non-reversing intensity component of the shorter helix bands levels off at the end of the primary crystallization, a further non-reversing increase of helices greater or equal to 12 repeating units was observed, involving the increase of sample crystallinity. This stage can be related to secondary crystallization.

In agreement with Zhu et al.[17], the present research shows that in the melt phase only the helix sequences shorter than 12 repeating units are in equilibrium with the coil structure in the melt. Furthermore, the secondary non-reversible crystallization involves only the formation of helices greater or equal to 12 repetitive units (Figures 2A, 5A), suggesting that helices above the critical length ($n \approx 11$) are unstable in amorphous conditions, but they can form if stabilized by an adjacent crystalline surface.

5.3.2 Quasi isothermal studies on reversibility of the crystallization

In order to study and quantify in detail the reversible phenomena related to the semi-crystalline phase of iPP, QIFTIR experiments were carried out and the results were compared to that obtained from quasi isothermal DSC analysis. The quasi isothermal protocol, in respect to the temperature modulated scan, allows to investigate the truly reversible transformation by holding the modulate temperature program for an arbitrary equilibration time at each investigated mean temperature. Therefore, any possible slow kinetic transformations, e.g. reorganization of the crystal phase, is brought at completion and the stationary condition achieved, in contrast to the temperature modulated protocol in which the equilibration time is heating/cooling rate dependent. Hence, a distinction of the “reversing” term from “reversible” has been made in the following section, indicating with “reversing” the transitions that occur in not proved stationary conditions (MTFTIR), and using “reversible” for transformations that are studied in stationary conditions (QIFTIR, QIDSC).

Figure 5.6 shows the comparison between the QIFTIR and TMFTIR experiments performed on the iPPs sample. The first derivative of the reversible intensity $(dI^R/dT)^\infty$ and of the reversing intensity dI^R/dT of the bands located at 1100, 998, 840 and 1220 cm^{-}1 were plotted as function of the mean temperature.

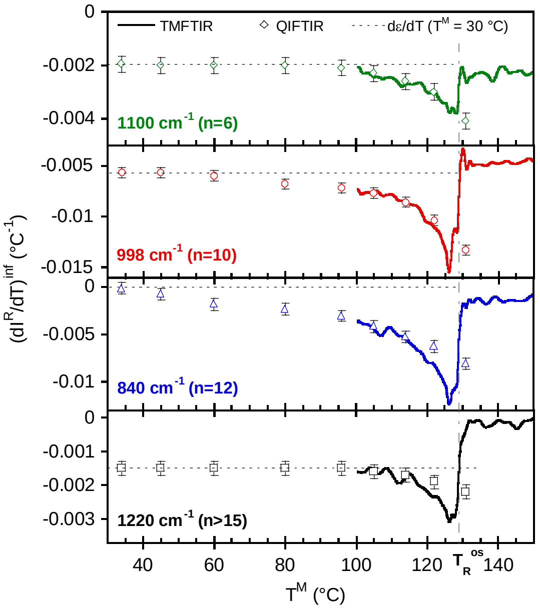

Figure 5.6. First derivative of the reversing intensity (solid lines) from iPPs TMFTIR experiment and first derivative of reversible intensity (open symbols) from QI-iPPs QIFTIR experiment of the bands at 1100, 998, 840 and 1220 cm^{-1} as function of the mean temperature. The horizontal short-dashed lines indicate the reversible intensity calculated at 30 °C. Vertical dash-dot line indicates the onset of the reversing transition T_R^{os} calculated in the iPPs experiment.

Regarding the iPPs non-isothermal melt crystallization (TMFTIR experiment), dI^R/dT (solid lines, Figure 5.6) remain constant from 150 °C to the onset of the reversing transition, evidenced by the rapid decrease at T_R^{os}= 129 °C (Figure 5.2). At 126 °C, the minima of dI^R/dT of all the reported bands represent the maximum change of reversing intensity with the mean temperature. Below 126 °C, dI^R/dT increases, indicating the decrease of the reversing transition with temperature decrease. Nevertheless, as seen in Figure 5.2, it is difficult to calculate the end of the transition, that is the achievement of the dI^R/dT constancy. A previously noticed, the first derivative of the reversing intensity depends on density, absorption coefficient and helix concentration variation with temperature. In absence of non-reversible transitions, the density (ρ) and the absorption coefficient (ε) change almost linearly with the temperature ($d\varepsilon/dT$, $d\rho/dT$=const.). Therefore, the deviation of dI^R/dT from a constant value is caused principally by the reversing variation of helix concentration.

The melt-crystallized iPPs sample was cooled at RT after the TMFTIR experiment to execute the QIFTIR measurements from 30 °C to 130 °C (open symbols, Figure 5.6). In this temperature region the helix of different length behaved distinctly. The bands located at 1100 (n=6) and 1220 cm^{-1} (n>15) shows a $(dI^R/dT)^\infty$ constant value from 30 to about 95 °C, where a rapid decrease occurs. Nevertheless, the bands at 998 (n=10) and 840 cm-1 (n=12) shows the deflection at 60 °C and 40 °C, respectively. These evidences strongly suggests that the reversible transition depends on helix length.

It is also interesting to observe that at 120 °C, differently from the shorter helices (n=6 and n=10), the $(dI^R/dT)^\infty$ values (QIFTIR) of longer helices (n=12 and n>15) are lower than those of dI^R/dT (MTFTIR). This is indicative of reversibility decrease of longer helices, involved in the slow non-reversing reorganization of the secondary crystallization.

The reversible transition of iPP was also investigated by quasi isothermal DSC technique (QIDSC) on an iPP sample, melt-crystallized with the same linear cooling rate of the iPPs experiment (0.2 °C/min). QIDSC results were reported in Figure 5.7, in a temperature range between 25 and 130 °C.

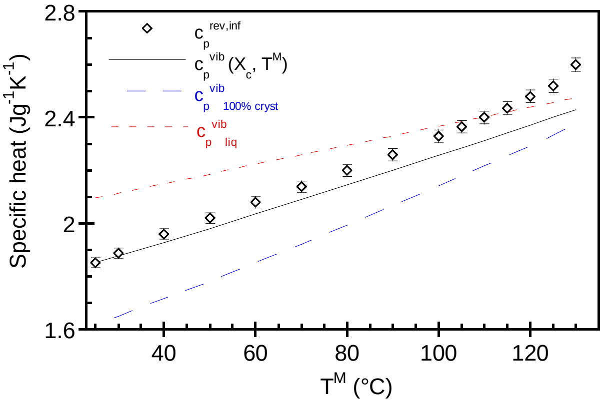

Figure 5.7. QIDSC measurement of iPP melt-crystallized at -0.2 °C min^{-1}. Reversible specific heat in stationary condition (open symbols) and the thermodynamic vibrational specific heat of

the semi-crystalline sample (solid line), of the liquid state (short-dash line) and of the crystal (long-dash line) as function of the mean temperature.

The values of reversible specific heat after the equilibration period (stationary condition) of semi-crystalline iPP as function of the mean temperature are in agreement with those reported by of Androsh et al.,[4] showing from 30 °C to 130 °C a reversible specific heat in excess of the thermodynamic vibrational c_p, (solid line, Figure 5.7).

In order to compare the FTIR and DSC results, an appropriate parameter must be chosen. For calorimetric measurements the average specific reversibility was utilized (Equation 5.2). This parameter considers that all the excess of the reversible specific heat was due totally to a reversible crystallization and melting. So, the $c_p^{rev,\infty}$ was normalized by the temperature dependent enthalpy of fusion of the 100% crystalline iPP and by the sample crystallinity. The obtained average specific reversibility $R^{DSC}(T^M)$ indicates the reversible percentage variation of the crystal phase per temperature unit.

Analogously, a parameter, called spectroscopic reversibility R^{FTIR}, was evaluated for FTIR measurements. It was defined as the reversible percentage variation of helix population per unit of Celsius (Equation 1). Then, for the R^{FTIR} calculation, it is necessary to know the reversible intensity excess. Unfortunately, the relationship between a regularity band intensity and the related helix population is not direct, because of the variation of the band absorptivity (ε) with temperature must be considered. Generally, ε changes linearly with the temperature and, in absence of phase transitions, $d\varepsilon/dT = const$. The other contribution to the reversible intensity, namely the conformational population change, could be highlighted as a departure of the first derivative of the reversible intensity $(dI^R/dT)^\infty$ from the absorptivity contribution $d\varepsilon/dT$. Hence, the spectroscopic reversibility R^{FTIR} as function of temperature can be determined by Equation 5.1. Here, the reversible excess is taken as the absolute value of the difference between the first derivative of the reversible intensity calculated at a generic temperature ($\frac{dI_{\bar{\nu}}^R}{dT}(T)$) and at the lowest temperature reached by QIFTIR ($\frac{d\varepsilon}{dT}_{(30\,°C)}$, T^M = 30 °C), where sample transitions are nearly absent. Finally, R^{FTIR} was obtained by normalizing the reversible excess by the total intensity of the band at 30 °C ($I_{\bar{\nu}\ (30\,°C)}$), representative of the helix population absorbing at that wavenumber.

Figure 5.8 shows the average specific reversibility R^{DSC} from QIDSC experiments and the spectroscopic reversibility R^{FTIR} of the bands at 1100, 998, 840 and 1220 cm^{-1} from QIFTIR experiments.

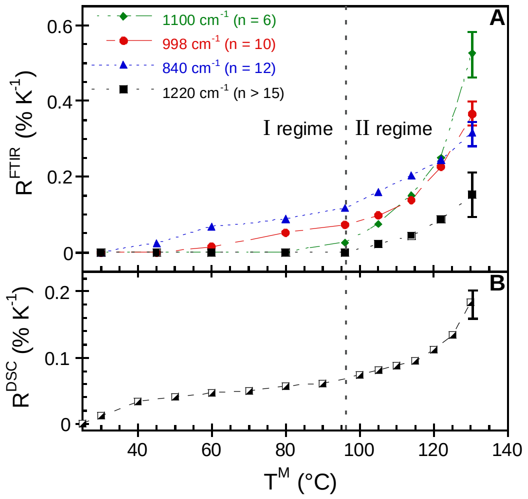

Figure 5.8. Spectroscopic reversibility (A) and average specific reversibility (B) as function of the mean temperature. Vertical dashed line at T^M = 96 °C shows the change of the reversible transition regime.

The spectroscopic reversibility of all the bands starts to zero at 30 °C, at which no transitions were expected.[4,37] Then, the spectroscopic reversibility shows a complex dependence with temperature, specific for each absorption.

According to the results reported in Figure 5.8, the explored temperature range was divided into two regions where two different general behaviour can be observed. They were called *regime I*, between 30 and 96 °C, and *regime II*, ranging from 96 °C and 140 °C (Figure 5.8A). In *regime I*, R^{FTIR} of shortest (n=6) and longest (n >15) helices was null, while the intermediate length helices showed the onset the reversible transition at 45 °C (n=12) and 60 °C (n=10). Above 96 °C, in the *regime II*, an intense reversible transition involved all the helix populations. In this temperature range, the shorter was the helix length the higher the spectroscopic reversibility, reaching the maximum value at T^M = 130 °C for the n= 6 helix structure.

In Figure 5.8B the average specific reversibility, calculated from reversible specific heat, was reported as function of the mean temperature. The QIDSC experiment shows that R^{DSC} rapidly increased from 30 °C and, then, stabilized nearly at 0.06 % C^{-1}, between about 50 °C and 96 °C, into the *regime I* region. Successively, a second specific reversibility increase occurred up to 130 °C, reaching R^{DSC}=0.18 % C^{-1}. The average specific reversibility in *regime II* was comparable to the spectroscopic reversibility of helices longer than 15 repetitive units, meanwhile the magnitude of the reversible transition for shorter helix is higher. On the other hand, in the *regime I*, the calorimetric reversibility was similar to the spectroscopic one related to the reversible formation and disruption of the intermediate length helices (n=10-12).

5.4 DISCUSSION

The comparison of the results about the reversible transformation occurring in semi-crystalline isotactic polypropylene observed by two different techniques, DSC and infrared spectroscopy, allowed to establish the correlation between the calorimetric data with those related to the microstructural sample evolution.

Typically, the Quasi-isothermal DSC experiments furnishes the specific heat in stationary conditions and exclude any contribute of the latent heat exchange involved kinetics phenomena. Then, the reversible specific heat can be considered as the sum of all reversible enthalpic contributions associated to the sample thermodynamic state, namely vibrational, conformational and structural (e.i. heat of reversible fusion/crystallization). The first contribution could be easily obtained from ATHAS database, but the separation of the last two is difficult because of the undifferentiated calorimetric response. Then, the average specific reversibility (R^{DSC}), calculated from QIDSC at selected temperatures and reported in figure 5.8 B, cannot give further information on the different mechanisms involved in the reversible transition and on the microstructural evolution observed in the *regime I* and *regime II* temperature ranges.

A further step towards the interpretation of the reversible transition of iPP in term of conformation evolution was accomplished by Quasi isothermal FTIR measurement on a sample characterized by the same thermal history to that used in QIDSC analysis. The measurement was carried out by using a small temperature modulation amplitude (2.5 °C) in order to obtain a linear response of the spectroscopic signals.[30]

The structure of the semi-crystalline isotactic polypropylene can be considered comprised of conformationally disordered chain segments and a distribution of 3_1 helix sequences of different length. The intensity of each regularity band of the mid-infrared spectrum represents a fraction of the overall helix population.[16,17,22] Then, quasi isothermal FTIR analysis allowed to measure the reversible concentration variation of specific helix populations due to the reversible conformational transition, namely helix formation and disruption. This involves the existence of a stationary state between disordered chain segments and helix structures, whose interconversion excludes the presence of thermally activated phenomena and, hence, supercooling. From the analysis of spectroscopic reversibility of the four regularity bands (Figure 5.8A), the following observations can be drawn:

- the spectroscopic reversibility, as far as its intensity and temperature dependence, showed a complex relationship with helix length;
- tentatively, two temperature regions could be identified, according to the dependence of spectroscopic reversibility onset and intensity on helix length;
- below 96 °C (*regime I*), the extension of reversible helix formation-disruption process was low and it was active only for helices of intermediate length (10 -12 repeating units);
- above 96 °C (*regime II*), the spectroscopic reversibility intensity showed a considerable increase involving all helix lengths (from 6 to >15 repeating units). At 130 °C, the R^{FTIR} maximum value increased with decreasing helix length.

Moreover, the reversible specific heat in the sample semi-crystalline temperature range (25-130 °C) was obtained by quasi-isothermal DSC analysis (Figures 7). For the comparison of the spectroscopic results, the average specific reversibility ($R^{DSC}(T^M)$), defined in equation 5.2, was used (Figure 5.8A). Similarly to the spectroscopic reversibility result analysis, the $R^{DSC}(T^M)$ dependence with tempertaure could be divided in two regions with the same temperature limits, namely *regime I* between 25 and 96 °C, and *regime II*, between 96 and 130°C. For sake of clarity, the molecular mechanism of the high temperature reversibility (*regime II*) is discussed first.

In *regime II*, the spectroscopic reversibility of helices longer than 15 repetitive units and the average specific reversibility (Figure 5.8) shows a similar intensity. Their maximum values at 130 °C are $R^{FTIR}_{n>15} = 0.15\ \%\ °C^{-1}$ and $R^{DSC} = 0.18\ \%\ °C^{-1}$. Neverthless, the shorter helices exibit much higher spectroscopic reversibility, 0.31 , 0.36 and 0.52 % °C^{-1} for= 12, 10 and 6 repetitive units, respectively. The similar values of spectroscopic reversibility related to the 1220 cm^{-1} regularity band and calorimetric reversibility can be explained taking into account that the polymer chains in the lamellar structure, estimated to be 10 nm thick for a melt-crystallization at about 125 °C [32], have 3_1 helix structures longer han 15 repeating units. These results provide the evidence that the reversible crystallization and melting of iPP proceeds trough reversible formation and disruption of helix structures longer than 15 monomer, corresponding to about 3.34 nm.[17]

According to the iPP microstructural models reported in literature[10,14,15], at the end of the primary crystallization at about 125 °C, the semi-crystalline iPP can be considered composed of crystalline lamellae surrounded by an interlamellar amorphous region. At the lamellar lateral surface, the mobility of conformationally ordered amorphous chain segments in the growth front layer (GFL) are reduced by the topological constrains caused by neighbouring lamellae and by entanglement or loose fold. Thus, this amorphous fraction experiences a local equilibrium condition,[10] in which the thermodynamic force that drives chain segments in the crystal phase is balanced by the elastic force involved in the movement of the chain. The equilibrium condition implies that the melting temperature of the crystalline chain segments is equal to the deposition temperature. If the temperature is decreased, the further progressive deposition of ordered stems produces a crystalline phase at the lamellar edge, characterized by a decreasing melting temperature. Anyway, the equilibrium condition occurs if the macromolecular segments participating to the reversible crystallization find a stable molecular nucleus on the crystalline substrate[1,4,37].

Hence, the reversible crystallization and melting proceeds via the formation-attachment or disruption-detachment of the longer helix structures on crystalline substrate. In this stage, the reversibility of the shorter helices could be associated to the formation-disruption of an intermediate conformationally ordered phase in GFL and, presumably, on the fold surface. The *regime II* reversible crystallization and melting proceeds until the temperature is higher than 96 °C.

Below this temperature (*regime I*), the reversible attachment-detacment of helices with n>15 ceases and the coil-helix transition remains active only for intermediate helix structures (n=10-12). The evidence that in regime I the calorimetric average specific reversibility persists implies the growth of a very thin crystalline phase at the edge of lamellae up to about 30 °C and/or the formation of an intermediate ordered phase composed of interacting helices stabilized by the adjiacent crystalline surface. Anyway, the melting and formation of this phase have to bring an enthalpic contribution ($c_p^{rev,\infty}$ excess) to the reversible process. Indeed, Androsh et al. have stated that the enthalpy variation associated only to the pure conformational coil-helix transition is very low or null.[4] As far as the shortest helices (n=6), it may supposed that their concentration remains almost constant with temperature and that the related reversibility is nearly null. Indeed, at this low temperature and high crystallinity, the fold formation as well as new lamellar basal plane should be excluded.

5.5 CONCLUSION

In the present research, two key advantages of the new modulated temperature FTIR technique have been exploited to give a description at molecular level of the iPP non-isothermal melt crystallization. Indeed, the modulated temperature program allowed to separate the overall variation of the absorption band intensities as a function of temperature in their reversing and non-reversing components. Moreover, the IR spectroscopic analysis gave the opportunity to distinguish the behaviour of the different structural features involved in the transitions. During the sample cooling from the melt state, the analysis of iPP spectra evolution highlighted a non-reversing primary crystallization and a reversing transition. The reversing process was manifested as an increase of regularity band intensities, which took place few degrees below the crystallization onset and continued at lower temperature, where the non-reversing transition ceased. The extent of the intensity variation depended on the regularity band, hence, on the concentration change of helices with different lengths.

The temperature profile of the spectroscopic reversibility for each regularity band, calculated by Quasi-isothermal FT-IR, was compared to the average specific reversibility measured by means of Quasi-isothermal DSC, in a temperature range between 30 and 130 °C. The results evidenced that the reversing transition, highlighted by MTFTIR and Quasi-isothermal, can be associated to the reversible crystallization-melting process occurring to the lateral edges of crystalline lamellae. The conformational mechanism involved in the reversible crystallization was recognized as the reversible helix formation and disruption, that took place soon after the non-reversing crystallization and involved the establishment of local equilibria between helical structure and coil segments. Furthermore, two different regimes of reversibility were highlighted according to the extent of the reversible crystallization. From high to low temperature, starting soon after the non-reversible crystallization up to 96 °C the so-called *regime II* reversibility took place, involving the reversible formation and disruption of the overall helix population. This transition occurred at the lateral surface of lamellae, where longer helical stems attach and detach from the crystal structure reversibly. Hence, by decreasing the temperature from 130 to 96 °C lamellae continued to grow laterally by the reversible mechanism of formation and disruption of longer helix that forms the crystalline stems. This mechanism involved that the new crystallinity at the lamellar edge possessed a lower melting temperature respect to the core lamella formed during the non-reversible crystallization, being equal to the stem deposition temperature. Below 96 °C the *regime II* ceased, and the regime I reversibility took place up to 30 °C. Here, the slight reversible transition was associated to the reversibility of the intermediate helix lengths (n=10-

12) that were too short to form a complete lamellar stem. However, Quasi-isothermal DSC revealed a slight increase of the reversible crystallinity by decreasing the temperature below 96 °C. Hence, the reversible formation and disruption of intermediate helices may support the hypothesis of a progressive lamellar thinning in the *regime I* reversibility by decreasing the temperature. Else, the formation of a metastable crystalline phase on the growth front layer adjacent to the lamellar structures could be hypothesized.

5.6 REFERENCES

(1) Okazaki, I.; Wunderlich, B. Reversible melting in polymer crystals detected by temperature-modulated differential scanning calorimetry. *Macromolecules* **1997**, *30*, 1758-1764.

(2) Okazaki, I.; Wunderlich, B. Reversible local melting in polymer crystals. *Macromol. Rapid Commun.* **1997**, *18*, 313-318.

(3) Righetti, M. C. Reversible melting in poly (butylene terephthalate). *Thermochim. Acta* **1999**, *330*, 131-135.

(4) Androsch, R.; Wunderlich, B. Reversible crystallization and melting at the lateral surface of isotactic polypropylene crystals. *Macromolecules* **2001**, *34*, 5950-5960.

(5) Androsch, R.; Wunderlich, B. Analysis of the degree of reversibility of crystallization and melting in poly (ethylene-co-1-octene). *Macromolecules* **2000**, *33*, 9076-9089.

(6) Androsch, R.; Wunderlich, B. Specific reversible melting of polyethylene. *J. Polym. Sci., Part B: Polym. Phys.* **2003**, *41*, 2157-2173.

(7) Wunderlich, B. Evidence for coupling and decoupling of parts of macromolecules by temperature-modulated calorimetry. *J. Polym. Sci., Part B: Polym. Phys.* **2004**, *42*, 1275-1288.

(8) Wunderlich, B. Reversible crystallization and the rigid–amorphous phase in semicrystalline macromolecules. *Prog. Polym. Sci.* **2003**, *28*, 383-450.

(9) Wurm, A.; Merzlyakov, M.; Schick, C. Reversible melting probed by temperature modulated dynamic mechanical and calorimetric measurements. *Colloid Polym. Sci.* **1998**, *276*, 289-296.

(10) Wurm, A.; Merzlyakov, M.; Schick, C. Reversible melting during crystallization of polymers studied by temperature modulated techniques (TMDSC, TMDMA). *J. Therm. Anal. Calorim.* **2000**, *60*, 807-820.

(11) Goderis, B.; Reynaers, H.; Scherrenberg, R.; Mathot, V. B.; Koch, M. H. Temperature reversible transitions in linear polyethylene studied by TMDSC and time-resolved, temperature-modulated WAXD/SAXS. *Macromolecules* **2001**, *34*, 1779-1787

(12) Pan, P.; Zhu, B.; Dong, T.; Yazawa, K.; Shimizu, T.; Tansho, M.; Inoue, Y. Conformational and microstructural characteristics of poly (L-lactide) during glass transition and physical aging. *J. Chem. Phys.* **2008**, *129*, 184902.

(13) Martinelli, A.; D'Ilario, L.; Caminiti, R. Poly (p-phenylene sulfide) nonisothermal cold-crystallization. *J. Polym. Sci., Part B: Polym. Phys*. **2005**, *43,* 2725-2736.

(14) Cong, Y.; Hong, Z.; Qi, Z.; Zhou, W.; Li, H.; Liu, H.; Chen, W.; Wang, X.; Li, L. Conformational ordering in growing spherulites of isotactic polypropylene. *Macromolecules* **2010**, *43*, 9859-9864.

(15) Cong, Y.; Hong, Z.; Zhou, W.; Chen, W.; Su, F.; Li, H.; Li, X.; Yang, K.; Yu, X; Qi, Z; Li, L. Conformational ordering on the growth front of isotactic polypropylene spherulite. *Macromolecules* **2012**, *45*, 8674-8680.

(16) Zhu, X.; Yan, D. In situ FTIR spectroscopy study on the melting process of isotactic poly (propylene). *Macromol. Chem. Phys.* **2001**, *202*, 1109-1113.

(17) Zhu, X.; Yan, D.; Fang, Y. In situ FTIR spectroscopic study of the conformational change of isotactic polypropylene during the crystallization process. *J. Phys. Chem. B* **2001**, *105*, 12461-12463.

(18) Jiang, Q.; Zhao, Y.; Zhang, C.; Yang, J.; Xu, Y.; Wang, D. In-situ investigation on the structural evolution of mesomorphic isotactic polypropylene in a continuous heating process. *Polymer* **2016**, *105*, 133-143.

(19) Li, X.; Ding, J.; Liu, Y.; Tian, X. A new model for mesomorphic-monoclinic phase transition of isotactic polypropylene. *Polymer* **2017**, *108*, 242-250.

(20) Hanna, L. A.; Hendra, P. J.; Maddams, W.; Willis, H. A.; Zichy, V.; Cudby, M. E. A. Vibrational spectroscopic study of structural changes in isotactic polypropylene below the melting point. *Polymer* **1988**, *29*, 1843-1847.

(21) Zhu, X.; Fang, Y.; Yan, D. A possible explanation to the structure change of isotactic polypropylene occurring at about 135° C. *Polymer* **2001**, *42*, 8595-8598.

(22) Reddy, K; R., Tashiro, K.; Sakurai, T.; Yamaguchi, N.; Sasaki, S.; Masunaga, H.; Takata, M. Isothermal crystallization behavior of isotactic polypropylene H/D blends as viewed from time-resolved FTIR and synchrotron SAXS/WAXD measurements. *Macromolecules* **2009**, *42*, 4191-4199.

(23) Xu, H.; Ince, B. S.; Cebe, P. Development of the crystallinity and rigid amorphous fraction in cold-crystallized isotactic polystyrene. *J. Polym. Sci., Part B: Polym. Phys*. **2003**, *41*, 3026-3036.

(24) Righetti, M. C.; Tombari, E.; Di Lorenzo, M. L. Crystalline, mobile amorphous and rigid amorphous fractions in isotactic polystyrene. *Eur. Polym. J.* **2008**, *44*, 2659-2667.

(25) Strobl, G. R.; Hagedorn, W. Raman spectroscopic method for determining the crystallinity of polyethylene. *J. Polym. Sci., Part B: Polym. Phys*. **1978**, *16*, 1181-1193.

(26) Yao, S. F.; Chen, X. T.; Ye, H. M. Investigation of Structure and Crystallization Behavior of Poly (butylene succinate) by Fourier Transform Infrared Spectroscopy. *J. Phys. Chem. B* **2017**, *121*, 9476-9485.

(27) Schawe, J. E. Mobile amorphous, rigid amorphous and crystalline fractions in isotactic polypropylene during fast cooling. *J. Therm. Anal. Calorim.* **2017**, *127*, 931-937.

(28) Zia, Q.; Mileva, D.; Androsch, R. Rigid amorphous fraction in isotactic polypropylene. *Macromolecules* **2008**, *41*, 8095-8102.

(29) Lamberti, G.; Brucato, V. Real-time orientation and crystallinity measurements during the isotactic polypropylene film-casting process. *J. Polym. Sci., Part B: Polym. Phys*. **2003**, *41*, 998-1008.

(30) Doi, M.; Edwards, S. F. The Theory of Polymer Dynamics; Oxford University Press: New York, 1986; pp. 350-380.

(31) Strobl, G. From the melt via mesomorphic and granular crystalline layers to lamellar crystallites: A major route followed in polymer crystallization? *The European Physical Journal E* **2000**, *3*, 165-183.

(32) Alamo, R. G., Brown, G. M., Mandelkern, L., Lehtinen, A., Paukkeri, R. A morphological study of a highly structurally regular isotactic poly (propylene) fraction. *Polymer* **1999**, *40*, 3933-3944.

(33) Hiejima, Y., Takeda, K., Nitta, K. H. Investigation of the Molecular Mechanisms of Melting and Crystallization of Isotactic Polypropylene by in Situ Raman Spectroscopy. *Macromolecules* **2017**, *50*, 5867-5876.

(34) Kissin, Y. V., & Rishina, L. A. (1976). Regularity bands in the ir spectra of C3H6□ C3D6 copolymers. *European Polymer Journal*, *12*(10), 757-759.

(35) Khafagy, R. M. (2006). In situ FT-Raman spectroscopic study of the conformational changes occurring in isotactic polypropylene during its melting and crystallization processes. *Journal of Polymer Science Part B: Polymer Physics*, *44*(15), 2173-2182.

(36) Gaur, U., Wunderlich, B. (1981). Heat capacity and other thermodynamic properties of linear macromolecules. IV. Polypropylene. *Journal of Physical and Chemical Reference Data*, *10*(4), 1051-1064.

(37) Androsch, R., Wunderlich, B. (2003). Specific reversible melting of polymers. *Journal of Polymer Science Part B: Polymer Physics*, *41*(17), 2039-2051.

6. CONCLUSIONS

In the research described in this thesis a new investigation technique has been proposed and employed to study thermal transition of polymers. According to the obtained results, we believe that it can be profitably combined with other experimental analysis to deeply investigate the mechanisms ruling material transformations. We extensively exploited the potentiality of the Infrared spectroscopy, able to investigate the conformational changes of the macromolecular chains as a result of thermal treatments. The new Modulated Temperature FTIR technique results were compared with calorimetric data to obtain wider insights of the phenomena involved in physical aging, glass transition and crystallization of different polymers. Moreover, the early findings obtained from MTFTIR stimulated the design of further experiments rarely reported in literature, such as the annealing above Tg or new modulated procedures, as Quasi-isothermal FTIR analysis. Through this kind of experiment, we highlighted and interpreted some phenomena otherwise not or poorly accessible by other experimental methods.

7. APPENDIX

During the collaboration period of five month at Material Physics Center (CFM) of San Sebastian, Spain, the common efforts with researcher Daniele Cangialosi and PhD Natalia Gutierrez Perez-de-Eulate, focused on the improvement of calorimetric information obtained by Fast Scanning Calorimetry (FSC), brought to the publish of "Glass Transition and Molecular Dynamics in Polystyrene Nanospheres by Fast Scanning Calorimetry". The link to the paper is attached below.

https://pubs.acs.org/doi/abs/10.1021/acsmacrolett.7b00484

Perez-de-Eulate, N. G., Di Lisio, V., & Cangialosi, D. (2017). Glass Transition and Molecular Dynamics in Polystyrene Nanospheres by Fast Scanning Calorimetry. *ACS Macro Letters*, *6*(8), 859-863.